Data Integration and Simulation of Population Immunity at the Beginning of a Pandemic

Siyu Chen

Linacre College

University of Oxford

A thesis submitted for the degree of

Doctor of Philosophy

Trinity Term 2023

Acknowledgements

First of all, a massive thank you to my supervisors, Lisa J White, Katrina A Lythgoe and Jennifer A Flegg– thank you for your extremely valuable insights and advice, and for always finding the time to meet or to read manuscripts. Lisa – the vast amount of time you have dedicated to my academic development since we first met in China, without which I would not be where I am today, is hugely appreciated. A big thanks to Katrina and Jen, past and present, for your endless mental support and emotional help.

This thesis would not have been possible without the collaborators who contributed to the publications from which the research chapters of this thesis are adapted: Ricardo Aguas (Chapter 2), Fatima Arifi (Chapter 4) and Nathaniel Hupert, Yawei J. Yang, Elisabeth A. Murphy (Chapter 5). Thank you to the CoMo Consortium where I started my first academic research collaboration and worked in a big team, to the Linacre College for providing a brilliant opportunity for me to give a talk for my DPhil studies, to Pan who invited me to visit MORU Tropical Medicine Research in Bangkok.

To my parents, Liping and Jingyun. Dad, you've always been the backbone of my life. Apart from being my superman; you are also a human being with emotions and I realized that when I saw you getting emotional about my departure. Mom, you're the most amazing person on earth; your life philosophy always motivates me to become a better person. I wouldn’t be where I am today without your help and guidance. You are the best parents in this world. I love you, my mom and dad! To my love, David. It was such a perfect coincidence that we first met in Nankai and a deterministic moment that we met again four years later in London. Thank you for always being with me whenever I need you. I love you, my love, forever! To myself, from Changsha to Tianjin to Oxford, you never stop chasing your dream and your love for one second. Now you are going to complete a big jump in your academic life and become a researcher. You deserve that! Go and become a real scientist!

Abstract

Accurate knowledge of population exposure at the outset of a pandemic has critical ramifications for preparedness plans for future epidemic waves. In this thesis, I developed a mechanistically informed statistical model to integrate multiple epidemiological datasets in different settings and in different population and to estimate key epidemiological parameters as well as population exposure using Bayesian inference.

First, I present a dynamic model to link together three key metrics for evaluating the progress of COVID-19 epidemic in England: seroprevalence, PR-PCR test positivity and death. While estimating the IgG antibody seroreversion rate and region-specific infection fatality ratios, I find that epidemic progression resulted in an increasing gap between measured serology prevalence levels and cumulative population exposure to the virus. Ultimately, this may mean that twice as many, or more, people have been exposed to the virus relative to the number of people who are seropositive by the end of 2020.

Moreover, I demonstrate that the model could reconstruct the first, unobserved, epidemic wave of COVID-19 in England from March 2020 to June 2020 as long as two or three serological measurements are given as inputs, with the second wave during the winter of 2020 validated by the estimates from the ONS Coronavirus Infection Survey. Comparing with the inferred exposure, I find that the UK official COVID-9 online dashboard reported COVID-19 cases only accounted for less than ten percent by the end of October 2020. I then generalise the model to account for the undocumented COVID-19-related mortality and sparse measurements of seroprevalence. I apply this in the context of Afghanistan COVID-19 epidemic and find the population exposure in nine regions of Afghanistan were all higher than the seroprevalence survey suggested by July 2020.

Finally, I assess the impact of shielding among pregnant patients by comparing their exposure with the estimated exposure of the general population. To approach this, I develop a dynamic model to link RT-PCR and antibody testing results from patients who gave birth and then apply Bayesian inference to estimate transmission parameters and exposure among pregnant patients. I find that after considering the duration of each pregnancy pre-COVID onset and after, the impact of shielding on reducing the level of exposure among pregnant patients during early 2020 who gave birth in this New York City hospital were approximately 50%.

Contents

Contents i
Chapter 1 Introduction 1
1.1 Progression of exposed individuals through the various clinical and diagnostic stages during COVID-19 infections 4
1.1.1 Within-host virologic kinetics and diagnosis 4
1.1.2 Within-host serologic kinetics and diagnosis 8
1.1.3 T cells in immunity to SARS-CoV-2 and cross-recognition against other human coronaviruses 10
1.1.4 Seroepidemiology 12
1.2 Mathematical models to reconstruct population exposure 14
1.3 Using Bayesian inference to estimate parameters in Rstan 18
1.4 Thesis overview 20
Chapter 2 Data integration to estimate exposure to SARS-CoV-2 in England 23
2.1 Introduction 24
2.2 Data sources and availability 29
2.2.1 Regional daily deaths 29
2.2.2 Regional adjusted seroprevalence 29
2.2.3 Regional test-positivity ratios 30
2.2.4 Regional population age structure and non-COVID epidemiological indices 30
2.3 Materials and Methods 30
2.3.1 Mechanistic model 30
2.3.2 Observation model for statistical estimation of model parameters 33
2.3.3 Sensitivity analyses 35
2.3.4 Relationship between demographic and epidemiological factors and estimated regional IFRs 35
2.4 Results 36
2.4.1 Time-independent IFR model results 36
2.4.2 Time-varying IFR model results 39
2.5 Discussion 41
Chapter 3 Data integration to estimate exposure to SARS-CoV-2 in data-scarce scenarios – at the beginning of the pandemic in England 45
3.1 Introduction 46

3.2 Data sources and availability 47
3.2.1 ONS estimated incidence 48
3.2.2 Model estimated exposure 48
3.2.3 7-day average of reported COVID-19 cases in England 49
3.3 Materials and Methods 49
3.3.1 Model predicted incidence 49
3.3.2 Case detection ratio 50
3.4 Results 50
3.4.1 Reconstruction of the early epidemic 50
3.4.2 Validation from ONS Coronavirus Infection Survey 51
3.4.3 Relationship between model performance and data abundance 52
3.4.4 Time-varying case detection rate 55
3.5 Discussion 56
Chapter 4 Data integration to estimate exposure to SARS-CoV-2 in data-scarce scenarios – serological data was limited in Afghanistan 59
4.1 Introduction 60
4.2 Materials and Methods 62
4.2.1 Data sources and availability 62
4.2.2 Seroprevalence adjusted by the performance of the test 63
4.2.3 Exposure estimates 64
4.3 Results 67
4.4 Discussion 69
Chapter 5 Data integration to estimate the shielding impact among pregnant women on reducing exposure to SARS-CoV-2 in New York City 74
5.1 Introduction 75
5.2 Data source and availability 76
5.2.1 Pregnant women data 76
5.2.2 General Population Data 78
5.3 Materials and Methods 78
5.3.1 Exposure Inference in Pregnant Patients 78
5.3.2 Exposure Inference in General Population 82
5.4 Results 82
5.4.1 Dynamic model of SARS-CoV-2 infection 82
5.4.2 Longitudinal cross-sectional RT-PCR and serology results 84
5.4.3 Fitting data from pregnant patients to the dynamic model 85

5.4.4 Transmission parameters of COVID-19 in pregnant patients are estimated to be consistent with those estimated for general population 87
5.4.5 Estimated SARS-CoV-2 exposure in pregnant patients is higher than seropositivity rates would suggest..... 87
5.4.6 SARS-CoV-2 exposure in pregnant patients at the time of birth rose from half that of the general population to equal that of the general population by late 2020 89
5.5 Discussion 91
Chapter 6 Discussion 95
6.1 Summary of findings and implications 96
6.2 Ongoing and future research 101
6.2.1 Using serology data to inform the assessing of the impact of non-pharmaceutical interventions (NPIs) targeted on COVID-19 on other respiratory diseases 101
6.2.2 Linking individual-level virologic and serologic kinetics to inform epidemic progression 102
6.2.3 Simulation of population assessments and economic impact of a hypothetical long-acting antibody (LAAB) on a vulnerable population 102
6.3 Conclusion remarks 103
Appendix Figures and Tables 105
Bibliography 129

List of Figures

Figure 1-1. Dynamics of RNA viral loads and infectious virus and its correlation with symptoms for ancestral SARS-CoV-2 in patients with mild-to-moderate disease (*16*).....7
Figure 1-2. Dynamics of diagnostic test results (RT-PCR, IgM antibody, and IgG antibody) for detection of SARS-CoV-2 infection relative to symptom onset (*59*).....10
Figure 2-1. Progression of exposed individuals through the various clinical (below the timeline) and diagnostic (above the timeline) stages of infection and recovery. 26
Figure 2-2. Time course of the SARS-CoV-2 pandemic up to 7 November 2020 for the seven regions in England in the constant IFR model. 37
Figure 2-3. Time course of the SARS-CoV-2 pandemic up to 7 November 2020 for the seven regions in England in the time-varying IFR model. 40
Figure 3-1. Comparison of model predicted daily incidence of SARS-CoV-2 in England.52
Figure 3-2. Comparison of estimates of exposure in seven regions of England in 2020 as more serological measurements are included in the model inputs (left to right). 55
Figure 3-3. Comparison between estimates of daily incidence with reported cases of SARS-CoV-2 in England and case detection rate that is defined as the ratio between reported cases and inferred underlying incidence. 55
Figure 4-1. Adjusted seroprevalence by region by the sensitivity and specificity of the serology test for IgG-positive and/or IgM-positive. 67
Figure 4-2. Time course of the COVID-19 pandemic up to 21 July 2020 for the nine regions in Afghanistan, for all age groups. 68
Figure 5-1. Schematic diagram of the dynamic model structure for RT-PCR and serology status. 79
Figure 5-2. Time evolution measurements and fitted test-result model estimates of the SARS-CoV-2 RT-PCR and antibody status among patients who gave birth between 20 April 2020 and 21 December 2020.....86
Figure 5-3. Time evolution of SARS-CoV-2 exposure and seroprevalence among patients who gave birth between 20 April 2020 and 21 December 2020. 88
Figure 5-4. Comparisons of estimates of exposure in patients who were giving birth from four models and general population. 89

Appendix Figure 1. Marginal posterior distributions for parameters in the constant IFR model. 110
Appendix Figure 2. Probability of seropositivity persistence after seroconversion. 110
Appendix Figure 3. Cumulative deaths in the seven regions of England. 111
Appendix Figure 4. Relationship between demographic and epidemiological factors and estimated regional IFRs. 111
Appendix Figure 5. Relevant epidemiological metrics in England over the course of the pandemic. 112
Appendix Figure 6. Marginal posterior distributions for parameters in the time-varying IFR model. 113
Appendix Figure 7. Posterior predictive distribution of the time-varying IFR. 113
Appendix Figure 8. Comparison of the time course of the SARS-CoV-2 pandemic up to 7 November 2020 for the seven regions in England. 114
Appendix Figure 9. Comparison of time course of the SARS-CoV-2 pandemic up to 7 November 2020 for the seven regions in England for the time-varying IFR model. 115
Appendix Figure 10. Daily deaths with COVID-19 on the death certificate and deaths within 28 days of positive test by date of death. 116
Appendix Figure 11. Comparison of marginal posterior distributions for estimated parameters in the constant IFR model. 116
Appendix Figure 12. Comparison of marginal posterior distributions for estimated parameters in the time varying IFR model. 117
Appendix Figure 13. Comparison of the time course of the SARS-CoV-2 pandemic up to 7 November 2020 for the seven regions in England for the constant IFR model between using death within 28 days of a positive COVID-19 test and death certificate data as model inputs. 118
Appendix Figure 14. Comparison of the time course of the SARS-CoV-2 pandemic up to 7 November 2020 for the seven regions in England for the time-varying IFR model between using death within 28 days of a positive COVID-19 test and death certificate data as model inputs. 119
Appendix Figure 15. Ratio between relative rates of deaths of people who died within 28 days of their first positive test (per 100,000 population) in the winter wave of 2020 vs. the 2020 spring wave. 120
Appendix Figure 16. Comparison of parameter posterior distributions for the time-varying IFR model. 121

Appendix Figure 17. Comparison of IFR estimates for seven regions in England for time-varying IFR model. 121
Appendix Figure 18. A map showing the nine regions in Afghanistan where the study was conducted (the eight regions of Afghanistan plus Kabul province). 123
Appendix Figure 19. Time course of the SARS-CoV-2 infection among general from January 1st, 2020 to December 31st, 2020. 126
Appendix Figure 20. Comparisons of posteriors with different significant levels (50%, 90% and 95%) for the proportion of pregnant patients who were not exposed previously by 20 April 2020. 127
Appendix Figure 21. Comparisons of priors and posteriors for the proportion of pregnant patients who were not exposed previously by 20 April 2020. 127
Appendix Figure 22. Comparison of estimates of 'instrumental parameters' among the four models. 128

List of Tables

Table 2-1. Marginal median parameter estimates and 95% CrI for the constant IFR model. 38
Table 5-1. Demographics table for women who giving birth prior to August 2020 and from August 2020 onwards. 77
Table 5-2. A list of patient compartments or model variables and their definitions. 81
Table 5-3. Parameter estimates (associated 90% credible intervals) among pregnant patients for each model fit. 84
Appendix Table 1. The effective sample size and the Gelman-Rubin diagnostic for the eight model parameters in the default model (constant infection fatality ratio, IFR). 105
Appendix Table 2. The effective sample size and the Gelman-Rubin diagnostic for the 15 model parameters in the time-varying IFR model. 105
Appendix Table 3. Marginal median parameter estimates and 95% CrI for the time-varying IFR model. 106
Appendix Table 4. Summary of sensitivity analyses performed for $\delta p, \delta \epsilon$, death inputs and β prior for both constant IFR and time varying IFR models. 107
Appendix Table 5. Summary of parameter estimates for all models explored as defined in Appendix Table 4. 108
Appendix Table 6. Linear regression models exploring relationships between demographic and epidemiological factors and estimated regional IFRs. 109
Appendix Table 7. Sample size for the regional serology survey 122
Appendix Table 8. Characteristics of respondents 122
Appendix Table 9. A list of parameters, definitions and priors used in the Bayesian inference in the model of pregnant patients and general population. 124
Appendix Table 10. Posterior estimates of parameters in general population. 125
Appendix Table 11. The effective sample size and the Gelman-Rubin diagnostic for the four models. 125
Appendix Table 12. Estimation of effectiveness of shielding from the four models. 126

Acronyms

CDR Case detection rate

CFR Case fatality ratio

CI Confidence interval

CIS Coronavirus Infection Survey

CrI Credible interval

EIDs Emerging infectious diseases

HICs High-Income Countries

IFR Infection fatality ratio

IgM Immunoglobulin M

IgG Immunoglobulin G

LMICs Low- and Middle-income Countries

MCMC Markov chain Monte Carlo

NPIs Non-pharmaceutical interventions

ODE(s) Ordinary differential equation(s)

RT-PCR Reverse transcription polymerase chain reaction

WHO World Health Organisation

Chapter 1 Introduction

Rationale

Emerging infectious diseases (EIDs) with endemic and pandemic potential remain a substantial threat to global health (*1-4*). The first few months of the COVID-19 pandemic were rife with conflicting information, controversy and anxiety. This was engendered not only by the nature of the disease itself and limited medical and therapeutic measures, but also by the urgent political and public health interventions required in response to the menacing developments. My research was motivated by the need to understand what precisely was transpiring epidemiologically at the outset, what aspects could be measured with the limited data available, and how these measurements could be integrated into a coherent model of the initial trajectory of the pandemic. This would not only be a contribution to the study of COVID-19, but should also be a resource for those confronting, as they emerge, future outbreaks of infectious diseases that threaten regional or global health. Essential to this project was to combine all relevant datasets, examine their interrelations, take account of as many potentially important factors as possible and to use rigorous and robust methods to characterize the progress of the disease.

The COVID-19 pandemic that started in 2019 has had a devastating impact, with 6.9 million deaths reported worldwide as of 29th June 2023 (*5*). In different stages of the pandemic different types of epidemiological datasets were established and collected. Integrating these datasets and modelling the progress of the pandemic provides vitally important scientific evidence for public health policy. Here I consider the progress of the pandemic in terms of the exposure level in a population, with the focus on the early stages when the population consists almost entirely of naïve hosts and a vaccination campaign has yet to be conducted.

Background

Exposure level in the population has strong implications for vaccination prioritization strategy. In the early stage of the COVID-19 vaccination campaign, when dose supply and administrative capacity were initially limited worldwide, a modelling study (*6*) explored how uncertainty regarding previous exposure levels and about a vaccine's characteristics affects the prioritization strategies for reducing deaths and transmission. This model showed that the individual-level serological data can be used to inform the dosing priority to seronegative individuals, which will improve the marginal impact of each dose and reduce vaccination inequities in COVID-19 impact.

Moreover, exposure level is an important metric for evaluating the effectiveness of non-pharmaceutical interventions (NPIs). Most studies of estimating the impact of NPIs in the real-world relied on health-related outcomes at the population level associated with COVID-19 (*7*) (e. g., hospitalisations (*8*) and deaths (*9*)), and epidemiological outcomes characterizing infection dynamics such as reproduction numbers (*10, 11*) or transmission rates. However, compared with the downstream measurements including hospitalisation and death, exposure level is a more relevant marker of transmission in the population when it comes to assessing the impact of NPIs where the intended purpose was to reduce transmission, for example, school closure (*12*).

Approach

In this thesis, I develop novel mechanistic mathematical models and use Bayesian inference to estimate exposure level by linking multiple datasets. Ordinary differential equations are classical tools to understand the population dynamics of infectious disease, and here I have adapted them to explore 'cross-scale' dynamics of pathogens: from within-host dynamics to the population scale. I used Bayesian methodology to conduct inference of important epidemiological characteristics in case of limited data, thereby allowing for reliable uncertainty quantification.

Overview

I applied these methodologies to different populations, including the general population (Chapter 2 & Chapter 5) and pregnant women (Chapter 5), and in different settings, including High-Income Countries (HICs), where datasets are relatively rich and have relatively low bias (Chapter 2 and Chapter 3) and Low- and Middle-income Countries (LMICs) where datasets are limited and biased because of reporting issue (Chapter 4). In addition, in Chapter 5, I compared the estimates of exposure in the pregnant patients vs. general population in New York City. By considering the duration of pregnancy pre- and post-shielding, I demonstrated a dramatic real-world effectiveness of shielding on reducing exposure to SARS-CoV-2.

I framed the remainder of this introductory chapter in terms of a complex and multi-scale system. This includes the immune scale with mechanisms that operate at the individual level, and the epidemiological scale with mechanisms that are inter-individual. The core of this thesis revolves around the interaction between these two scales. In details, I first review the progression of exposed individuals during the various clinical and diagnostic stages of COVID-19 infection (Section 1.1) in terms of the within-host virologic kinetics (Section 1.1.1), within-host serologic kinetics (Section 1.1.2), T cells in immunity to SARS-CoV-2 and cross-recognition against other human coronaviruses (Section 1.1.3) and seroepidemiology (Section 1.1.4). This review forms the basis of model development for exploring 'cross-scale' dynamics of pathogens: from within-host dynamics to the population scale. Then I summarise previously published methodologies on the process of exposure (Section 1.2) and parameter inference (Section 1.3), techniques that I use and adapt throughout this thesis. Due to length limitations, I do not attempt to provide an encyclopaedic account of the epidemiological modelling or the parameter inference literature but focus on those methods that directly relate to the research presented in this

thesis. I then conclude this introductory chapter by providing an outline of the main research chapters of this thesis.

1.1 Progression of exposed individuals through the various clinical and diagnostic stages during COVID-19 infections

Once invaded the host, the SARS-CoV-2 starts replicating inside cells and infects more cells, evoking human immune responses. There are two broad types of immune response: innate responses and adaptive responses. The innate responses usually include physical barriers, such as the skin, as well as the activities of immune cells, such as macrophages and natural killer cells. The adaptive responses target specific pathogens or foreign substances and can take several days to develop (*13*). They involve two types of cells:

- immune B cells, which help to hunt down invaders circulating in the bloodstream by producing antibodies
- T cells, which seek out and destroy cells that have been infected by the invading pathogen by recognising tell-tale proteins on their surface

The indicators of T cells immunity are usually hard to measure compared with B cells immune responses, typically antibodies. Throughout the thesis, I did not use any measurements directly related with T cells immunity and am not relating the serology and exposure with immunity. I discussed the limitations of the study around this in the Discussion chapter.

1.1.1 Within-host virologic kinetics and diagnosis

After an individual is infected with SARS-CoV-2, the virus starts replicating inside cells and infects more cells (*14*). Studies showed that SARS-CoV-2 initially infects targets cells in the upper respiratory tract (URT) (*15*) but also spreads to the lower respiratory tract (LRT), where it infects alveoli, causing reduced gas exchange, inflammation and pulmonary

pathologies (*16*). Exposed individuals shed the virus through the URT and transmit the virus leading to secondary infections with emission of infectious virus (*17*). The gold standard for laboratory diagnosis of an infection is quantitative reverse transcription polymerase chain reaction (RT-PCR). This is used to recognize the presence of specific target RNA through an enzymatic process of amplification (*18*).

Viral load, a measure of the total number of viral particles inside the individual, as determined by RT-PCR, is either expressed as the number of viral RNA copies per millilitre of viral transport medium or per swab (*19-21*) or by the arbitrary test-specific Cycle threshold (Ct) value (*22*). Ct value is defined as the number of amplifications required for a target gene to cross the threshold determined by real-time PCR. Arbitrary test-specific Ct values inversely correlate with viral load (*17*). There are different types of RT-PCR assays worldwide used for COVID-19 surveillance. The assays differ from each other in multiple ways, including the threshold (sensitivity) – the lowest concentration of virus that can be detected by the assay, chemistry of reagents, gene targets, cycle parameters, analytical interpretive methods, sample preparation and extraction techniques (*23*). Therefore, Ct values cannot be directly compared among assays of different types.

It is important to note that RT-PCR detects the presence of viral RNA in a sample but is not able to distinguish whether infectious virus is present. In a COVID-19 hamster model, the timeframe of transmission is correlated with the detection of infectious virus using cell culture instead of viral RNA (*24*). The gold standard for detecting the presence of infectious virus in respiratory specimens is the replication of virus in cell culture, termed virus isolation (*17*).

Viral load determines the Ct value reported from a RT-PCR test and then determines RT-PCR testing status (positive or negative). Infectious viral load determines the culture probability and then determines the infectiousness (or infectivity) and transmission. In the

literature, many studies have tried to capture the kinetics of viral titer or Ct value or RT-PCR sensitivity since exposure or onset of symptom (*25-27*). A literature review during early 2020 showed it is more likely that the virus would be detected from nasopharyngeal sampling between 0- and 4- days post-symptom onset, 89% (95% CI (83%, 93%)) vs. 54% (95% CI (47%, 61%)) after 10 to 14 days (*27*). However, RT-PCR positivity is highly likely to have started before the onset of symptoms, namely during the incubation period (*28*). Other studies tried to model the time-varying relationship between infectiousness and time since exposure or onset of symptoms (*19-21, 29, 30*). During the incubation period, infected individuals are highly likely to be infectious (*31, 32*).

Comparing the kinetics of Ct value and culture probability shows that the viral load increased earlier in the early stage of infections and decreased later in the late stage of infections than the infectious viral load (*33*). This implies that the earlier detection of viral load using PT-PCR tests can help capture early infections but might lead to unnecessary isolation days or absenteeism in the late stage of infection (*28*) as illustrated by Figure 1-1 (*17*).

Along with the viral kinetics, infected individuals experience various clinical stages. Here I review the estimates of mean time of symptom onset, hospitalisation, and death since exposure. These quantities vary across virus variants and vaccination status. Since most of work in this thesis deals with the early stage of the pandemic, the literature review below mainly focuses on studies in 2020.

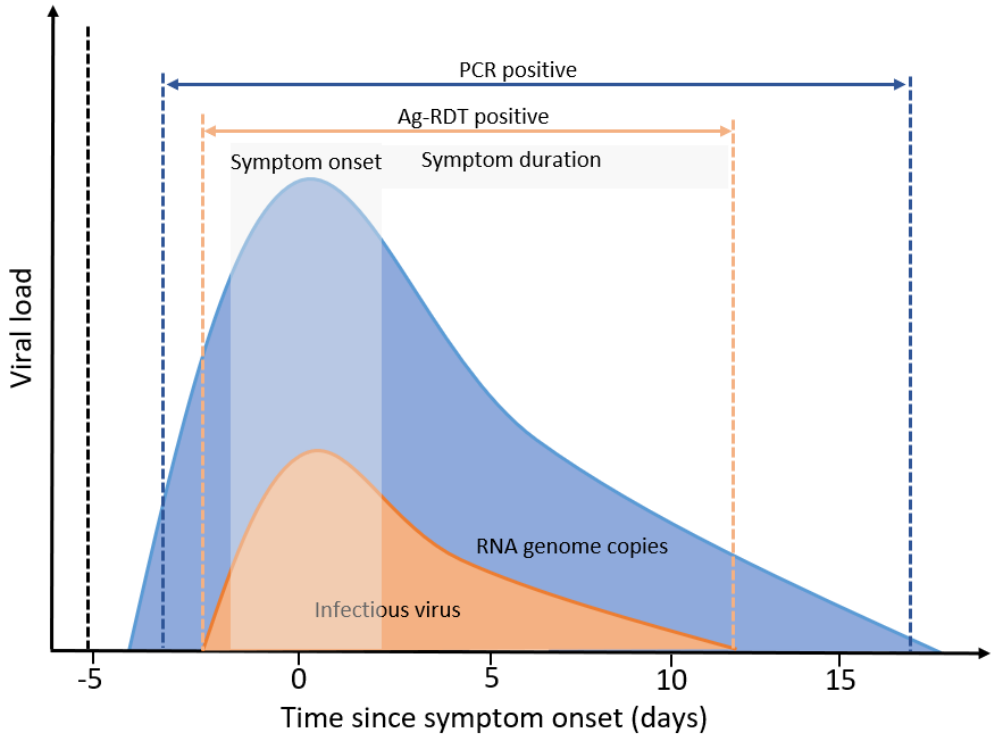

Figure 1-1. Dynamics of RNA viral loads and infectious virus and its correlation with symptoms for ancestral SARS-CoV-2 in patients with mild-to-moderate disease (*17*).
The orange area shows the window of infectious virus presence that can be captured by Ag-RDT positivity while the blue area shows the window of RNA genome presence that can be captured by RT-PCR positivity.

Most individuals, once infected, experience an incubation period of approximately 4.8 days (95% confidence interval (CI): 4.5–5.8) (*34*). followed by the development of symptoms, which include fever, dry cough, and fatigue, although some individuals will remain asymptomatic throughout. Symptomatic individuals may receive a diagnostic RT-PCR test at any time after symptom onset; the time lag between symptom onset and date of test varies by country and area, depending on local policies and testing capacity. Some individuals might, as their illness progresses, require hospitalization, oxygen therapy, or even intensive care, eventually either dying or recovering. The day of symptom onset, as the first manifestation of infection, is a critical point for identifying when specific events occur relative to each other along the infection timeline. The mean time from symptom onset to death is estimated to be 17.8 days (95% credible interval (CrI): 16.9–19.2 days) and to hospital discharge is 24.7 days (22.9–28.1 days) (*35*) (*36*).

1.1.2 Within-host serologic kinetics and diagnosis

When individuals are exposed to the virus, their immune systems can recognise the proteins on the surface of the virus, namely antigens. Then the immune cells, such as 'B cells', produces antibodies that bind to the virus and signals for other cells in the immune system to neutralize the virus (*37*). The role of T cells in immunity to SARS-CoV-2 is briefly discussed in the following subsection.

The SARS-CoV-2 RNA genome encodes 29 structural and non-structural proteins, including the spike (S), envelope (E), membrane (M) and nucleocapsid (N) proteins, as well as the ORF1a/b polyprotein (*38*) which should elicit an antibody response (IgM and IgG) following infection. Many serological assays (also called response assays) have been developed to detect anti-spike (S) protein and anti-nucleoprotein (N) antibody response, because the two proteins are highly immunogenic (*39, 40*).

Spike S protein is found on the surface of the virus. It contains several regions, such as the Receptor-Binding Domain ('RBD') which enables the virus to enter human cells. Anti-S antibody tests may target the entire S protein, or only certain regions (for example, RBD) (*41, 42*). The nucleocapsid ('N') protein plays a crucial role in subgenomic viral RNA transcription and viral replication and assembly (*39*). Some anti-S antibodies, including those targeting the receptor binding domain (RBD) of the S protein, display neutralizing activity. Neutralizing antibody levels detected by functional assays such as plaque neutralization assays, microneutralization assays or inhibition of infection assays are highly predictive of immune protection from symptomatic SARS-CoV-2 infection (*43*). Delayed production of neutralizing antibodies correlates with fatal COVID-19 (*44*).

The commercial immunoassays used for COVID-19 diagnosis are mainly chemiluminescence immunoassays (CLIAs), enzyme-linked immunosorbent assay (ELISAs) and rapid diagnostic tests such as lateral flow immunoassays (LFIAs) (*45*). They detect the

viral structural proteins or IgM and IgG antibodies against viral antigens (*46-48*). The dynamics of IgG and IgM antibodies after infection have been widely studied during the pandemic because of its potential power for tracking disease burden and population immunity.

The time lag from exposure to SARS-CoV-2 until seroconversion was estimated to be 1-3 weeks (*49-51*). Here, seroconversion is defined as the timing that exposed individuals start generating detectable antibody. After infection, however, 5-22% of individuals remain serology negative (*52-54*), which is more common among individuals with mild symptoms than with severe disease (*53*) and among asymptomatic compared to symptomatic individuals (*52*). The duration of antibody detection varied among antigen and immunoglobulin targets; anti-spike and total Ig assays demonstrated more stable longitudinal reactivity than anti-nucleocapsid and IgG assays (*46*). The half-life of anti-spike IgG antibodies was estimated to be from 36 to 244 days while estimates of the half-life of anti-nucleocapsid IgG was reported to be between 35 and 85 days (*55-58*). These estimates also show the half-life of IgG antibodies varies across age and disease severity and depends on the assay used. A recent systematic review and meta-analysis of SARS-CoV-2 serology studies assessed the sensitivity decay of seroassays for detecting SARS-CoV-2 infections; it showed sensitivity waning highly correlated with the antigen and the analytic technique used by the assay. The average sensitivities ranging between 26% and 98% at 6 months after infection, depending on assay characteristics (*59*). Figure 1-2 illustrated the time course of diagnosis variation relative to symptom development.

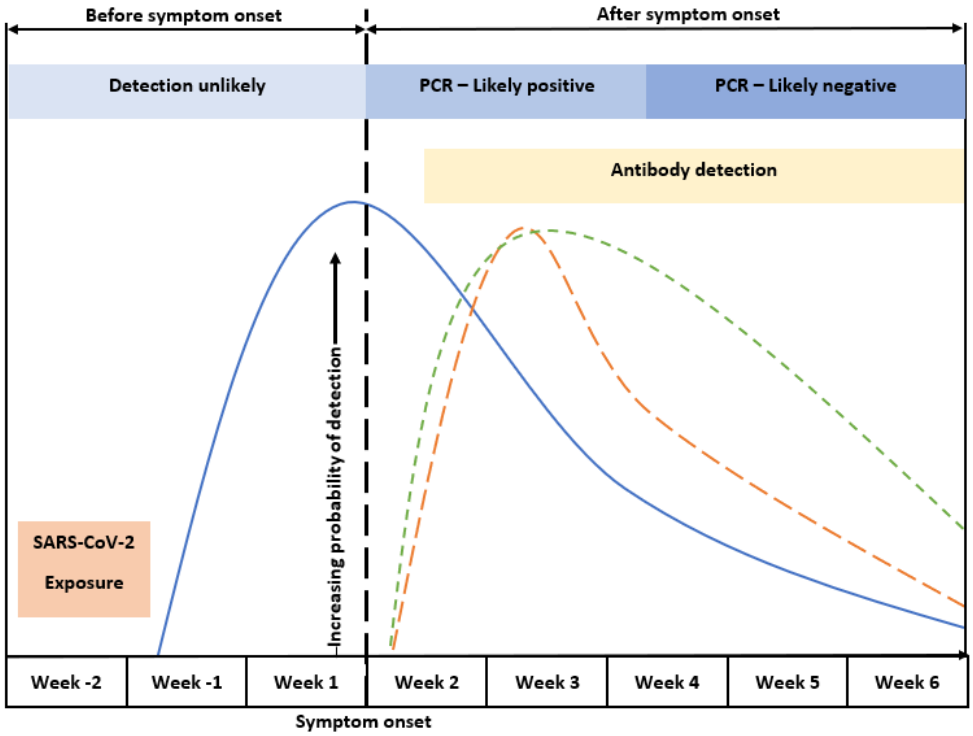

Figure 1-2. Dynamics of diagnostic test results (RT-PCR, IgM antibody, and IgG antibody) for detection of SARS-CoV-2 infection relative to symptom onset (*60*).
The blue solid curve stands for the nasopharyngeal swab RT-PCR, the orange dashed curve indicates IgM antibody, and the dashed green curve represents IgG antibody. RT-PCR can detect infections much earlier than antibody tests prior symptom onset.

1.1.3 T cells in immunity to SARS-CoV-2 and cross-recognition against other human coronaviruses

Many individuals with substantial exposure to SARS-CoV-2, such as healthcare workers, demonstrate virus-specific cellular responses without virus-specific antibodies (*61-63*), indicating a potential role for the cellular immune system in clearing infection before it is fully established, known as 'cellular sensitization without seroconversion' (*64*). This implies that exposure level inferred from serology data might underestimate the population immunity.

Cellular immune system might cooperate with humoral immune system to fight with the virus and provide protection against severe disease. Studies show that CD4+ dominated spike-specific T cell responses are likely to support antibody generation, with follicular helper T cells correlating with humoral immunity in the memory phase (*65-67*). CD8+ T cell

responses against the $NP_{105–113}$ epitope restricted by B*07:02 demonstrate strong anti-viral activity and correlate with protection from severe disease (*67*).

As for the duration of SARS-CoV-2-specific T cells presence, there is hope that they will be maintained for many years, although this may depend on the clinical severity of the initial infection (*68*). Robust immunity is certainly maintained by 6 months (*69*) and beyond (*70*), while prospective studies show some refocusing of T cell specificity over time (*71*) and an estimated half-life of around 200 days for virus-specific cells (*72*).

Studies also showed that T cells exist within the body as resident memory cells within tissue and play an important role in protection against reinfection. The number of SARS-CoV-2-specific resident memory T cells in the lungs correlates with clinical protection (*73*), and as they can be detected for at least 10 months after infection, it is likely that they play an important role in limiting the severity of reinfection (*74*).

As for the T cell cross-recognition against other human coronaviruses, some studies show that children and young adults demonstrate higher levels of antibody cross-reactivity between human coronaviruses and SARS-CoV-2 (*75*). Individuals with robust HCoV-specific T cells may potentially be primed for superior protective cellular immunity following exposure to SARS-CoV-2, and recent infection with an human coronaviruses appears to be associated with a better clinical outcome after SARS-CoV-2 infection (*76-78*).

A study examined how the presence of these T cells induced by other coronaviruses at the time of SARS-CoV-2 exposure influences whether someone becomes infected and found high levels of pre-existing T cells, created by the body when infected with other human coronaviruses like the common cold, can protect against COVID-19 infection (*79, 80*).

Another study at the early days of COVID-19 pandemic reflected on the immunological and epidemiological aspects and implications of pre-existing cross-reactive immune memory to SARS-CoV-2, which largely originates from previous exposure to circulating common cold

coronaviruses (*81*). They proposed four immunological scenarios for the impact of cross-reactive CD4+ memory T cells on COVID-19 severity and viral transmission and discussed its implications for the dynamics of herd immunity. They found in any scenario wherein cross-reactive T cell memory affects SARS-CoV-2, there would still be substantial implications for understanding disease severity and risk stratification. The implications of immunological processes on other aspects of SARS-CoV-2 epidemiology are worthy of future study.

1.1.4 Seroepidemiology

Serologic studies provide important information about the current disease burden, i.e., what proportion of a population has been infected, as well as future pandemic trends, i.e., what proportion of a population is immune to disease or infection. However, because of the complexity of serologic dynamics as stressed above the answers to these two questions require further thought. I firstly outline some benefits of using serology data to inform pandemic progress as follows.

Seroprevalence data can be useful to calculate important epidemiologic parameters

Linking the syndrome surveillance data where COVID-19 cases and deaths are recorded with the seroprevalence data, one can calculate the case detection rate, symptom development rate, severity development rate, infection fatality rate and so on. However, to calculate the infection fatality rate, the total infections must be further estimated from the seroprevalence data as described below.

Seroprevalence data can be used to fit dynamic models

Susceptible-Exposure-Infection-Recovery-Susceptible (SEIRS)-based mechanistic models have been widely developed and applied during the pandemic to inform intervention design and vaccination campaigns. COVID-19 related case, hospitalisation, and death data are the three main sources used to fit the models (*82, 83*). Seroprevalence should be another

important source of data that can be used to anchor model parameters and improve the performance of prediction models.

I also summarise some limitations of using serology data to understand exposure and immunity as follows.

Antibody waning should be considered while inferring exposure

The antibody generated after infection decays rapidly. The rate of decay varies across the antigen and immunoglobulin targets, leading eventually to seronegative status in exposed individuals over time, also called as 'seroreversion'. This implies that seroprevalence assays miss this proportion of exposed individuals and underestimates the true exposure in the population over time. To compensate, in order to estimate the true exposure, one has to 'add back' the impact of antibody decay.

Cellular immunity and cross protection against other human coronaviruses have to be taken into account while interpreting the relation between serology and immunity

Studies have shown that the existence of anti-spike or anti-nucleocapsid IgG antibodies is correlated with a substantial risk reduction of SARS-CoV-2 reinfection at least during the first six months after primary infection (*84-88*). Comparing the incidence rate of reinfection in the antibody-positive cohort to the incidence rate of infection in the comparator antibody-negative cohort, one study concluded that natural infection elicits strong protection against reinfection with an efficacy more than 90% for at least seven months (*89*). Based on an antibody level of 28ng ml^{-1} that was estimated to be associated with 50% protection against new infection (*43*), one study estimated that IgG antibodies will be present up to 869 (482–3145), 600 (376–1123), 667 (407–1710) and 520 (343–962) days among white females, white males, non-white females and non-white males, respectively, aged 60 years. Based on a threshold of 6 ng ml^{-1} that was estimated to provide 50% protection against severe infection (neutralizing antibody levels 3% of peak) (*90*), the estimated time was 1500 (871–

5973), 1017 (685–1909), 1070 (669–2827) and 826 (571–1532) days, respectively. Besides the study of humoral immunity, other studies focus on the T cell response and found that antibody and T cell responses may work in a compensatory manner to provide protection (*91*). Sero-reversion does not prevent the establishment of population immunity and many other factors including T cells immunity and cross protection from other human coronaviruses may play important roles in understanding population immunity.

1.2 Mathematical models to reconstruct population exposure

In the literature, many studies aim to quantify the exposure to SARS-CoV-2 over time in the population. In this section I categorise them into two major approaches: the simulation approach, and the deconvolution approach. I summarise each of them below.

Simulation approach

I use 'simulation approach' to represent an approach to estimate the population exposure in the past or to predict the population exposure in the future. It usually involves developing a transmission model under a series of assumptions about the underlying mechanism, parameterising the model by fitting real-world observation data and/or using the parameters estimated from studies. Two types of models are usually developed in the literature, namely compartmental models, and agent-based models (ABM). An agent-based model that tries to include the uncertainty of individual behaviour is often referred to as an individual-based model.

The use of compartmental models to study infectious diseases can be traced back to the early 20th century when Kermack and McKendrick first introduced the well-known susceptibility-infected-removed (SIR) model (*92*). Since then, compartmental models have been widely applied to very diverse epidemics. As the name implies, such a model divides the whole population into three groups: susceptible (S), infected (I), and removed (R), based on a series of assumptions, e.g., homogeneous mixing of the infected and susceptible

populations. In practice the modelling exercises during the COVID-19 pandemic aiming to estimate population exposure have taken many factors into account, for example, the heterogenous contact pattern in a population structured by age and context (*93*), household structure (*94, 95*), clinical progress pathway (*96*), waning immunity and reinfection (*97*), and time-varying impact of non-pharmaceutical interventions (e.g. mask wearing, social distancing, school closure, working from home, etc) (*83, 98*) , and so on. To account for the uncertainty of model structure and parameters, some studies used stochastic versions of the discretised compartmental model (*99, 100*).

Agent-based models for infectious diseases usually include three key components: (1) a realistic synthetic population generated with demographic characteristics and household structure representative of the studied population, (2) a contact network among single individuals in the population, and (3) a disease model linking contact network into infection probabilities (*101-104*).

In both compartmental and agent-based models, model predictions are used to fit the observed data including COVID-19 related reported cases, mortality, hospitalisation (stratified by ICU and ventilation) (*99*), so that all model parameters can be estimated at the same time. Once the model is fully parameterised, estimates of population exposure over time can be easily generated.

Deconvolution approach

Mathematically, epidemiological measurements such as daily reported cases can be described as a convolution of the underlying time series of new exposure with a delay distribution— the probability distribution that describes time from exposure to measurements such as cases reporting. Recovering the infections curve from measurable metrics is a deconvolution operation (*105*). Similarly, COVID-19 related mortality, hospitalisation, and even the estimates of prevalence from large-scale infection surveys

(*106*) can also be used as the inputs in the deconvolution approach. Equation (1.1) gives a discrete version of the mathematical representation of the convolution-deconvolution process

$$z(t) \leftarrow (f * g)(t) = \sum_{x=m}^{n} f(x)g(t-x) \tag{1.1}$$

Here, z is the observed epidemiological time-series data, e.g., daily reported cases (*107*), daily hospitalisation (*105*), and daily death (*108*) etc, f is the new exposure time-series to be inferred, g is the delay distribution, e.g. the probability distribution that describes the time from exposure to reporting, and m and n is the lower and upper bound of summation window. Calculating z given f and g is defined as 'convolution', while inferring f given g and z is defined as 'deconvolution'. Because not all infections result in hospitalisation or mortality, some time-independent or time-varying probabilities of clinical pathway have to be included into Equation (1.1). For example, the infection fatality ratio (IFR) should be accounted for while using mortality data as input.

Intuitively, new exposures can be seen as a weighted sum of reported observations with the weights as the probabilities given by the delay distributions. In the absence of a model, new exposures are just identified—the number of exposures to be inferred is equal to the number of observed data points. Without observation noise, the convolution matrix can be inverted, and true exposure rates can be identified. With observation noise, the data alone cannot distinguish signal from noise, leading to fundamentally unstable estimation. A recent study imposed structure on the solution of the deconvolution based on prior information in order to separate out the noise and obtain robust estimates of exposure (*105*). Using similar ideas based on the COVID-19 related mortality and a given delay distribution from infection to

mortality, another study estimated the cumulative exposure to SARS-CoV-2 in 2020 across 15 countries (*109*).

Using the deconvolution framework, some studies make full use of serological survey data to reconstruct the exposure curve (*108, 110*). However, the deconvolution formula has to be used 'twice' in this case; along with the process from exposure to seropositivity there is another process called seroreversion whereby seropositive individuals become seronegative due to antibody decay as discussed in Section 1.1.2, besides the process of delay between exposure to seroconversion. One study developed a full stochastic framework to account for the delay between exposure and seroconversion and the delay between seroconversion and seroreversion and estimated the reversion rate as well as the infection fatality ratio (IFR) using mortality and seroprevalence data in New York City and Connecticut. The daily seroprevalence and cumulative incidence of SARS-CoV-2 infection predictions can then be easily generated once the model is parameterised (*108*). This deconvolution framework of reconstructing the exposure curve using seroprevalence and mortality as input has been widely applied in many populations since then (*111-113*).

In Chapter 2 and Chapter 5, I developed two novel mathematical models to link multiple datasets in the general population and pregnant women and applied Bayesian inference to estimate the population exposure over time. Compared with the SEIR-type compartmental models in the Simulation Approach, the model that I developed in Chapter 2 is simpler in terms of the model structure and requires fewer datasets as demonstrated in Chapter 3 but provides accurate estimates of parameters that can be validated by clinical observation study. Compared with the Deconvolution Approach, the model that I developed in Chapter 5 can reconstruct the exposure history by integrating multiple underlying dynamics including virologic kinetics and serologic kinetics, and then fitting to multiple real-world datasets.

1.3 Using Bayesian inference to estimate parameters in Rstan

Throughout this thesis, I estimate parameter values of different mathematical models by fitting the models to a variety of data types using Bayesian inference using Markov chain Monte Carlo (MCMC). A brief introduction to Bayesian inference and its implementation in Rstan is given below.

Bayesian statistics describe all characteristics of a parameter θ are made in terms of probability. The probability is conditional on the observed data of y, written as $p(\theta|y)$. The joint probability mass or density function can be written as a product of two densities that are often referred to as the prior distribution $p(\theta)$ and 'likelihood' $p(y|\theta)$, respectively:

$$p(\theta, y) = p(\theta)p(y|\theta) \tag{1.2}$$

Simply conditioning on the known value of the data y, using Bayes' rule, yields the posterior density:

$$p(\theta|y) = \frac{p(\theta, y)}{p(y)} = \frac{p(\theta)p(y|\theta)}{p(y)} \tag{1.3}$$

where $p(y) = \sum p(\theta)p(y|\theta)$, and the sum is over all possible values of θ (or $p(y) = \int p(\theta)p(y|\theta)d\theta$ in the case of continuous θ). Once the data y is given, then it can be considered as a constant. This allows to omit the factor $p(y)$ from Equation (1.3) which does not depend on θ, yielding the unnormalized posterior density,

$$p(\theta|y) \propto p(\theta)p(y|\theta) \tag{1.4}$$

The second term in the expression, $p(y|\theta)$, is taken here as a function of θ, not of y (*114*). It is generally challenging to work out the posterior in closed form due to the complexity of

models. MCMC methods provide a family of approaches for obtaining a sample from the posterior distribution, $p(\theta|y)$ (*115*).

One of the simplest MCMC algorithms is the Metropolis-Hastings algorithm. Briefly, this algorithm generates a sequence of values of the model parameters, $\theta = \theta_n$ (where $n = 0, \ldots, N$ for some N), that converges to a sequence of samples from the posterior distribution for large n. In each step, a candidate value of $\theta = \theta_{prop}$ is sampled from a proposal distribution $Q\left(\theta_{prop}\middle|\theta_{n-1}\right)$, where the proposal distribution can be any distribution that is symmetric in the sense of satisfying $Q(\theta) = Q\left(\theta\middle|\tilde{\theta}\right)$, although this algorithm can also be adapted for non-symmetric proposal distributions. The proposed value of θ is accepted (i.e. we set $\theta_n = \theta_{prop}$) with a probability that depends on the relative posterior densities at θ_{prop} and θ_{n-1} (where the proposal is always accepted if the posterior density is higher at θ_{prop} than at θ_{n-1}), and is otherwise rejected (i.e. we set $\theta_n = \theta_{n-1}$). While the chain eventually converges to the posterior distribution of θ, initial estimates (i.e., θ_n for small n) may not follow this distribution (*82*).

Stan is a C++ library for Bayesian modelling and inference that primarily uses the No-U-Turn sampler (NUTS) (*116*) to obtain posterior simulations given a user-specified model and data. The R package rstan provides RStan, the R interface to Stan. The rstan package allows one to conveniently fit Stan models from R and evaluate the output, including posterior inferences and intermediate quantities such as evaluations of the log posterior density and its gradients (*117*). To assess the convergence of the Markov chains, one can plot the time series of the posterior draws or calculate the split $\hat{R}$ statistic (*118*). At convergence $\hat{R} = 1$ and the time series of the posterior draws are well mixing. Throughout this thesis, I conducted Bayesian inference using the R package rstan.

1.4 Thesis overview

The whole relationship between immune responses, exposure to SARS-CoV-2 and other human coronaviruses forms a very big picture of COVID-19 ecosystem, which is extremely complex and beyond the scope of my thesis. I am focusing on a few data types that were available namely seroprevalence, COVID-19 related mortality and RT-PCR testing results. Through my analysis, I am offering evidence on a piece of the puzzle by focussing on methods for inferring the population exposure from available epidemiological datasets and not making any statement about the presence or absence with the immunity as a result of this.

The overall aim of this thesis is to develop mechanistic models with Bayesian inference to reconstruct the hidden exposure history of SARS-CoV-2 infections in a population. I approach this problem by first conducting a literature review about the average timeline of virologic and serologic dynamics during an infection at the population level as presented in Sections 1.2-1.3. Then I developed mechanistic models to link multiple datasets and applied Bayesian inference to simultaneously estimate quantities of epidemiological interest from the models (see following chapters). The summaries of each chapter are:

- **Chapter 2:** Data integration to estimate exposure to SARS-CoV-2 in England. In this chapter, I aim to estimate exposure to SARS-CoV-2 in different regions of England after accounting for the antibody decay. I first presented a new mechanistic model with Bayesian inference that combines multiple datasets (time-series of serology, mortality, and virus positivity ratios) to estimate seroreversion rate and infection fatality ratios (IFR) and simultaneously infer population exposure levels. Secondly, I collected publicly available datasets in different regions of England including mortality, seroprevalence and RT-PCR positivity rates and applied this method to estimate exposure. The results indicate that the average time to seroreversion is around six

months, while the true exposure may be more than double the seroprevalence levels reported at the time for several regions of England. This chapter is mainly based on my first-author paper published in PLOS Computational Biology (*36*).

- **Chapter 3:** Data integration to estimate exposure to SARS-CoV-2 in data-scarce scenarios – at the beginning of the pandemic in England. In this chapter, I described how the model developed in Chapter 2 can be useful to accommodate the uncertainty of limited epidemiological information at early time and how it can be validated by large-scale population level infection survey when it is available. This Chapter is mainly based on a first-author manuscript submitted to MedRxiv (*119*).
- **Chapter 4:** Data integration to estimate exposure to SARS-CoV-2 in data-scarce scenarios – serological data was limited in Afghanistan. In this chapter, I revised the methodology that I developed in Chapter 2 to allow for the estimation to be conducted using a single seroprevalence and then applied this to data from Afghanistan as an example. The method also addressed the underreporting issue of COVID-19 related mortality in Afghanistan. This Chapter is mainly based on a co-author paper published in BMJ Open (*120*).
- **Chapter 5:** Data integration to estimate the shielding impact among pregnant women on reducing exposure to SARS-CoV-2 in New York City. In this chapter, my aim was to estimate exposure to SARS-CoV-2 in pregnant women and in the general population separately in New York City and, based on that, to infer the effectiveness of shielding behaviour during pregnancy on reducing exposure among pregnant women. I first developed a new mechanistic model and used Bayesian inference to estimate exposure in pregnant women and applied the methodology that I developed in Chapter 2 to infer exposure in the general population in New York City. I compared the estimate of exposure in these two populations and discussed/considered? the effectiveness of

shielding during pregnancy, making full use of the approximately 40-week duration of pregnancy. The model showed that patients already pregnant at the onset of the pandemic had around a 50% decrease in exposure compared to those who became pregnant after the onset of the pandemic as well as to members of the general population. This Chapter is mainly based on a first-author paper published in Viruses (*121*).

- **Chapter 6:** In this chapter, I summarise the findings of the thesis and discuss directions for future work.

Chapter 2 Data integration to estimate exposure to SARS-CoV-2 in England

I have published the research underlying this chapter in the journal PLOS Computational Biology with me as the first author (*36*): Siyu Chen, Jennifer A Flegg, Lisa J White, and Ricardo Aguas. (2021) Levels of SARS-CoV-2 population exposure are considerably higher than suggested by seroprevalence surveys. PloS Computational Biology 17(9): e1009436. https://doi.org/10.1371/journal.pcbi.1009436.

Accurate knowledge of prior population exposure has critical ramifications for preparedness plans for future SARS-CoV-2 epidemic waves and vaccine prioritization strategies. Serological studies can be used to estimate levels of past exposure and thus position populations in their epidemic timeline. To circumvent biases introduced by the decay in antibody titers over time, methods for estimating population exposure should account for seroreversion, to reflect that changes in seroprevalence measures over time are the net effect of increases due to recent transmission and decreases due to antibody waning.

This chapter aims to present a mathematical model to link together three key metrics for evaluating the progress of an epidemic and apply to the context of SARS-CoV-2 in England: antibody seropositivity, infection incidence and number of deaths. I use data on these three metrics to estimate the antibody seroreversion rate and region-specific infection fatality ratios. In doing so, the cumulative number of infections in England are estimated, showing that cross-sectional seroprevalence data underestimate the true extent of the SARS-CoV-2 epidemic in England to date. Estimates for the IgG (spike) seroreversion rate and IFR are broadly consistent with other studies, which supports the validity of these findings.

2.1 Introduction

The COVID-19 pandemic has inflicted devastating effects on global populations and economies (*122*). Levels and styles of reporting epidemic progress vary considerably across countries (*123*) with cases consistently being under-reported and case definitions changing considerably over time. Therefore, the scientific and public health communities turned to serological surveys as a means to position populations along their expected epidemic timeline and thus provide valuable insights into COVID-19 lethality (*124, 125*). Those prospects were frustrated by apparent rapid declines in antibody levels following(*126*) infection. Population-wide antibody prevalence measurements can significantly underestimate the level of underlying population immunity, with obvious implications for intervention strategy design and vaccine impact measurement.

Continued research efforts to determine the correlates for protective immunity against disease and infection have found that while antibody titers are poor indicators of sustained immunity, cellular immunity can play a determinant role in limiting susceptibility to further SARS-CoV-2 challenges in previously exposed individuals (*61, 127*). Unfortunately, performing T cell assays at scale is technically challenging and expensive, which justified the decision to conduct a series of serology surveys (some of which are still underway) in many locations globally to provide a better understanding of the extent of viral spread among populations (*128*).

In England, a nationwide survey sampling more than 100,000 adults was performed from 20 June to 13 July 2020. The results suggested that 13% and 6% of the population of London and England, respectively, had been exposed to SARS-CoV-2, giving an estimated overall infection fatality ratio (IFR) of 0.90% (*129*). Although corrections were made for the sensitivity and specificity of the test used to infer seroprevalence, declining antibody levels were not accounted for. This is a limitation of the approach, potentially resulting in

underestimates of the true levels of population exposure (*129*) and an overestimate of the IFR.

We now have a much clearer picture of the time dynamics of humoral responses following SARS-CoV-2 exposure, with antibody titers remaining detectable for approximately 6 months (*130, 131*). Commonly used serological assays have a limit of antibody titer detection below which a negative result is yielded. Hence, a negative result does not necessarily imply an absence of antibodies, but rather that there is a dynamic process by which the production of antigen-targeted antibodies diminishes once infection has been resolved, resulting in decaying antibody titers over time. As antibody levels decrease below the limit of detection, seroreversion occurs.

We define the seroreversion rate as the inverse of the average time taken following seroconversion for antibody levels to decline below the cut-off point for testing seropositive. In a longitudinal follow-up study, antibodies remained detectable for at least 100 days(*126*). In another study (*132*), seroprevalence declined by 26% in approximately three months, which translates to an average time to seroreversion of around 200 days. However, this was not a cohort study, so newly admitted individuals could have seroconverted while others transitioned from positive to negative between rounds, leading to an overestimation of the time to seroreversion.

Intuitively, if serology were a true measure of past exposure, we would expect a continually increasing prevalence of seropositive individuals over time. However, data suggest this is not the case (*133*), with most regions in England showing a peak in seroprevalence at the end of May 2020. This suggests seroreversion plays a significant role in shaping the seroprevalence curves in England and that the time since the first epidemic peak will influence the extent to which subsequent seroprevalence measurements underestimate the underlying population attack size (proportion of the population exposed). We argue that the

number of people infected over the course of the epidemic can be informed by data triangulation, i.e., by combining numbers of deceased and seropositive individuals over time. For this linkage to be meaningful, we need to carefully consider the typical SARS-CoV-2 infection and recovery timeline (Figure 2-1).

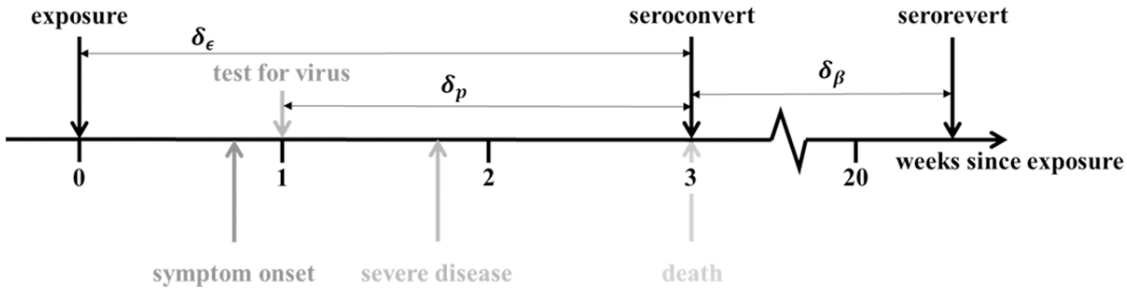

Figure 2-1. Progression of exposed individuals through the various clinical (below the timeline) and diagnostic (above the timeline) stages of infection and recovery.
Stages marked in grey represent events that may happen, with a probability consistent with the darkness of the shade of grey.

Most individuals, once infected, experience an incubation period of approximately 4.8 days (95% confidence interval (CI): 4.5–5.8) (*34*), followed by the development of symptoms, which include fever, dry cough, and fatigue, although some individuals will remain asymptomatic throughout. Symptomatic individuals may receive a diagnostic RT-PCR test at any time after symptom onset; the time lag between symptom onset and date of test varies by country and area, depending on local policies and testing capacity. Some individuals might, as their illness progresses, require hospitalization, oxygen therapy, or even intensive care, eventually either dying or recovering.

The day of symptom onset, as the first manifestation of infection, is a critical point for identifying when specific events occur relative to each other along the infection timeline. The mean time from symptom onset to death is estimated to be 17.8 days (95% credible interval (CrI): 16.9–19.2 days) and to hospital discharge 24.7 days (22.9–28.1 days) (*35*). The median seroconversion time for IgG (long-lasting antibodies thought to be indicators of prior exposure) is estimated to be 14 days post-symptom onset; the presence of antibodies

is detectable in less than 40% of patients within 1 week of symptom onset, rapidly increasing to 79.8% (IgG) at day 15 post-onset (*134*). We assume that onset of symptoms occurs at day 5 post-infection and that it takes an average of 2 additional days for people to have a RT-PCR test. Thus, we fix the time lag between exposure and seroconversion, δ_ϵ, at 21 days; the time lag between a RT-PCR test and death, δ_p ,at 14 days; and assume that seroconversion in individuals who survive occurs at approximately the same time as death for those who do not (Figure 2-1).

Thus, we propose to use population-level dynamics (changes in mortality and seroprevalence over time) to estimate three key quantities: the seroreversion rate, the IFR, and the total population exposure over time. We developed a Bayesian inference method to estimate said quantities, based on official epidemiological reports and a time series of serology data from blood donors in England, stratified by region (*133*) (see 2.3 Materials and Methods for more details). This dataset informed the national COVID-19 serological surveillance, and its data collection was synchronous with the 'REACT' study(*135*). The two serosurveys use different, but comparable, antibody diagnostic tests (*136*). While the 'REACT' study used the FORTRESS lateral flow immunoassay (LFIA) test for IgG (*129*), the data analyzed here were generated using the Euroimmun ELISA (IgG) assay (*46, 129*). The independent 'REACT' study acts as a validation dataset, lending credence to the seroprevalence values used. For example, seroprevalence in London was reported by 'REACT' to be 13.0% (95% CI: 12.3–13.6%) (*129*) for the period 20 June to 13 July 2020. In comparison, the London blood-donor time series indicated seroprevalence to be 13.3% (95% CI: 8.4–16%) (*137*) on 21 June 2020. Notably, the Abbott IgG antibody testing assay showed the most striking decline in sensitivity over time compared with other serological assays (*138, 139*), which limits comparisons across the two datasets as time progresses.

We developed a method that combines daily mortality data with seroprevalence in England, using a mechanistic mathematical model to infer the temporal trends of exposure and seroprevalence during the COVID-19 epidemic. We fit the mathematical model jointly to serological survey data from seven regions in England (London, North West, North East (North East and Yorkshire and the Humber regions), South East, South West, Midlands (East and West Midlands combined), and East of England) using a statistical observation model (see the 2.3 Materials and Methods section for more details on the input data sources, mechanistic model, and fitting procedure). We considered that mortality is perfectly reported and proceeded to use this anchoring variable to extrapolate the number of people infected 3-weeks prior. We achieved this by estimating region-specific IFRs (defined as γ_i), which we initially assumed to be time invariant, later relaxing this assumption. The identifiability of the IFR metric was guaranteed by using the serological data described above as a second source of information on exposure. From the moment of exposure, individuals seroconvert a fixed 21 days later and can then serorevert at a rate, β, that is estimated as a global parameter. We thus have both mortality and seropositivity prevalence informing SARS-CoV-2 exposure over time. Extending from the baseline model thus described, we conducted sensitivity analyses on key assumptions to evaluate the robustness of the results presented in the main paper. These sensitivity analyses explore how estimates for IFRs and seroreversion rates depend on assumptions around the timelines of infection/testing and the data sources used (see the sensitivity analysis subsection in the 2.3 Materials and Methods section for more details).

Several other research groups have used mortality data to extrapolate exposure and as a result provide estimates for IFR. Some IFR estimates have been published assuming serology cross-sectional prevalence to be a true reflection of population exposure, while others used infection numbers generated by mechanistic dynamic models fit to mortality

data (*140*). Most recently, sophisticated statistical techniques, which take into account the time lag between exposure and seroconversion, have been used to estimate the underlying population exposure from seroprevalence measurements (*141*), with some also considering seroreversion (*108, 110, 142, 143*). Our method is very much aligned with the latter studies but is applied at a regional level while using a dataset that has been validated by an independent, largely synchronous study (*137*) and uses test positivity data to help inform time-varying transmission intensity.

2.2 Data sources and availability

We used publicly available epidemiological data to infer the underlying exposure to SARS-CoV-2 over time, as described below. All data, code, and materials used in the analyses can be accessed at: https://github.com/SiyuChenOxf/COVID19SeroModel/tree/master. All parameter estimates and figures presented can be reproduced using the codes provided.

2.2.1 Regional daily deaths

The observed daily mortality data for each of seven English regions (London, North West, North East (contains both the North East and Yorkshire and the Humber regions), South East, South West, Midlands (East and West Midlands combined) and East of England), from 1 January 2020 to 11 November 2020, relate to daily deaths with COVID-19 on the death certificate by date of death. This information was extracted from the UK government's official COVID-9 online dashboard (*144*) on 8 March 2021. The age dependent regional death rate data used to compare spring and winter 2020 waves was extracted from the same source.

2.2.2 Regional adjusted seroprevalence

Region-specific SARS-CoV-2 antibody seroprevalence measurements, adjusted for the sensitivity and specificity (82.5% and 99.1%, respectively) of the Euroimmun antibody test,

were retrieved from the national COVID-19 surveillance reports produced by Public Health England (*133*).

2.2.3 Regional test-positivity ratios

Time series of region-specific RT-PCR test-positivity ratios were downloaded from the UK government's official dashboard (*144*) on 16 May 2021.

2.2.4 Regional population age structure and non-COVID epidemiological indices

Region-specific population structures were obtained from the UK Office for National Statistics 2018 population survey (*145*). Other demographic and epidemiological indicators such as number of care home beds and incidence of diabetes, e.g., were extracted from the PHE online database (*146*), using the search terms: 'care home'; 'diabetes'; 'pulmonary disease'; 'heart disease'.

2.3 Materials and Methods

2.3.1 Mechanistic model

We developed a mechanistic mathematical model that relates reported daily deaths from COVID-19 to seropositive status by assuming all COVID-19 deaths are reported and estimating an IFR that is congruent with the observed seroprevalence data. For each region, $i = 1, \ldots 7$, corresponding to London, North West, North East, South East, South West, Midlands and East of England respectively; we denote the IFR at time t by $\alpha_i(t)$ and the number of daily deaths by $m_i(t)$. While we formulate the model in terms of a general, time-dependent IFR, we assume its default shape to be time invariant and later allow IFR to vary with the stage of the epidemic.

Using the diagram in Figure 2-1 as a reference and given a number of observed deaths at time t, $m_i(t)$, we can expect a number of infections $\frac{1}{\alpha_i(t-d_i)} m_i(t-d_i)$ to have occurred d_ϵ days before. Of these infected individuals, $m_i(t)$ will eventually die, while the remaining $\frac{1-\alpha_i(t)}{\alpha_i(t)} m_i(t)$ will seroconvert from seronegative to seropositive. This assumes that seroconversion occurs, on average, with the same delay from the moment of infection as death.

Assuming that seropositive individuals convert to seronegative (serorevert) at a rate β, the rate of change in the number of seropositive individuals in region i, $X_i(t)$ is given by:

$$\frac{dX_i(t)}{dt} = \frac{1-\alpha_i(t)}{\alpha_i(t)} m_i(t) - \beta X_i(t) \tag{2.1}$$

Solving Equation (2.1), subject to the initial condition $X_i(t_0) = 0$, where t is time since 1 January 2020, gives:

$$X_i(t) = e^{-\beta t} \int_{t_0}^{t} e^{\beta w} \frac{\big(1-\alpha_i(w)\big)}{\alpha_i(w)} m_i(w) dw \tag{2.2}$$

Discretizing Equation (2.2) with daily intervals ($\Delta w = 1$) gives:

$$X_i(t) = e^{-\beta t} \sum_{w=t_0}^{t} \left[\frac{1-\alpha_i(w)}{\alpha_i(w)} e^{\beta w} m_i(w) \right] \tag{2.3}$$

The model-predicted proportion of seropositive individuals in each population, $x_i(t)$, is calculated by dividing $X_i(t)$ in Equation (2.3) by the respective region population size at time t, $P_i - \sum_{w=t_0}^{t} m_i(w)$, where P_i is the reported population in region i before the COVID-19 outbreak (*145*) :

$$x_i(t) = e^{-\beta t}\left[P_i - \sum_{w=t_0}^{t} m_i(w)\right]^{-1} \sum_{w=t_0}^{t}\left[\frac{1-\alpha_i(w)}{\alpha_i(w)} e^{\beta w} m_i(w)\right]$$

(2.4)

This is relatively straightforward when the serology data are already adjusted for test sensitivity and specificity, as is the case with the datasets used here. For unadjusted antibody test results, the proportion of the population that would test positive given the specificity (k_{sp}) and sensitivity (k_{se}) can be calculated as:

$$z_i(t) = k_{se} x_i(t) + \big(1 - k_{sp}\big)\big(1 - x_i(t)\big)$$

As mentioned earlier, the method that we present here allows for the IFR, $\alpha_i(t)$, to be (a) constant or (b) vary over time with the stage of the epidemic:

a) For a constant IFR, we have

$$\alpha_i(t) = \gamma_i$$

b) For a time-varying IFR, we first define the epidemic stage, $ES(t)$, as the normalized cumulative positivity ratio:

$$ES_i(t) = \frac{\sum_{w=t_0}^{t} y_i\big(w - \delta_p\big)}{\sum_{w=t_0}^{T} y_i\big(w - \delta_p\big)}$$

(2.5)

where $y_i(t)$ is the confirmed case positivity ratio at time *t* in the proportion of individuals testing positive for the virus, δ_p is the average time between testing positive and seroconversion (see Figure 2-1) and T is the total number of days from t_0 until the last date of positivity data. In this work, we fixed δ_p = 14 days (see Figure 2-1 and the main text). We assume that the IFR is a linear function of the normalized cumulative positivity ratio as follows:

$$\alpha_i(t) = \gamma_i\big(1 - \eta_i ES_i(t)\big)$$

(2.6)

where $\eta_i \in [0,1]$ and $\gamma_i \in [0,1]$ are coefficients to be estimated. At the start of the epidemic, when the epidemic stage is 0 (see Equation (2.5)), then $\alpha_i(t) = \gamma_i$, whereas when the epidemic stage is 1, $\alpha_i(t) = \gamma_i - \eta_i \times \gamma_i \leq \gamma_i$.

In Equation (2.5), $y_i(t)$ is taken from the daily regional positivity ratios provided in the UK government's data dashboard (*144*).

Once the model is parameterized, we can estimate the total proportion of the population that has been exposed, E_i, using the following formula:

$$E_i(t - \delta_\epsilon) = \left[P_i - \sum_{w=t_0}^{t} m(w)\right]^{-1} \sum_{w=t_0}^{t} \frac{1 - \alpha_i(t)}{\alpha_i(t)} m_i(w) \tag{2.7}$$

where δ_ϵ is fixed to 21 days (Figure 2-1)

2.3.2 Observation model for statistical estimation of model parameters

We developed a Bayesian model to estimate the model parameters θ and present the posterior predictive distribution of the seroprevalence in Equation (2.4) and exposure in Equation (2.7) over time. The results are presented as the median of the posterior with the associated 95% credible intervals (CrI). We assumed a negative binomial distribution (*147*) for the observed number of seropositive individuals in region i over time, $X_i^{obs}(t)$:

$$X_i^{obs}(t) = x_i^{obs}(t) \times \left(P_i - \sum_{w=t_0}^{t} m_i(w)\right) \tag{2.8}$$

where $x_i^{obs}(t)$ is the observed seroprevalence in region i over time. Then, the observational model is specified for region i with observations at times $t_{i1}, t_{i2}, \ldots, t_{in_i}$:

$$X_i^{obs}(t) \sim NB(X_i(t), \phi), t = t_{i1}, \ldots, t_{in_i} \tag{2.9}$$

where $NB(X_i(t), \phi)$ is a negative binomial distribution, with mean $X_i(t)$ –given by Equation (2.3)–and ϕ is an overdispersion parameter. We set ϕ to 100 to capture additional uncertainty in data points that would not be captured with a Poisson or binomial distribution. We assume uninformative beta priors for each of the parameters, according to the assumption made for how the IFR is allowed to vary over time:

a) For a constant IFR, we have $\theta = \{\{\gamma_i\}_{i=1}^{7}, \beta\}$ and take priors:

$$\gamma_i \sim beta(1,1), \beta \sim beta(1,1) \tag{2.10}$$

b) For a time-varying IFR, we have $\theta = \{\{\gamma_i\}_{i=1}^{7}, \{\eta_i\}_{i=1}^{7}, \beta\}$ and take priors:

$$\gamma_i \sim beta(1,1), \eta_i \sim beta(1,1), \beta\ (1,1) \tag{2.11}$$

We use Bayesian inference (Hamiltonian Monte Carlo algorithm) in RStan (*117*) to fit the model to seroprevalence data by running four chains of 20,000 iterations each (burn-in of 10,000). We use 2.5% and 97.5% percentiles from the resulting posterior distributions for 95% CrI for the parameters. The Gelman–Rubin diagnostics ($\hat{R}$) given in Appendix Table 1 and Appendix Table 2 show values of 1, indicating that there is no evidence of non-convergence for either model formulation. Furthermore, the effective sample sizes (n_{eff}) in Appendix Table 1 and Appendix Table 2 are all more than 10,000, meaning that there are many samples in the posterior that can be considered independent draws.

2.3.3 Sensitivity analyses

The results in the main text explore two model formulations: one that assumes IFR is constant over time and another that relaxes that assumption. These models share several underlying assumptions, particularly relating to time delays between events in the life history of infection, prior distributions, and data sources. To ascertain the robustness of our main results, we estimated the relevant parameters using a series of different models as listed in Appendix Table 4. Essentially, we explore how our estimates change as we:

- assume different values for the delay between testing RT-PCR positive and death, δ_p, and for the delay between infection and death, δ_ϵ.
- use a different prior distribution for seroreversion rate.
- use a different set of mortality data. These are sourced from the same official database (*144*) but obey different criteria. The main results were generated using a dataset of death certificates with COVID-19 named as the cause of death, but we also apply our method to the 'Deaths within 28 days of a positive test' dataset.

The parameter estimates for the different models considered are summarized in Appendix Table 5. Note that parameter δ_p does not appear in Equation (2.1), thus, estimates using the constant IFR model are only sensitive to changes in δ_ϵ (Appendix Figure 8). Interestingly, the time-varying IFR model is relatively insensitive to δ_p (Appendix Figure 16) since changes in δ_p have a limited impact on the shape of the Epidemic Stage (ES) curve and consequently IFR over time (Appendix Figure 17).

2.3.4 Relationship between demographic and epidemiological factors and estimated regional IFRs

Our estimates for regional IFRs were noticeably lower for London and higher for the North East, South East and South West. Since treatment outcomes are identical across regions (*148*), we explored which demographic and epidemiological factors could help interpret our

results (Appendix Table 6). Our objective here was not to build the most accurate predictive regression model (as this is beyond the scope of this paper), but rather to explore a multitude of covariates which might display a statistically significant correlation with the obtained IFR trends. We thus built several linear regression models with a single covariate using regional estimates (Model 2 in Appendix Table 4) for IFR as the dependent variable, which are summarized in Appendix Table 6. Linear regression models exploring relationships between demographic and epidemiological factors and estimated regional IFRs. Each row refers to a unique linear regression model and indicates which covariate was used, alongside the resulting slope and intercept estimates (with accompanying 95% CIs) and p-value. The independent variables explored were:

- Proportion of the population over a certain age breakpoint (40 to 75 years of age in 5-year intervals). We only show the results for the two most significant age breakpoints, 45 and 60.
- Deaths in the community relative to deaths in care homes.
- Care home beds per 100 people over 75 years of age.
- Diabetes prevalence.
- Chronic liver disease mortality rate (per 100,000).
- Chronic obstructive pulmonary disease mortality rate (per 100,000).

2.4 Results

2.4.1 Time-independent IFR model results

Results from the fixed IFR inference method show excellent agreement with serological data (Figure 2-2). We found that, after seroconverting, infected individuals remain seropositive for about 176 days on average (95% CrI: 159–197 days) (Table 2-1, Appendix Table 1 and Appendix Figure 1). This relatively rapid (approximately six months) seroreversion is

similar to estimates from experimental studies (*130, 131, 139, 149, 150*), and the choice of an exponential distribution for seroreversion seems to be validated by long follow-up longitudinal studies showing antibody persistence up to 1 year (*139, 150, 151*), with 59% (95% CrI: 50–68%) of seropositive individuals seroreverting after 52 weeks (Appendix Figure 2). These seroreversion rates are also broadly consistent with the observation of 83% protection against reinfection within 6 months of disease in UK patients (*87*).

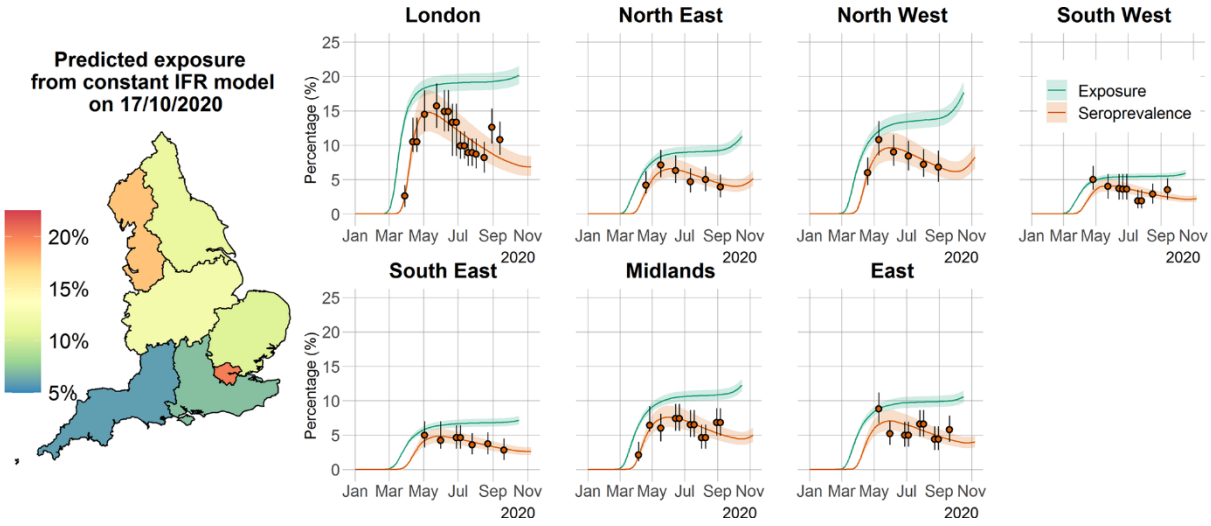

Figure 2-2. Time course of the SARS-CoV-2 pandemic up to 7 November 2020 for the seven regions in England in the constant IFR model.
The solid orange circles and black error bars in each regional panel represent the observed seroprevalence data and their credible intervals, respectively, after adjusting for the sensitivity and specificity of the antibody test. The green and orange lines show the model predictions of median exposure and seroprevalence, respectively, while the shaded areas correspond to the 95% CrI. The regional predicted exposure levels (expressed as the proportion of the population that has been infected) as of 17 October 2020 are shown on the map of England.

As a consequence of this rapid seroreversion, epidemic progression will result in an increasing gap between measured serology prevalence levels and cumulative population exposure to the virus. Ultimately, this may mean that more than twice as many people have been exposed to the virus relative to the number of people who are seropositive (Figure 2-2), highlighting the importance of our method in aiding interpretation of serological survey results and their use for informing policy decisions moving forward. Seroreversion is responsible for decreased seropositivity over periods of continued transmission (as

evidenced by mortality and case data) and thus why we had to resort to mortality data to inform the true exposure of populations to SARS-CoV-2. This is made clear by comparing the shapes of the regional cumulative death curves (Appendix Figure 3) with those of the estimated cumulative total exposure (Figure 2-2).

Table 2-1. Marginal median parameter estimates and 95% CrI for the constant IFR model.
β is the rate of seroreversion and γ denotes the IFR. The estimated median time to seroreversion given by $1/\beta$ is 176 (95% CrI: 159–197 days).

Parameter	*Median (95% CrI)*
β	0.0057(0.0051-0.0063)
γ_{London}	0.0049(0.0046-0.0063)
$\gamma_{NorthEast}$	0.0080(0.0073-0.0087)
$\gamma_{SouthEast}$	0.0103(0.0095-0.0112)
$\gamma_{NorthWest}$	0.0094(0.0087-0.0101)
$\gamma_{SouthWest}$	0.0118(0.0109-0.0129)
$\gamma_{Midlands}$	0.0085(0.0079-0.0091)
γ_{East}	0.0083(0.0077-0.0090)

We also estimated age-independent IFRs for the seven English regions (means ranging from 0.49% to 1.18%; Table 2-1) that are in very good agreement with other estimates for England (*152*). The estimated IFRs were noticeably lower for London and higher for the North East, South East and South West, indicating a clear signal for a lower probability of death per infection in London. Given there are no significant disparities in treatment outcomes across regions (*148*), we explored several demographic and epidemiological factors that could explain the observed trend (Appendix Figure 4). There is a strong positive correlation between the proportion of the population over the age of 45 years (when disease and mortality risk start to increase significantly) and the estimated IFR. Interestingly, not only is the population in London younger but there is also a lower proportion of the population

comprising elderly people living in care homes, which may explain the proportionally lower contribution of care-home deaths to the overall mortality in London. This covariate appears to explain more than 75% of the variance observed in estimated IFRs across regions (Appendix Table 4 (B)). Note that other mortality risk factors, such as diabetes and pulmonary and liver disease, seem to have no correlation with estimated IFR at all (Appendix Table 6).

2.4.2 Time-varying IFR model results

An alternative formulation of our modelling approach allows IFR to vary over time according to the stage of epidemic progression, i.e., allowing for IFR to potentially decrease as the population gains immunity, shielding of vulnerable people is optimized and patient treatment is improved. Unfortunately, it is extremely difficult to extrapolate the underlying risk of infection (a proxy for epidemic progression) from reported case data due to the volatility in testing capacity. Hence, we propose that the optimal metric for epidemic progression is the cumulative test positivity ratio. In the absence of severe sampling biases, the test positivity ratio is a good indicator of changes in underlying population infection risk, as a larger proportion of people will test positive if infection prevalence increases. In fact, it is clear from Appendix Figure 5(D) that the test positivity ratio is a much better indicator of exposure than the case fatality ratio (CFR) or the hospitalization fatality ratio (HFR), as it mirrors the shape of the mortality incidence curve Appendix Figure 5(B). For the time-varying IFR, we took the normalized cumulative test positivity ratio time-series and applied it as a scalar of the maximum IFR value estimated for each region (more details can be found in the 2.3 Materials and Methods section).

The results from the time-varying IFR model are consistent with the results from the constant IFR model and in very good agreement with serological data (Figure 2-3). The mean seroreversion rate in this model was estimated to be 162 days (95% CrI: 148–186 days), a

5.5–6.9% difference compared with the constant IFR model, meaning that the estimation for the seroreversion rate was robust to the assumption of the shape of the IFR. Critically, predictions for cumulative exposure in the population are very robust to the assumption of the shape of IFR, with both models forecasting the same levels of overall exposure (comparing Figure 2-2 and Figure 2-3). Estimates for the time-varying IFR model (Appendix Table 3 and Appendix Figure 6 and Appendix Figure 7) suggest a slight decrease in IFR from March to November 2020 in several regions of England; this was most significant in London.

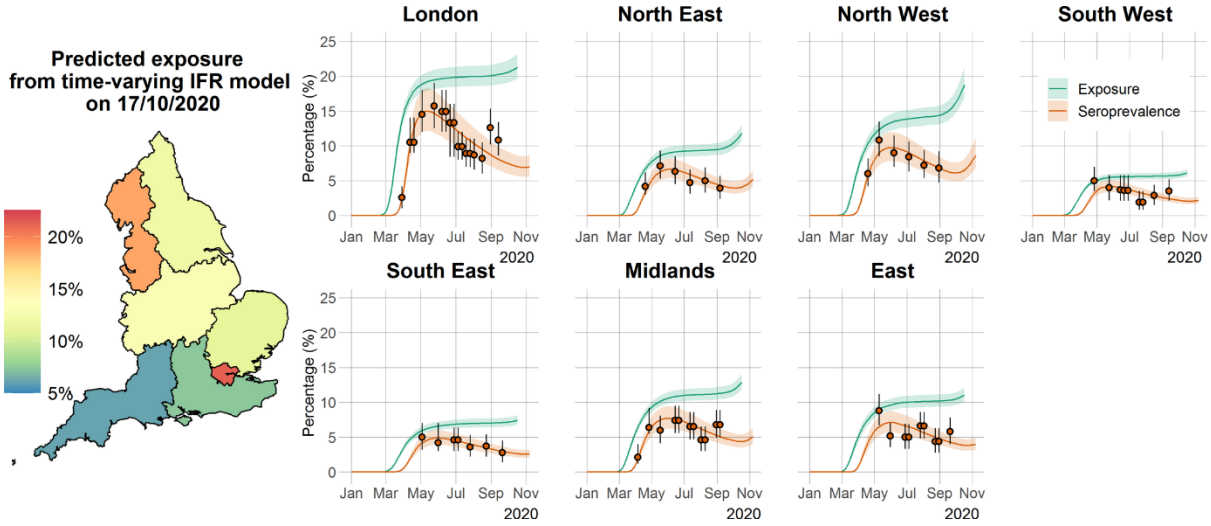

Figure 2-3. Time course of the SARS-CoV-2 pandemic up to 7 November 2020 for the seven regions in England in the time-varying IFR model.
The orange solid circles and black error bars in each regional panel represent the observed seroprevalence data and their credible intervals after adjusting for the sensitivity and specificity of the antibody test. The green and orange lines show the median time-varying IFR model predictions for exposure and seroprevalence, respectively, while the shaded areas correspond to the 95% CrI. The regional median predicted exposure levels (expressed as the proportion of the population that has been infected) as of 17 October 2020 are shown on the map of England.

The methodology for estimating the cumulative exposure in the population proposed in this paper rests on several key assumptions that might be violated in practice, the first of which is the assumption of fixed delays in the infection time history as depicted in Figure 2-1. This is admittedly a simplification of delay-distribution approaches used elsewhere but, as

determined by our sensitivity analysis, has no significant implications for the estimates of IFR and seroreversion rates for either the constant IFR model or the time-varying IFR model (Appendix Figure 8 and Appendix Figure 9). Indeed, relaxing the fixed delays assumption would only result in a shift in predicted exposure during the very early stages of the pandemic. Second, our methodology relies on mortality data to infer the true shape of the cumulative exposure curve. The official English government data dashboard provides two mortality datasets: 'Deaths with COVID-19 on the death certificate' and 'Deaths within 28 days of positive test' by date of death (*144*). We opted for the former as the default source of mortality data used, because the latter dataset significantly underestimates COVID-19-associated deaths at the beginning of the pandemic, at a time when transmission was very high and RT-PCR testing capacity was at its lowest (Appendix Figure 10). Note that once testing capacity reached the tens of thousands of tests per day, the two mortality data streams report essentially the same figures. If we use 'Deaths within 28 days of positive test by date of death' as a model input, we obtain a seroreversion rate that is 8.8–12.8% shorter, along with 16–32% lower regional IFRs (Appendix Figure 11 and Appendix Figure 12). This is an expected consequence of having the model fit to the same serology data, while assuming there were 17,000 fewer deaths during the spring 2020 epidemic wave. More importantly, the cumulative exposure predictions are extremely robust to the explored mortality inputs (Appendix Figure 13 and Appendix Figure 14).

2.5 Discussion

Given the current polarization of opinion around COVID-19 natural immunity, we realize that our results are likely to be interpreted in one of two conflicting ways: (1) the rate of seroreversion is high, therefore achieving population (herd) immunity is unrealistic, or (2) exposure in more affected geographical areas, such as London, is much higher than previously thought, and population immunity has almost been reached, which explains the

decrease in IFR over time. We would like to dispel both interpretations and stress that our results do not directly support either. Regarding (1), it is important to note that the rate of decline in neutralizing antibodies, reflective of the effective immunity of the individual, is not the same as the rate of decline in seroprevalence. Antibodies may visibly decline in individuals yet remain above the detection threshold for antibody testing (*126*). Conversely, if the threshold antibody titer above which a person is considered immune is greater than the diagnostic test detection limit, individuals might test positive when in fact they are not effectively immune. The relationship between the presence and magnitude of antibodies (and therefore seropositive status) and protective immunity is still unclear, with antibodies that provide functional immunity only now being discovered (*130*). Furthermore, T cell-mediated immunity is detectable in seronegative individuals and is associated with protection against disease (*61*). Therefore, the immunity profile for COVID-19 goes beyond the presence of a detectable humoral response. We believe our methodology to estimate total exposure levels in England offers valuable insights and a solid evaluation metric to inform future health policies (including vaccination) that aim to disrupt transmission. With respect to (2), we must clarify that decreasing IFR trends can result from a combination of population immunity, improvement in patient treatment, better shielding of those at highest risk, and selection processes operating at the intersection of individual frailty and population age structure. We can eliminate exposure levels as the main driver of this process as there is no clear temporal signal for IFR for regions other than London. This is confirmed by data on age-dependent mortality rates at different stages of the epidemic, which show that mortality rates in London have decreased substantially since the first spring wave, much more so than in other regions (Appendix Figure 15).

As no significant disparities in treatment outcomes across regions were found (*148*), an alternative interpretation of IFR trends in England is that individuals who are more likely to

die from infection (due to some underlying illness, being in a care home, being over a certain age or any other risk factors) will do so earlier. This means that as the epidemic progresses, selection (through infection) for a decrease in average population frailty (a measure of death likelihood once infected) is taking place and, consequently, a reduction in the ratio of deaths to infections. The lower estimated IFR for London can be attributed to the city's relatively younger population and lower rates of elderly persons in care homes when compared with populations in the other regions of England (Appendix Figure 4, top right panel), indicating that if this selection process does exist it will be more pronounced in younger populations with a smaller subset of very frail individuals.

We should mention some details that potentially limit the applicability of the methodology presented here to other countries, especially low- and middle-income countries (LMICs). The most pertinent detail is one of data quality. Whereas our assumption that COVID-19 deaths are nearly perfectly reported in England is a plausible one, this is very unlikely to hold for other countries across the globe (*153*). To account for potential under-reporting, we could include a constant or time-varying reporting ratio to transform reported deaths into 'likely' deaths. The direct consequence of using predicted deaths as a model input would be that any IFR estimates would be very difficult to disentangle from the underlying reporting ratio. The quality of the seroprevalence data itself is paramount, and the data collection protocol can have a major influence on the obtained estimates, as evidenced by two concurrent seroprevalence studies conducted in Manaus, Brazil. Whereas one study reports a raw seroprevalence of approximately 40% (*154*) using the Abbot test, the other reports an antibody positivity of approximately 13% (*155*) using the WONDFO SARS-CoV-2 antibody test, with both measured in May 2020. A significant difference is that the former study used blood donor samples, whereas the latter relates to household surveys. Another issue that is likely to be relevant to many LMICs is that the provision of a reliable level of

uncertainty around the seroreversion estimate relies on having several sequential seroprevalence measurements. In countries with a very limited capacity for conducting serosurveys, we suggest using the posterior distribution for seroreversion provided here as an informative prior and proceed to estimate infection fatality ratios and total exposure profiles. However, we should note that the thresholds of seropositive and seronegative assignment vary across assays, hindering the applicability of estimates resulting from data generated with a specific assay to other settings where different assays might be used. Through its structure, the model assumes that all infections result in in seroconversion. If this is not the case, then this approach would underestimate exposure. One study used a different method and where large levels of exposure had been inferred from the model structure using mortality data (*156*).

In conclusion, we propose a new method to forecast the total exposure to SARS-CoV-2 from seroprevalence data that accounts for seroreversion and uses daily mortality and test positivity ratio data to aid inference. The associated estimate of time to seroreversion of 176 days (95% CrI: 159–197 days) lies within realistic limits derived from independent sources (*130, 131, 139, 149, 150*). The total exposure in regions of England estimated using this method is more than double the latest seroprevalence measurements. Implications for the impact of vaccination and other future interventions depend on the, as yet uncharacterized, relationships between exposure to the virus, seroprevalence, and population immunity. To assess vaccination population impact, one can consider the population at risk to be those individuals who are seronegative, those with no past exposure (confirmed or predicted), or those with no T-cell reactivity. Here, we offer an extra dimension to the evidence base for immediate decision-making, as well as anticipating future information from the immunological research community about the relationship between SARS-CoV-2 exposure and immunity.

Chapter 3 Data integration to estimate exposure to SARS-CoV-2 in data-scarce scenarios – at the beginning of the pandemic in England

I have published the research underlying this chapter as first author on MedRxiv (*119*): Siyu Chen, Jennifer A Flegg, Katrina A Lythgoe, Lisa J White. (2023). Reconstructing the first COVID-19 pandemic wave with minimal data in the UK. *medRxiv*: 2023-03. https://www.medrxiv.org/content/10.1101/2023.03.17.23287140v2

In this chapter, I aim to describe how the model developed in Chapter 2 (termed 'exposure model' below) can be useful to accommodate the uncertainty of limited epidemiological information at early times and how it can be validated by a large-scale population level infection survey when it is available. To approach that, I re-examined and evaluated the exposure model in the context of reconstructing the first COVID-19 epidemic wave in England from three perspectives: validation from ONS Coronavirus Infection Survey, relationship between model performance and data abundance and time-varying case detection rate. The results showed that our exposure model can recover the first but unobserved epidemic wave of COVID-19 in England from March 2020 to June 2020 as long as two or three serological measurements are given as additional model inputs, with the second wave during winter of 2020 validated by the estimates from ONS Coronavirus Infection Survey. Moreover, our exposure model estimated that by the end of October in 2020 the UK government's official COVID-9 online dashboard reported COVID-19 cases only accounted for 9.1% (95%CrI (8.7%,9.8%)) of cumulative exposure, dramatically varying across two epidemic waves in England in 2020 (4.3% (95%CrI (4.1%, 4.6%)) vs 43.7% (95%CrI (40.7%, 47.3%))).

3.1 Introduction

The COVID-19 pandemic has inflicted devastating effects on global populations and economies(*157, 158*) and is now still affecting countries in many different ways. Reviewing the challenges posted by the COVID-19 pandemic and evaluating previous responses is vitally important for future pandemic preparedness (*93, 159-161*). Accurate estimation of exposure remains crucial for understanding the dynamics of disease transmission and assessing the impacts of interventions during the different stages of the pandemic. However, this was particularly challenging in the early phase since most of the characteristics of the pathogen were unknown and at the same time epidemiological data were sparse.

Confirmed COVID-19 cases were typically the first type of data to be collected and reported mostly due to the syndrome surveillance systems (*162, 163*). However, this underestimates the true exposure in the population because of the limited capacity of diagnoses, the lack of clear definition of cases, testing criteria, etc. Large-scale viral infection surveys in the community can help to solve the testing issue. For example, the UK Office for National Statistics (ONS) conducted a nation-wide COVID-19 viral testing survey, namely Coronavirus Infection Survey (CIS) (*164*) that has successfully tracked the trajectories of COVID-19 infections in the UK community since April of 2020. Because of its representative sampling across households in the general population this study is recognised to have a strong power to capture asymptomatic infections which might be missed out by symptomatic testing scheme in the early pandemic and can provide reliable estimates of prevalence over time (*106*). However, this study started collecting samples from April of 2020 and reporting the estimates of daily incidence from May of 2020 while the first death due to COVID-19 disease in the UK was documented in February 2020 (*144*). This implies that the transmission of COVID-19 in the community began earlier than the survey, and the survey might not be able to recover the early epidemic curve.

Serologic studies that measure how many people have antibodies against the virus are a promising tool for pinning down the stage of the pandemic because of its ability of capturing past infections regardless of clinical symptoms (*165*). If the antibody elicited by the virus lasts for lifetime, representative sampling in a population followed by the antibody testing will provide robust estimates of exposure. However, cohort studies following individuals over time after they've had a known COVID-19 infection were able to determine that antibodies are only measurable up to 6–9 months (*51, 90, 166*), on average, varying across testing assay (*167*) and antigen types (*58*). The immediate implication is that serological studies will inevitably under-estimate the number of people exposed, since some will have a lower antibody count when the study is conducted and test negative. Linking multiple publicly available datasets, I proposed a method that I published previously (*36*) and is described in Chapter 2 (termed 'exposure model' below) to estimate the true level of exposure after considering antibody decay. Here I further examined and evaluated the exposure model in the context of reconstructing the first COVID-19 pandemic in England from three perspectives: validation from the ONS Coronavirus Infection Survey (Section 3.4.2), the relationship between model performance and data abundance (Section 3.4.3) and time-varying case detection rate (Section 3.4.4).

3.2 Data sources and availability

I used publicly available epidemiological data to conduct the analysis, as described below. All codes and materials used in the analyses can be accessed at: https://github.com/SiyuChenOxf/Exposure_ONS-modelling. All parameter estimates and figures presented can be reproduced using the code provided.

3.2.1 ONS estimated incidence

The Office for National Statistics (ONS) launched the Coronavirus (COVID-19) Infection Survey in England on 26 April 2020 to estimate how many people across England, Wales, Northern Ireland and Scotland would have tested positive for COVID-19 infection, regardless of whether they report experiencing symptoms as one of the primary goals of the survey. The survey was based on a random sample of households to provide a nationally representative survey. Everyone aged 2 years and over in each household sample was asked to take a nose and throat swab for SARS-CoV-2, which was tested using the reverse transcriptase polymerase chain reaction (RT-PCR). Every participant was swabbed once. they were then invited to have repeat tests every week for another four weeks and then monthly. More descriptions about the survey design can be found in (*164*). Using Bayesian multilevel generalised additive regression models to model the swab test results (positive or negative) as a function of age, sex, time, and region, the study estimated community prevalence of SARS-CoV-2 in England since April 2020 (*164*). Combining the estimates of community prevalence and estimates of duration of RT-PCR testing positivity, the survey modelling team also published the estimates of daily incidence based on a deconvolution model (*168*).

To conduct the comparison of estimates of incidence from our exposure model (*36*) and ONS Coronavirus Infection Survey, we first retrieved the SARS-CoV-2 daily incidence in England in 2020 from the Office for National Statistics (ONS) (*106*) on 17 March 2023.

3.2.2 Model estimated exposure

Cumulative exposure to SARS-CoV-2 in seven regions of England estimated by our exposure model were obtained from (*36*). Here, we transformed the cumulative exposure to daily incidence in different regions of England using Equation (3.1) and then aggregated to the total daily incidence in the whole England using Equation (3.2).

3.2.3 7-day average of reported COVID-19 cases in England

7-day average of reported COVID-19 daily cases in England in 2020 were retrieved from the UK government's official COVID-9 online dashboard (*144*) on 17 March 2023.

3.3 Materials and Methods

3.3.1 Model predicted incidence

The incidence of COVID-19 in the whole England estimated by our exposure model (*36*) was calculated by computing the difference of cumulative exposure in two successive days by region and adding together over all England:

$$I_i(t) = E_i(t+1) - E_i(t), t = 1,2, \dots, n, i = 1,2, \dots, 7 \tag{3.1}$$

$$I_{England}(t) = \sum_{i=1}^{7} I_i(t) \tag{3.2}$$

Here, $E_i(t)$ is the daily exposure at region i estimated by our exposure model (*36*), n is the total number of days from 1 January 2020 to 7 November 2020, $i = 1, \dots 7$ represents London, Southwest, Southeast, Northeast, Northwest, East, Midland. $I_{England}(t)$ represents the total daily incidence of COVID-19 in England.

The 7-day average model-predicted incidence as shown by the green lines in Figure 3-1 and Figure 3-3 was given by

$$\bar{I}_{England}(t) = \frac{1}{7} \sum_{i=t-3}^{t+3} I_{England}(i), \qquad t = 4, 5, \dots, n-4 \tag{3.3}$$

Here, $t = 4$ refers to the fourth day of 2020, n is the end date of the comparison exercise, 7 November 2020.

3.3.2 Case detection ratio

The estimated case detection ratio as shown by the bottom figure of Figure 3-3 was calculated by

$$r(t) = \frac{\bar{I}_{England}(t)}{C(t)} \tag{3.4}$$

Here, C is the 7-day average of reported cases in England from the UK government's official COVID-9 online dashboard (*144*).

While examining the relationship between model performance and data abundance as shown in Figure 3-2, we first obtained all the data and codes from our exposure model (*36*) and reran the model by adding the seroprevalence measurements one-by-one into the model.

3.4 Results

3.4.1 Reconstruction of the early epidemic

In Chapter 2, I presented a simple model to link together three key metrics for evaluating the progress of an epidemic applied to the context of SARS-CoV-2 in England: antibody seropositivity, infection incidence and number of deaths. We use these three metrics to estimate the antibody seroreversion rate and region-specific infection fatality ratios. In doing so, the cumulative number of infections in England are estimated, showing that cross-sectional seroprevalence data underestimate the true extent of the SARS-CoV-2 epidemic in England in the early pandemic. Estimates for the IgG (spike) seroreversion rate and IFR are broadly consistent with other studies, which supports the validity of these findings.

The model was set up based on the important observation about the COVID-19 infection timeline that seroconversion in individuals who survive occurs at approximately the same time as death for those who do not. Therefore, a simple ordinary differential equation (ODE) was formulated to model the rate of change in the number of seropositive individuals in different regions of England. This rate will increase as new infections are generated as calculated by the daily number of deaths divided by infection fatality ratio and will decrease as antibody decays. The model-predicted proportion of seropositive population is fitted to observed seroprevalence using a Bayesian observation model. More details can be found in Chapter 2.

3.4.2 Validation from ONS Coronavirus Infection Survey

Comparing the incidence of SARS-CoV-2 in England estimated by our exposure model (*36*) with that inferred by the ONS Coronavirus Infection Survey (Figure 3-1), we found that our model could reveal the first but unobserved epidemic wave of COVID-19 in England from March 2020 to June 2020 as well as the second wave validated by the estimates from ONS Coronavirus Infection Survey. Further, we found our model results were highly consistent with those using SEIRS type compartmental models with time-varying force of infection (*99, 169*).

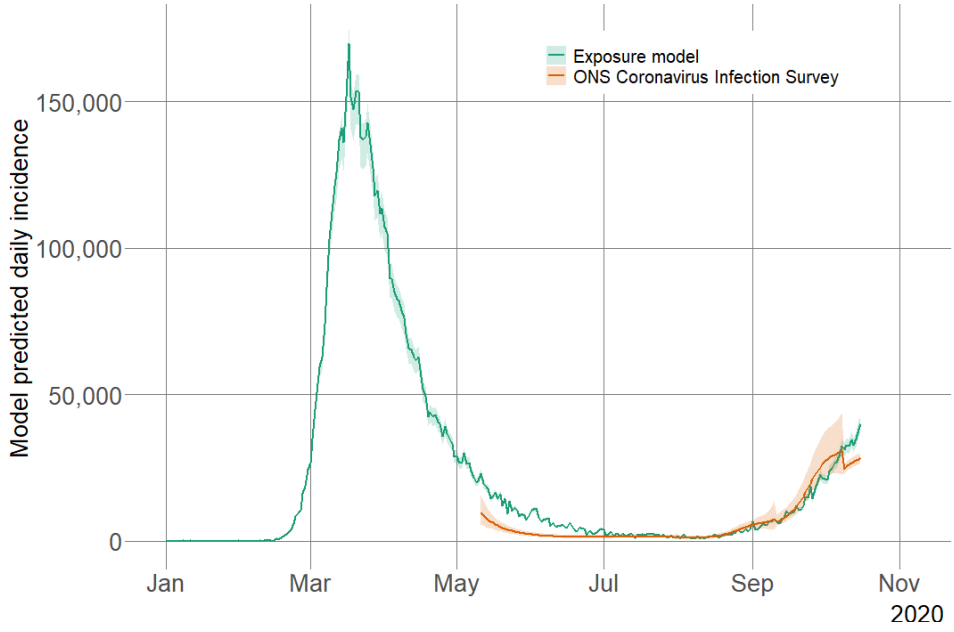

Figure 3-1. Comparison of model predicted daily incidence of SARS-CoV-2 in England.
The green lines show the predictions of median daily incidence from our model (*36*) based on Equation (3.1) - Equation (3.3). The orange lines show the predictions of median daily incidence from the ONS Coronavirus Infection Survey while the orange shaded areas correspond to the 95% CrI.

3.4.3 Relationship between model performance and data abundance

We then examined the relationship between model performance and data abundance - how estimates of exposure from our exposure model change with more serological data points being added into the fitting procedure one-by-one over time (Figure 3-2). We found that, in general, a highly robust pattern of exposure across different regions of England was estimated. Specifically, the model could only estimate the quantities of interest: exposure and the two parameters (infection fatality ratio and antibody decaying rate) when at least two serological measurements from April to June 2020 in each region were given as inputs. However, these estimates were already highly consistent with those when more serological measurements were added although the credible bands were wider. The wide credible bands indicate a larger uncertainty around the estimates when little information was available. When three serological measurements in each of region were included, the estimates of exposure level became largely consistent with the results of using all the serological

measurements. This might be attributed to the timing of these third serological measurements since by then the seroprevalence in most regions started decreasing. With the addition of more and more serological measurements, the credible bands of estimates of exposure gradually narrowed.


n=2 London
n=3 London
n=4 London
n=5 London
n=6 London
n=7 London
South East
North West
South West
Midlands
North East
East
Exposure
Seroprevalence
Percentage (%)
0
5
10
15
20
25
30
Jan Mar May Jul Sep Nov

Figure 3-2. Comparison of estimates of exposure in seven regions of England in 2020 as more serological measurements are included in the model inputs (left to right).
The green and orange lines show the model predictions of median exposure and seroprevalence, respectively, while the shaded areas correspond to the 95% CrI.

3.4.4 Time-varying case detection rate

When comparing the reported cases with the incidence estimated by our exposure model (Figure 3-3), we found the UK government's official COVID-9 online dashboard (*144*) reported COVID-19 cases in England only accounted for 9.1% (95%CrI (8.7%,9.8%)) of cumulative exposure by the end of October 2020. Further, the relative sizes of the two infection waves in England in 2020 estimated by our exposure model, the Spring wave from February to June and the Autumn wave from September to November, were reversed compared to those reported as confirmed cases.

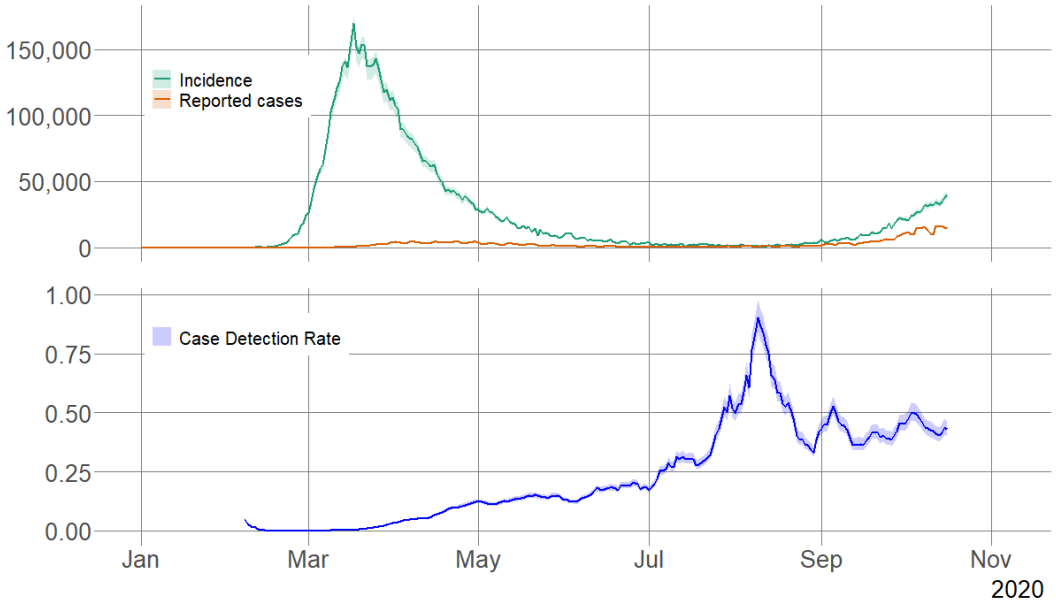

Figure 3-3. Comparison between estimates of daily incidence with reported cases of SARS-CoV-2 in England and case detection rate that is defined as the ratio between reported cases and inferred underlying incidence.

Here, all serological measurements were used in the model fitting to generate the green lines. In the top figure, the green lines show the predictions of median daily incidence by our exposure model based on Equation (3.1) - Equation (3.3) while the shaded areas correspond to the 95% CrI. The orange lines show the reported confirmed cases in England downloaded

from GUV.UK dashboard. In the bottom figure, the blue lines show the estimates of median case reporting rate in England based on Equation (3.4) while the shared areas correspond to the 95% CrI.

The case detection rate relative to the total exposure was also dramatically different in these two-epidemic waves. In separating the two waves at the first of August 2020, we found during January 2020 to August 2020 the case detection rate was only 4.3% (95%CrI (4.1%, 4.6%)) which increased to 43.7% (95%CrI (40.7%, 47.3%)) during August 2020 to October 2020, highlighting the dominant effect of testing effort in shaping the case curve in the early stage of a pandemic. The testing issue, e.g. the limited capacity of tests and symptom-based testing strategy posed a big challenge for understanding the early pandemic. Viral surveys in the general population can solve the sampling issue, but still have the problem of not sampling early on. Serological data, even from some convenient samples, e.g., blood donors, can help to pin down the progress of the pandemic when antibody decay is teased out.

3.5 Discussion

Accurate reconstruction of exposure time series is necessary to assess how policies influenced transmission over time, in particular when reporting is lagged, and multiple interventions may have been undertaken in succession. For example, (*121*) made use of the comparison of exposure between general population and pregnant women in New York City to conclude the effectiveness of shielding during pregnancy. Moreover, the prior exposure level in the population can be used to inform future intervention design, e.g., vaccination prioritisation. For example, in the early stage of the COVID-19 vaccination campaign, when dose supply and administrative capacity were initially limited worldwide, a modelling study (*6*) explored how uncertainty about previous exposure levels and about a vaccine's characteristics affects the prioritization strategies for reducing deaths and transmission. This

model showed that the use of individual-level serological tests to redirect doses to seronegative individuals improved the marginal impact of each dose while potentially reducing existing inequities in COVID-19 impact.

Here, we evaluated a simple dynamical model that we published previously and demonstrated its ability to reconstruct the first epidemic wave in England before large-scale survey sampling by providing robust estimates of exposure over time. One key element of the model was fitting it to serologic data that was generated from healthy adult blood donors supplied by the NHS Blood and Transplant (NHS BT collection) serum samples using the Euroimmun anti-spike IgG assay and reported in the Weekly national Influenza and COVID-19 surveillance report. This suggests that convenient samples, such as serum samples from blood donors, have the promising power to provide primary information of epidemic progress in a short timeframe especially during the emergency of a new outbreak from a novel pathogen.

It is also important to understand the limitations of the blood donor data. For example, testing samples were provided by healthy adult blood donors aged 17 years and older, supplied by the NHS Blood and Transplant (NHS BT collection); this might mean that the seroprevalence cannot well represent the exposure level among young people who are below 17 years and some individuals who are not eligible for blood donation. Since week 26 (June 22, 2020), an exclusion of donors aged 70 years and older donating throughout lockdown was lifted, and therefore data from recent sampling periods include donors in this older age group; this mean that before June 22, 2020 the seroprevalence data might not represent the true exposure level among people who are 70 years old and older.

Because of the rigorous sampling design and robust estimation power, the ONS Coronavirus Infection Survey can almost be seen as the gold standard for estimating community prevalence. Our model does not take any results or estimates from the survey as inputs, so

that the comparison exercise that we conducted here between estimates of exposure from our model with the ONS Coronavirus Infection Survey provides a real-world validation. However, it is also important to note that there are some limitations of ONS study, including 1) some data in the questionnaires can be incorrect or missing. For example, participants sometimes misinterpret questions or, in the case of remote data collection, may stop filling in the questionnaire part way through; 2) the testing results are limited by the performance of testing kits. There will be false-positives and false-negatives from the test, and false-negatives could also come from the fact that participants in this study are self-swabbing.

Moreover, we showed the modelling approach is a valuable early pandemic diagnostic tool and can clearly recover the first epidemic wave that the survey was unable to capture because of its late start. Using the inferred daily incidence, we explicitly demonstrated the variation of case detection rates over two epidemic waves in England in 2020. This provides quantitative information for studying the association between the capacity, behaviour and strategy of testing with the evolution of the epidemic and further supports the argument that confirmed case reports largely underestimate the extent of disease transmission.

Moreover, the simple structure of the model presented here avoids the unnecessary complexity and structure-based uncertainty of a full dynamic model where compartmental models simulating disease spread in different groups of the population including susceptible, exposed, infected and recovered are developed. The exercise of studying the model performance against data abundance suggests the modelling results remain highly robust in a data-sparse setting that would be particularly important, for example, in Low- or Middle-Income Countries (LMICs).

Chapter 4 Data integration to estimate exposure to SARS-CoV-2 in data-scarce scenarios – serological data was limited in Afghanistan

I have co-authored a paper on the research underlying this chapter in the journal BMJ Open (*120*): Sayed Ataullah Saeedzai1, Mohammad Nadir Sahak, Fatima Arifi, Eman Abdelkreem Aly, Margo van Gurp4, Lisa J White, **Siyu Chen**, Amal Barakat, Giti Azim, Bahara Rasoly, Soraya Safi, Jennifer A Flegg, Nasar Ahmed, Mohmmad Jamaluddin Ahadi, Niaz M Achakzai, Alaa AbouZeid. (2022). COVID-19 morbidity in Afghanistan: a nationwide, population-based seroepidemiological study. BMJ open 12.7: e060739. doi: 10.1136/bmjopen-2021-060739.

My contribution in this paper was to develop methods to 1) estimate seroprevalence after adjusting the sensitivity and specificity of the antibody tests based on the serosurveys (as shown in Figure 2 in the original paper, 10.1136/bmjopen-2021-060739); 2) estimate the time course of exposure based on the seroprevalence calculated in 1) by accounting for antibody decay (as shown in Figure 3 in the original paper, 10.1136/bmjopen-2021-060739). To approach 2), I revised the method developed in Chapter 2 to allow for the estimation to be conducted using a single seroprevalence measurement at one time point.

All of the theoretical models that I developed are formulated in 4.2 Materials and Methods; results that I generated from these models are presented in 4.3 Results. A brief description about the serological measurements from the serological survey that was conducted by collaborators is included in the 4.1 Introduction. More details about the survey can be found in the publication (*120*).

4.1 Introduction

The first reported case of COVID-19 in Afghanistan was in Herat province, the national border with Iran where many returnees have seeded new cases in the country, on 24 February 2020 (*170*). A few days later, the highly infectious virus was reported to have spread to several other locations within the country. Many efforts had been made to mitigate the spread by the Ministry of Public Health of Afghanistan during the early days of the epidemic. For example, a screening program with quarantine requirements following symptoms and positive tests for those entering through the country's porous borders and airports was launched in January 2020 (*171*). Programmes on raising awareness in the population in preventing the spread of the virus were conducted since June 2020 (*172*). Lockdown was first imposed in Herat then subsequently in all major provinces including Kabul. Schools and universities were closed, and restrictions on mass gatherings were imposed from March 2020 to August 2020 (*170*). Despite these non-pharmaceutical interventions, a series of epidemic waves were still reported since 2020. As of 20 July 2021, Afghanistan has reported 156,363 confirmed cases of COVID-19 and 7,284 deaths from the disease (*173*).

COVID-19 deaths are a key indicator to track the evolution of the epidemic. However, due to a less comprehensive surveillance system and limited capacity of diagnostic testing, the percentage of documented COVID-19 deaths was estimated to be only 10% in the African region, compared with 90% in Europe (*174*). With the political transition in Afghanistan and disruption of the health system, public health efforts to tackle COVID-19 were completely disrupted (*175*), implying that the undocumented COVID-19 related deaths are highly likely substantial in Afghanistan. This posted a big challenge for tracking the exposure to SARS-CoV-2 in Afghanistan.

Serological testing of patients can be used to provide useful information about an individual's status in terms of a current or previous COVID-19 infection. Immunoglobulin

M (IgM) and G (IgG) antibodies arise at around the same time, between 1 to 3 weeks after infection (*60*); however, IgM antibodies decay more rapidly than IgG antibodies (*176*). Therefore, for public health studies, IgM is used as a marker of current infection while IgG is used as a marker of previous infection, i.e., within the previous few months.

To estimate levels of past exposure and thus the position of a population in their epidemic timeline, a national population-based, cross-sectional, age-stratified seroepidemiological survey was initiated by the Afghanistan Ministry of Public Health and conducted throughout Afghanistan between June and July 2020, including a questionnaire survey and antibody testing of participants for COVID-19 infection using RDTs (*120*). The World Health Organization (WHO) protocol for population-based age-stratified seroepidemiological investigations for COVID-19 infection was adapted for the Afghanistan context to obtain seroprevalence estimates (*177*).

Briefly, a two-stage cluster sampling was conducted in the eight regions of Afghanistan plus Kabul province where 9514 individuals were sampled in total and the number of participants required in each region was estimated proportionate to the population size of each region. More details about the survey design and sampling can be found in the publication (*120*). For each individual participant finger-prick blood samples were collected and tested using an antibody rapid test (RDT) of COVID-19. The COVID-19 RDT used was the COVID-19 IgG/IgM Rapid Test Cassette developed by Healgen Scientific LLC, USA with IgM relative sensitivity and specificity of 95.7% and 97.3%, respectively; IgG relative sensitivity and specificity of 91.8% and 96.4%, respectively; and both IgG-positive and/or IgM-positive specificity of 97.5% (*178*). A weighted analysis of accounting for the sampling weighting, non-response weighting, and poststratification weighting was applied to adjust for the complex survey design for reporting the survey results.

I briefly describe the survey results in the national level here since they will be used as one of the inputs of the model that I developed below in Section 4.2 to infer the population exposure after adjusting for test sensitivity and specificity and seroreversion. In total, 9514 participants aged from 5-17 years and >18 years were interviewed and tested for this survey. 2997 (31.5%) of individuals tested positive for antibodies against SARS-CoV-2. Kabul region had the highest proportion of participants who tested positive for antibodies against SARS-CoV-2 (534, 53%), then East, Central, West, Northeast, Southeast, North, South, Central Highland with the antibody positivity as (466, 42.9%), (333, 36.3%), (314, 34.1%), (371, 32.4%), (263, 32.2%), (308, 30.7%), (170, 25.8%), (147,21.1%) respectively (*120*).

As discussed in Chapter 1, serological survey results might underestimate the total exposure in a population (*179*) because of decaying antibody titres over time (*126, 139, 166*). To adjust the seroprevalence for test sensitivity and specificity, as well as seroreversion, I further adapted the methodology (*36*) that was originally developed for the English setting and used this to infer the population exposure after accounting for the undocumented mortality associated with COVID-19 in Afghanistan.

4.2 Materials and Methods

4.2.1 Data sources and availability

In this section, I describe the datasets that are given as the inputs of the model for inferring exposure level in different regions of Afghanistan. Survey serology data that are used for modelling are all available from (*120*) and described in Section 4.1. For adjusting the COVID-19 seroprevelance, all data, code and materials used in the analyses can be accessed at:

https://github.com/SiyuChenOxf/AfghanistanSerologyStudy/tree/master.

Regional daily deaths

The documented daily mortality data associated with COVID-19, which might be subject to underreporting, for each of the nine Afghanistan regions (Kabul, East, West, North, South, North-east, South-east, Central, and Central highlands) from 1 January 2020 to 4 August 2020, were extracted from the Afghanistan Ministry of Health DHIS2 database.

Regional serology data

The proportion of individuals with current or past COVID-19 infection in each region were obtained from the seroepidemiological study data (*120*). The serology survey provided a result for both IgM and IgG antibodies for each participant, using the COVID-19 IgG/IgM Rapid Test Cassette (*180*). The dynamics of IgM and IgG antibodies within an infected individual are complicated (*126*) as described in Section 1.2.1. Here, I take the simplified view that an individual who is either IgG positive and/or IgM positive has been exposed to COVID-19 (either past or current infection). Therefore, in the following modelling, the sensitivity and specificity provided by the manufacturer of the imperfect serology test for IgG+ and/or IgM+ was employed.

Sample size for the regional serology survey

The sample size for the serology survey in nine Afghanistan regions (Kabul, East, West, North, South, North-east, South-east, Central, and Central highlands) was obtained from the survey sampling protocol (*120*) as shown in Appendix Table 7. This will be used to correct the bias of proportion of population tested antibody positive caused by imperfect testing performance using Equation (5.1).

4.2.2 Seroprevalence adjusted by the performance of the test

I used a simple Bernoulli model to estimate the regional seroprevalence, after adjusting the proportion of individuals in each region with current or past COVID-19 infection according to the sensitivity and specificity of the serology test (*180*). (The term ‘seroprevalence’ below

denotes the serology positive ratio already adjusted by the test used) The Bayesian framework was as follows:

$$x_i(t_0) \sim Beta(1,1)$$

$$w_{ij} \sim bernoulli\left(k_{se} \times x_i(t_0) + \left(1 - k_{sp}\right) \times \left(1 - x_i(t_0)\right)\right)$$

$$w_{ij} = \begin{cases} 0, IgG + or\ IgM + \\ 1, IgG - and\ IgM - \end{cases}, j = \{1, \ldots, N_i\}$$

(5.1)

where in the first equation given above we have specified a uniform prior for $x_i(t_0)$, which is the proportion of the population in region i that is serology positive, either for IgM or IgG, at t_0, 21 July 2020; w_{ij} is the serology survey result for the j-th participant in the serology study from region i; N_i is the total number of participants in the serology survey for region i list in Appendix Table 7; and k_{se} (k_{sp}) is the median of the serology test cassette sensitivity (specificity) reported by the manufacturer (*180*). The posterior for seroprevalence on the date the serology survey was conducted, $t = t_0$, was estimated using a Markov chain Monte Carlo (MCMC) implemented in Rstan (*117*) and denoted as $\tilde{x}_i(t_0)$.

4.2.3 Exposure estimates

We revised the mathematical model developed in (*36*) to account for the underreporting of mortality in the Afghanistan setting according to the varying serology status of the population, $X_i(t)$, of each regional population (for each region $i = 1, \ldots, 9$, corresponding to Kabul, East, West, North, South, North-east, South-east, Central, and Central highlands, respectively). The population that has positive serology status increased with exposure of the population to COVID-19 and decreased due to the waning of antibodies.

Given that the constant age-averaged infection fatality rate by region is β_i, the documented mortality over time by region is $m_i(t)$, and the reporting rate of mortality associated with COVID-19 by region is q_i, which is assumed to be constant over time, then, at each time

step, of the $\frac{1}{q_i\beta_i}m_i(t)$ individuals who were exposed, $\frac{1}{q_i}m(t)$ die and the remaining number of individuals, $\frac{1-\beta_i}{q_i\beta_i}m_i(t)$, seroconvert from negative to positive. Then, assuming that positive individuals convert to negative at a rate of α, the equation for the rate of change of the number of seropositive individuals is given by:

$$\frac{dX_i(t)}{dt} = \frac{(1-\beta_i)}{q_i\beta_i}m_i(t) - \alpha X_i(t) \tag{5.2}$$

Solving Equation (5.2), subject to the initial condition $X_i(t=0) = 0$ where $t = 0$ is time since 1 January 1 2020, gives:

$$X_i(t) = \frac{(1-\beta_i)e^{-\alpha t}}{q_i\beta_i}\int_0^t e^{\alpha r}m_i(r)dr \tag{5.3}$$

Discretising Equation (5.3) with daily intervals ($\Delta r = 1$) gives:

$$X_i(t) = \frac{(1-\beta_i)e^{-\alpha t}}{q_i\beta_i}\sum_{r=0}^{t} e^{\alpha r}m_i(r) \tag{5.4}$$

Then, the proportion of the population that is serology positive over time, $x_i(t)$, is

$$x_i(t) = \frac{X_i(t)}{P_i - \frac{\sum_{r=0}^{t} m_i(r)}{q_i}} \tag{5.5}$$

Where P_i is the reported population in region i before the COVID-19 outbreak, and the total proportion of the population that has been exposed over time, $\varepsilon(t-\delta_\epsilon)$, is

$$\varepsilon_i(t-\delta_\epsilon) = \frac{\frac{1-\beta_i}{q_i\beta_i}\sum_{r=0}^{t} m_i(r)}{P_i - \frac{\sum_{r=0}^{t} m_i(r)}{q_i}} \tag{5.6}$$

where δ_ϵ is the time lag between exposure and seroconversion and is fixed at 21 days (*36*). We used the posterior samples of seroprevalence at t_0, $\tilde{x}_i(t_0)$, from the MCMC and combined it with Equations (5.4) and Equation (5.5) to calculate the posterior samples of reporting rate for mortality, $\tilde{q}_i$:

$$\tilde{q}_i = \frac{(1-\beta_i)e^{-\alpha t_0}\sum_{t=0}^{t_0} e^{\alpha t} m_i(t)}{x_i(t_0)\beta_i P_i} + \frac{\sum_{t=0}^{t_0} m_i(t)}{P_i} \tag{5.7}$$

Compared with the total population in Afghanistan prior to 2020 (approximately 38 million people), the cumulative mortality associated with COVID-19 by the date of serology survey, $\sum_{t=0}^{t_0} m(t)$, is small. Therefore, it is reasonable to neglect it from Equation (5.7), which then gives:

$$\tilde{q}_i \approx \frac{(1-\beta_i)e^{-\alpha t_0}\sum_{t=0}^{t_0} e^{\alpha t} m_i(t)}{x_i(t_0)\beta_i P_i} \tag{5.8}$$

Combining Equations (5.4), (5.5) and (5.8) we can obtain samples of seroprevalence over time, $\tilde{x}_i(t)$:

$$\tilde{x}_i(t) \approx \frac{x_i(t_0)}{e^{\alpha(t-t_0)}} \frac{\sum_{r=0}^{t} e^{\alpha r} m_i(r)}{\sum_{t=0}^{t_0} e^{\alpha t} m_i(t)} \tag{5.9}$$

From Equations (5.6) and Equation (5.8) we can obtain samples of the total proportion of the population that has been exposed over time, $\tilde{\varepsilon}_i(t-\delta_\epsilon)$:

$$\tilde{\varepsilon}_i(t-\delta_\epsilon) \approx x_i(t_0)e^{\alpha t_0} \frac{\sum_{r=0}^{t} m_i(r)}{\sum_{t=0}^{t_0} e^{\alpha t} m_i(t)} \tag{5.10}$$

Note that the seroprevalence in Equation (5.9) and exposure in Equation (5.10) over time are not dependent on β. We use the median estimation of α from the constant infection fatality ratio (IFR) model from (*36*) as an input to Equation (5.9) and Equation (5.10).

4.3 Results

Based on the analysis formulated in Equation (5.1), the seroprevalence by region adjusted by the sensitivity and specificity of the antibody tests is shown in Figure 4-1.

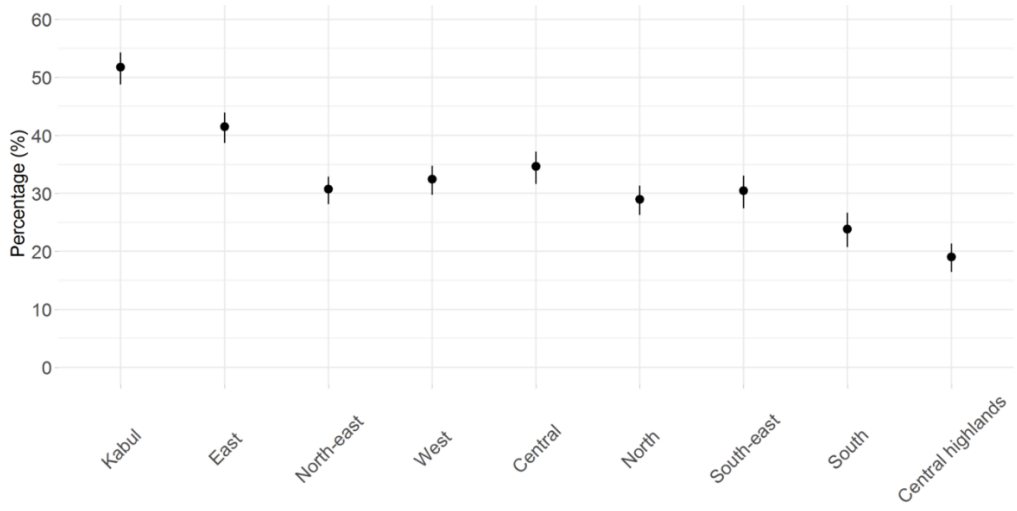

Figure 4-1. Adjusted seroprevalence by region by the sensitivity and specificity of the serology test for IgG-positive and/or IgM-positive.

By region, Kabul had the highest proportion of population who had COVID-19 infections according to the serological survey (51.8% CrI (48.8%, 54.8%)), while the Central highlands region had the lowest proportion, at (19.0% CrI (16.4%, 21.8%)).

Based on the mathematical relationship between adjusted seroprevalence and exposure formulated in Equation (5.10), I presented the predictions for cumulative exposure in the population up to 21 July 2020 in the nine regions of Afghanistan in Figure 4-2. Kabul was estimated to have around 60% population exposed while the Central highlands and South region had the lowest level of exposure, around 30%, suggesting a huge heterogeneity of exposure across different regions of Afghanistan in 2020.

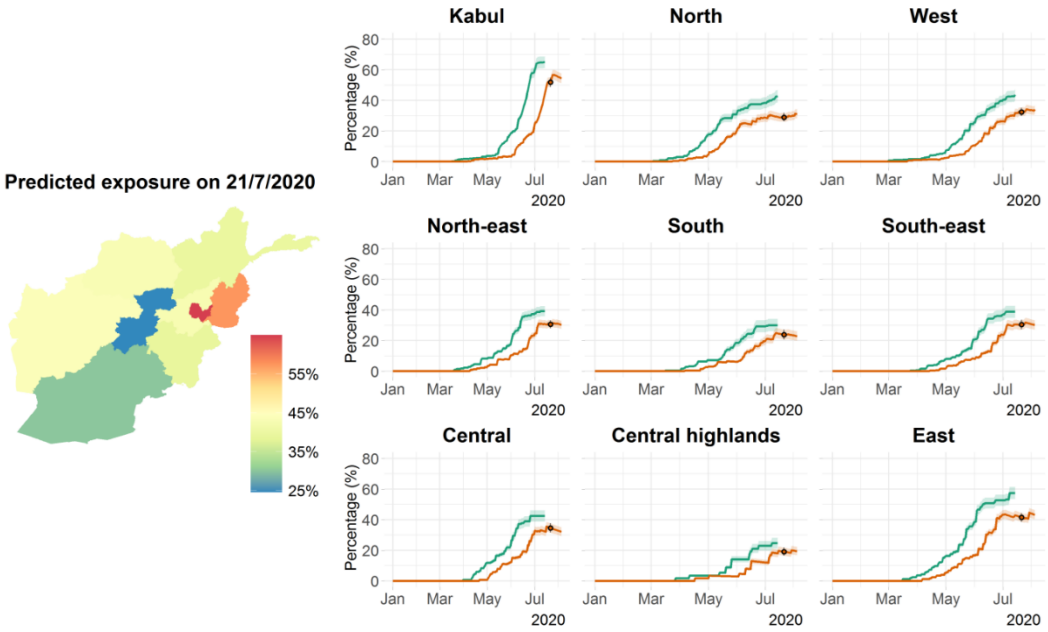

Figure 4-2**.** Time course of the COVID-19 pandemic up to 21 July 2020 for the nine regions in Afghanistan, for all age groups.
The solid orange circles and black error bars in the panel for each region represent the observed seroprevalence data and the associated credible interval (CrI) after adjusting for the sensitivity and specificity of the antibody test. The green and orange lines show the median predictions for exposure and seroprevalence, respectively, while the shaded areas correspond to 95% CrI. The median predicted exposure levels by region (expressed as the proportion of the population that has been infected) as of 21 July 2020 are shown on the map of Afghanistan.

This national survey of COVID-19 morbidity in Afghanistan, which was conducted during June and July 2021, revealed that around 10 million people (31.5% of the population) were seropositive for antibodies against SARS-CoV-2 and even higher proportion of population were estimated to have been exposed after accounting for the antibody decay. The population of Afghanistan is estimated to comprise approximately 33.6 million people (*181*). This finding is reasonably consistent with the results of another telephone survey conducted before July 2020 with a randomly selected sample of 713 healthcare workers to estimate COVID-19 morbidity in the country. The estimated proportion of individuals who had experienced COVID-19 signs and symptoms was 49.6%, which is close to the value for total infections for most regions reported in the present study, however, no laboratory testing was conducted for the phone survey, which only collected clinical information about symptoms. There is a discrepancy between the serosurvey results and the detected number of COVID-

19 infections reported to the surveillance system in the country (36 710 cases reported by the surveillance system as of 30 July 2020 and 156 363 cases as of 5 November 2021) in Afghanistan. The under-reporting of COVID-19 cases is a problem globally due to limited testing availability, flawed test sensitivity, poor surveillance and the indeterminate proportion of asymptomatic infections (*182*).

4.4 Discussion

In this Chapter, I presented a simple but powerful calculation tool to estimate the exposure to SARS-CoV-2 in a data scarce setting where COVID-19 related death was largely underreported and only one serological measurement at one time point was measured. I applied it to the context of Afghanistan and used the serological measurements from a large-scale survey conducted in nine regions of Afghanistan in June and July 2020 as model inputs. In this process, I made two key assumptions in the model which is 1) the reporting rate of COVID-19 in Afghanistan was time invariant; 2) the antibody decaying rate was consistent with the posterior estimates from the England study that I presented in Chapter 2. By doing so, a key epidemic parameter, infection fatality ratio, can be omitted from the model. The model results showed that the exposure level was higher than the serology survey suggested in all regions of Afghanistan but had great heterogeneity across different regions, suggesting a non-uniform transmission pattern of SARS-CoV-2.

The estimates of exposure informed the real practice of policy decision in Afghanistan. During the evolution of the COVID-19 epidemic in Afghanistan, I performed a series of modelling exercises to project the median- and long-term epidemic trends to inform policy decision using the CoMo model with collaborators from WHO EMRO as one active contributor in the CoMo Consortium. The CoMo model was developed by the Consortium (*93*). The CoMo Consortium adopted a participatory modelling approach (*183*), which places in-country subject matter experts at the forefront of model development to ensure that

contextual considerations, such as local infrastructure, human resources and sociocultural considerations, are fully taken into account. The CoMo model was used to estimate the peak incidence of COVID-19 in Afghanistan after fitting to the exposure level inferred in this Chapter under four scenarios: good, bad, very bad and appropriate, depending on the coverage of and adherence to various non-pharmaceutical interventions.

Regularly presenting the modelling results to the Afghanistan Ministry of Public Health, revising the model structure and parameters to incorporate changes of various non-pharmaceutical interventions conducted in the country, informing about emerging evidence of virus characteristics and summarising results from the updated model constituted the loop of collaboration. It became one of the successful community case studies for the CoMo consortium (*93*).

A highly relevant concept when discussing and interpreting exposure to the virus in the population is herd immunity, which is also a key metric used in decision-making in communicable disease epidemiology. Herd immunity occurs when a certain proportion of the population is immune to a given infectious disease, reducing the probability that the disease will be transmitted from one individual to another, thus helping to protect the entire population from that disease (*112*). Herd immunity can be achieved when the immunity level in the whole population is above a certain threshold, called the herd immunity threshold, either through individuals being exposed or vaccinated.

Under the simplest model, the herd immunity threshold depends on a single parameter known as R_0, or the basic reproduction number. R_0 indicates the average number of individuals one infected individual will go on to infect in a fully susceptible population. Mathematically, the herd immunity threshold is defined by $1 - 1/R_0$ (*184*). In the context of COVID-19 various herd immunity thresholds in different contexts have been estimated, ranging from 43% to 85% (*93, 185-188*). For example, one study indicated that if R0=3, i.e.

one infected individual can infect up to three others, meaning 67% of the population must be immune to achieve herd immunity (*189*). Estimates by Johns Hopkins University suggest that 70% of the population must be immune to achieve herd immunity and end restrictions on people's day to day lives (*93*), while another study suggested that R0 values of 1–2, 2–4 and >4 would require herd immunity thresholds of 50%, 56.1–74.8% and 77.9–85%, respectively (*185*)

Based on evidence from countries comparable to Afghanistan, assuming an R_0 in the country of 2–3, the herd immunity threshold would be between 56% and 75%. Kabul province, with a SARS-CoV-2 inferred exposure of 53%, was within range of this threshold. The Eastern and Central regions, with SARS-CoV-2 seroprevalences of 34% to 42%, seem in a relatively good position, but the remaining regions with SARS-CoV-2 seroprevalence of less than 35% seem in a worse position and not yet close to the assumed herd immunity threshold at the time of the study.

However, the above discussion of R_0 and its correlation to the herd immunity threshold represents the simplest interpretation of these terms. They depend on several key assumptions, including homogeneous mixing of individuals within a population and that all individuals develop sterilizing immunity—immunity that provides lifelong protection against reinfection—upon vaccination or natural infection (*190-192*). In real-world situations, these epidemiological and immunological assumptions are often not met. From what we have learned in the past three years especially the last year of the Omicron epidemic wave, the rising number of documented reinfections, as well as the high number of breakthrough infections with the Omicron variant among the fully vaccinated, means that the indirect protection from the overall population immunity might be very hard to achieve. There are situations when herd immunity might be achieved before the population immunity reaches the threshold. By accounting for the heterogeneity of population mixing due to age

and social contact, one study concluded that herd immunity can be achieved at a population-wide infection rate of ~40%, considerably lower than previous estimates (*193*). This shift is because transmission and immunity are concentrated among the most active members of a population, who are often younger and less vulnerable. However, this heterogenous transmission is also likely to be not very effective in terms of achieving the herd immunity threshold. One review paper pointed out that if super-spreading, one example of the heterogenous transmission, is driven by events rather than by individuals, or if control measures reduce or modify the set of potential super-spreaders, there may be limited impact on herd immunity (*194*).

As in many low- and middle-income countries, COVID-19 vaccination rates in Afghanistan are low, with just 12% of the population fully vaccinated by middle of 2021. With the disruptions to the health system as a result of the evolving political situation in the country, the COVID-19 response may deteriorate if control measures are not implemented and vigilantly maintained. In practice, after July 2021, the restrictions in many areas within the country were reduced and since then the country has only focused on school closures as a mitigation measure to balance the economy, social life and the impact of COVID-19 on the health system. It is worth mentioning that with the recent transition of government in Afghanistan and decreased funding for the country's health system, there are evolving challenges that will ultimately lead to the increased spread of COVID-19 and other infectious diseases. Greater levels of poverty, a displaced population and poor sanitation will further exacerbate this problem. The influx of refugees from Afghanistan to other countries might also facilitate the cross-border spread of disease. Particularly with the emergence of new variants and low vaccination coverage, it is crucial to have continued public health and social measures to mitigate the impact of COVID-19 in a conflict-affected and unstable country. For the continuation of health services, functional hospitals, surveillance systems

and laboratories, as well as a skilled healthcare workforce, are needed to mitigate the spread of COVID-19 and other infections within Afghanistan and prevent the regional and even global spread of disease. Given the large proportion of the population that remains susceptible to COVID-19 infection, and limited COVID-19 vaccination coverage, extra caution should be made when relying on the indirect protection from herd immunity and then lifting any non-pharmaceutical interventions in the country, in order to avoid larger epidemic waves and to protect the health system from an unmanageable burden of hospitalisations.

In this chapter, I revised the methodology developed in Chapter 2 to calculate the population exposure in Afghanistan to account for the sero-reversion and under-reporting of covid-19 related mortality. However, it is also important to note that sero-reversion does not prevent the establishment of herd immunity and many other factors including T cells immunity and cross protection from other coronavirus may play important roles in understanding population immunity. Since I only inferred the exposure level from serology data, further correlations with immunity are beyond this thesis.

Chapter 5 Data integration to estimate the shielding impact among pregnant women on reducing exposure to SARS-CoV-2 in New York City

I have published the research underlying this chapter in the journal Viruses with me as the first author (*121*): Siyu Chen*, Elisabeth A. Murphy, Angeline G. Pendergrass,Ashley C. Sukhu ,Dorothy Eng, Magdalena Jurkiewicz, Iman Mohammed, Sophie Rand, Lisa J. White, Nathaniel Hupert and Yawei J. Yang*. (2022). Estimating the Effectiveness of Shielding during Pregnancy against SARS-CoV-2 in New York City during the First Year of the COVID-19 Pandemic. Viruses, 14, 2408. https://doi.org/10.3390/v14112408

Pregnant patients have increased morbidity and mortality in the setting of SARS-CoV-2 infection. The exposure of pregnant patients in New York City to SARS-CoV-2 is not well understood due to early lack of access to testing and the presence of asymptomatic COVID-19 infections. Before the availability of vaccinations, preventative (shielding) measures, including but not limited to wearing a mask and quarantining at home to limit contact, were recommended for pregnant patients.

This chapter aims to develop a dynamic model to link serologic and virologic data from 2196 patients who gave birth from April through December 2020 in one institution in New York City and estimated the exposure in pregnant women. In comparison with exposure in general population in New York City as assessed by the method presented in Chapter 2, I demonstrated a dramatic real-world effectiveness of shielding in these pregnant patients after considering the duration of pregnancy.

5.1 Introduction

Pregnant patients make up a vulnerable patient population in any infectious disease outbreak. When New York City became the epicenter of COVID-19 pandemic in March 2020, the impact of SARS-CoV-2 infection on pregnant patients and their neonates was not well understood (*195*). In addition, the prevalence of the disease in the pregnant population was difficult to capture given the lack of early testing and the presence of asymptomatic infected patients (*195, 196*).

During this period of uncertainty early in the pandemic, most national and regional public health authorities and medical care professionals advocated for the enforcement of protective measures including wearing masks, quarantining at home when possible, and keeping social distancing. These non-pharmaceutical interventions or shielding measures have been shown to be highly effective in mitigating epidemic curves in the larger population especially during different "lockdown" periods in myriad countries (*10, 83, 197, 198*) but the effectiveness among pregnant patients at that time are still unknown.

Studies have shown that pregnant patients are at higher risk of getting seriously ill from SARS-CoV-2 compared to non-pregnant patients (*199, 200*). A meta-analysis showed that compared to non-pregnant patients of reproductive age with COVID-19, pregnant patients are at increased risk of severe disease from COVID-19, with increased risk of ICU admission mechanical ventilation, and death (*201, 202*) . In this study we aim to model exposure rates in the pregnant vs. general populations and evaluate the efficacy of both shielding and behaviour changes during pregnancy on reducing both infection exposure and its ramifications for morbidity and mortality to SARS-CoV-2 among pregnant patients. The estimation of effectiveness of shielding during pregnancy relies on the comparison of estimates of past exposure to infection between pregnant patients and the general population. Serology tests can identify past infections and enable estimation of the number of total

infections. However, naturally formed immunoglobulins targeting the virus (i.e., those generated by native infection and not vaccination) have been reported to wane below the detectable level of serological assays quite rapidly (e.g., after several months) (*36, 108*). The cumulative level of exposure to SARS-CoV-2 in a population therefore is not directly measurable and has to be inferred through modelling. Here, we propose a new method to estimate the cumulative exposure of SARS-CoV-2 among pregnant patients and employ a peer-reviewed model to estimate the cumulative exposure among general population in New York City, accounting for expected levels of antibody waning (seroreversion). These results have implications on future infectious disease prevention strategies in pregnancy.

5.2 Data source and availability

All code and materials used in the analyses can be accessed at: https://github.com/SiyuChenOxf/COVID-19Exposure-ShieldingPregnantWomen. All parameter estimates and figures presented can be reproduced using the code provided. The datasets from pregnant patients can be made available from the corresponding authors of the publication (*121*) on reasonable request. The seroprevalence data for general population in New York City Metro Area and the daily total (including confirmed and probability) mortality data were extracted from US Department of Health and Human Services Centers for Disease Control and Prevention CDC Data Tracker (*203*).

5.2.1 Pregnant women data

Pregnant patients giving birth at a single New York City hospital between 20 April 2020 and 27 December 2020 were included in this study. 2682 pregnant patients with clinical data capture and sample capture could have had either RT-PCR testing or serology testing or were untested (unknown). Among these 2682 patients in terms of RT-PCR, 97.7% were tested and 2.3% were unknown; in terms of serology tests, 89.9% were tested and 10.1%

were unknown. For testing results breakdown: 10% were RT-PCR negative but serology unknown; 0.3% were both RT-PCR and serology unknown; 8.1% were RT-PCR negative and serology positive, 0.075% were RT-PCR unknow and serology positive, 2.1% were both RT-PCR and serology positive, 77.18% were both RT-PCR and serology negative, 2.0% RT-PCR unknown and serology negative, and 0.56% were RT-PCR positive and serology negative. The demographics of these 2682 pregnant patients can be found in Table 5-1. After screening the distribution of unknown tests results for RT-PCR and serology on the calendar week, 2196 pregnant patients were included in the mathematical modelling.

Table 5-1. Demographics table for women who giving birth prior to August 2020 and from August 2020 onwards.

	Total	**Women Giving Birth Prior to August 2020**	**Women Giving Birth from August 2020 Onwards**	**Test**	***p*-value**
	n = 2682	*n* = 1781	*n* = 901		
Ethnicity				Chi Square: 5.82	0.324
Not Hispanic or Latino or Spanish Origin	1769 (66%)	1173 (65.9%)	596 (66.1%)		
Hispanic or Latino or Spanish Origin	219 (8.2%)	142 (8%)	77 (8.5%)		
African American	1 (0%)	1 (0.1%)	0 (0%)		
Multi-racial	1 (0%)	0 (0%)	1 (0.1%)		
Declined	600 (22.4%)	396 (22.2%)	204 (22.6%)		
Unknown	92 (3.4%)	69 (3.9%)	23 (2.6%)		
Race				Chi Square: 11.49	0.244
White	1346 (50.2%)	876 (49.2%)	470 (52.2%)		
Asian	336 (12.5%)	224 (12.6%)	112 (12.4%)		
Black or African American	169 (6.3%)	118 (6.6%)	51 (5.7%)		
American Indian or Alaska Nation	6 (0.2%)	2 (0.1%)	4 (0.4%)		
Nat. Hawaiian/Oth. Pacific Island	3 (0.1%)	2 (0.1%)	1 (0.1%)		
Ashkenazi Jewish	2 (0.1%)	1 (0.1%)	1 (0.1%)		
Multiple races reported	15 (0.6%)	7 (0.4%)	8 (0.9%)		
Other combinations not described	258 (9.6%)	170 (9.5%)	88 (9.8%)		
Declined	464 (17.3%)	319 (17.9%)	145 (16.1%)		
Unknown	83 (3.1%)	62 (3.5%)	21 (2.3%)		
Mom Age (SD) years				t-test: −0.47	0.636
	34.4 (5.0)	34.4 (5.0)	34.5 (5.0)		
Gestational Age at delivery (SD) weeks				t-test: 1.53	0.126
	38.8 (2.1)	38.8 (2.0)	38.7 (2.4)		

The serology was detected in the serum or plasma from peripheral blood collected during admission for delivery. The serology test was performed using the clinical testing Pylon 3D

platform (ET HealthCare, Palo Alto, CA). The Pylon 3D platform (*204*) utilizes a fluorescence-based reporting system that allows for the semiquantitative detection of antie-SARS-CoV-2 IgG and IgM with a specificity of 98.8% and 99.4%, respectively. In this paper, we denoted the serology status of every pregnant patient as positive if either IgG or IgM was positive and as negative if both IgG and IgM were negative. Pregnant patients underwent RT-PCR testing for SARS-CoV-2 using nasopharyngeal swabs.

The observed cross-sectional data for pregnant patients is restructured into four trajectories for model fitting: weekly proportion of RT-PCR and serology negative time-series, weekly proportion of RT-PCR positive and serology negative time-series, weekly proportion of RT-PCR positive and serology positive time-series and weekly proportion of RT-PCR negative and serology positive time-series.

5.2.2 General Population Data

The seroprevalence data for general population in New York City Metro Area (including Manhattan, Bronx, Queens, Kings and Nassau) from February 2020 to December 2020 and the daily total (including confirmed and probability) mortality data were extracted from US Department of Health and Human Services Centers for Disease Control and Prevention CDC Data Tracker (*203*). Details of the seroprevalence data used here can be found elsewhere (*108, 205*).

5.3 Materials and Methods

5.3.1 Exposure Inference in Pregnant Patients

We first develop a dynamic model diagramed in Figure 5-1 for the temporary changing status of RT-PCR and serology among pregnant patients based on the COVID-19 disease progression. The definition of each compartment and transmission parameter specific to pregnant patients is described in Table 5-2 and Table 5-3 respectively.

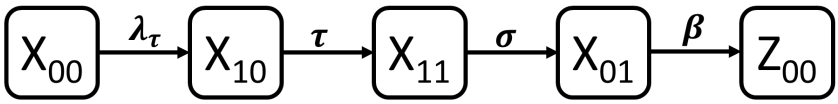

Figure 5-1. Schematic diagram of the dynamic model structure for RT-PCR and serology status.

A set of ordinary differential equations (ODEs) describing the time evolution of $X_{00}, X_{10}, X_{11}, X_{01}$ and Z_{00} can be written as follows:

$$\frac{dX_{00}(t)}{dt} = -\lambda_\tau(t)X_{00}$$

$$\frac{dX_{10}(t)}{dt} = \lambda_\tau(t)X_{00} - \tau X_{10}$$

$$\frac{dX_{11}(t)}{dt} = \tau X_{10} - \sigma X_{11}$$

$$\frac{dX_{01}(t)}{dt} = \sigma X_{11} - \beta X_{01}$$

$$\frac{dZ_{00}(t)}{dt} = \beta X_{01}$$

(5.1)

The initial conditions of $X_{00}, X_{10}, X_{11}, X_{01}$ and Z_{00} at $t = 0$ are denoted as $y_{00}, x_{10}, x_{11}, x_{01}$ and z_{00}. Here, $t = 0$ refers to 20 April 2020 (calendar week 17 in 2020) when the first data of pregnant patients was collected. The minimum time step in the ODEs is one week. We reparametrize the initial conditions as follows

$$x_{10} = k_{10}(1 - y_{00})$$

$$x_{11} = k_{11}\big(1 - y_{00} - k_{10}(1 - y_{00})\big)$$

$$x_{01} = k_{01}\Big(1 - y_{00} - k_{10}(1 - y_{00}) - k_{11}\big(1 - y_{00} - k_{10}(1 - y_{00})\big)\Big)$$

$$z_{00} = 1 - x_{10} - x_{11} - x_{01}$$

(5.2)

where $\{k_{10}, k_{11}, k_{01}\}$ are tool parameters and constrained between 0 and 1 so that $\{x_{01}, x_{11}, x_{10}, z_{00}\}$ can be constrained between 0 and 1. This is mainly for the convenience

of MCMC implementation in Rstan. The posterior estimates of $\{k_{10}, k_{11}, k_{01}\}$ in each model can be found in Table 5-3 and Appendix Figure 22.

In Equation (5.1), $\{\lambda_\tau(t)\}$ is the force of infection. We first assume $\lambda_{11}(t)$ is constant over time $(17 \leq t \leq 53)$ in Model 1 and then relax it by assuming a piece-wise constant at a fixed time step. To test the sensitivity, we try several different steps including 18 weeks in Model 2,

$$\begin{cases} \lambda_{21}, & 17 \leq t < 35 \\ \lambda_{22}, & 35 \leq t < 53 \end{cases} \tag{5.3}$$

12 weeks in Model 3,

$$\begin{cases} \lambda_{31}, & 17 \leq t < 29 \\ \lambda_{32}, & 29 \leq t < 41 \\ \lambda_{33}, & 41 \leq t < 53 \end{cases} \tag{5.4}$$

and 9 weeks in Model 4,

$$\begin{cases} \lambda_{41}, & 17 \leq t < 26 \\ \lambda_{42}, & 26 \leq t < 35 \\ \lambda_{43}, & 35 \leq t < 44 \\ \lambda_{44}, & 44 \leq t < 53 \end{cases} \tag{5.5}$$

and then compare main model results. We denote the numerical solutions of ODE system defined in Equation (5.1) as $\hat{X}_{00}, \hat{X}_{10}, \hat{X}_{11}, \hat{X}_{01}$ and $\hat{Z}_{00}$.

Following the dynamic model, we develop a Bayesian measurement model to model the data observation process so that the parameter estimation and model fitting can be conducted simultaneously using MCMC in Rstan (*117*).The model with associated parameters (Appendix Table 9) is described as follows:

$$\lambda_{ij} \sim uniform(0,1), \lambda_{ij} \in [0,1]$$

$$\sigma \sim uniform(0,1), \sigma \in [0,1]$$

$$\tau \sim gamma(4,3), \tau \in [0,5]$$

$$\beta \sim uniform(0,1), \beta \in [0,1]$$

$$y_{00} \sim beta(8,2), y_{00} \in [0,1] \tag{5.6}$$

$$\left(x_{00}^{obs}(t), x_{10}^{obs}(t), x_{11}^{obs}(t), x_{01}^{obs}(t)\right)$$

$$\sim Multinomial\left(N(t), \hat{X}_{00}(t) + \hat{Z}_{00}(t), \hat{X}_{10}(t), \hat{X}_{11}(t), \hat{X}_{01}(t)\right) \tag{5.7}$$

where $x_{00}^{obs}(t), x_{10}^{obs}(t), x_{11}^{obs}(t)$ and $x_{01}^{obs}(t)$ are the measured numbers of pregnant patients at calendar week t who were (a) both RT-PCR and serology negative, (b) RT-PCR positive and serology negative, c) both RT-PCR and serology positive and d) RT-PCR negative and serology positive respectively. $\hat{X}_{10}(t), \hat{X}_{11}(t), \hat{X}_{01}(t)$ are ODE-predicted individuals at calendar week t who were in RT-PCR positive and serology negative, RT-PCR positive and serology positive, RT-PCR negative and serology positive respectively. $\hat{X}_{00}(t) + \hat{Z}_{00}(t)$ is the ODE-predicted total number of pregnant patients at calendar week t who were either both RT-PCR and serology negative.

We use Bayesian inference (Hamiltonian Monte Carlo algorithm) in RStan to fit the model to RT-PCR and serology data by running four chains of 20,000 iterations each (burn-in of 10,000). We use 5% and 95% percentiles from the resulting posterior distributions for 90% CrI for the parameters. The Gelman–Rubin diagnostics ($\hat{R}$) given in Appendix Table 11 show values of 1, indicating that there is no evidence of non-convergence for either model formulation. Furthermore, the effective sample sizes (n_{eff}) in Appendix Table 11 are all more than 5000, meaning that there are many samples in the posterior that can be considered independent draws.

Table 5-2. A list of patient compartments or model variables and their definitions.

Variables	Definition
X_{00}	proportion of naïve population who are both RT-PCR and serology negative and never exposed
X_{10}	proportion of early-phase infected population who are RT-PCT positive but serology negative
X_{11}	proportion of middle-phase infected population who are both RT-PCR and serology positive
X_{01}	proportion of late-phase infected population who are RT-PCR negative but serology positive
Z_{00}	proportion of past infected population who are both RT-PCR and serology negative but previously exposed

5.3.2 Exposure Inference in General Population

For general population in New York City, we collected morality and seroprevalence time-series data as described in the Data Description section and fitted a published model under the assumption of constant infection fatality ratio (*36*). In the meanwhile, we got the estimates of cumulative exposure over time and two parameters related to the general population of New York City: they are infection fatality ratio, α and antibody decaying ratio, ω (Appendix Table 10). Through comparing the exposure level to SARS-CoV-2 among pregnant patients and general population, we estimated the effectiveness of shielding during pregnancy.

5.4 Results

5.4.1 Dynamic model of SARS-CoV-2 infection

The time course of SARS-CoV-2 infection among pregnant patients can be reconstructed utilizing both RT-PCR and serology testing results by following the timeline of a typical SARS-CoV-2 infection. Most individuals, once infected, experience an incubation period before developing some symptoms of COVID-19 infection, while some individuals will remain asymptomatic throughout. The onset of RT-PCR positivity varies across individuals

and types of clinical specimens (*206*) but systematic review studies showed that the highest percentage virus detection was from nasopharyngeal sampling between 0- and 4-days post-symptom onset at 89% (95% confidence interval (CI) 83% to 93%) dropping to 54% (95% CI 47 to 61) after 10 to 14 days (*27*). In addition to testing SARS-CoV-2 RNA load using RT-PCR testing SARS-CoV-2-specific IgM and IgG antibody (in the absence of vaccination) is another method for identifying history of infection. Although the precise timing of IgM and IgG antibody detectability depends on the testing kits and varies across different individuals (*90, 207*), on average the viral RNA is detectable one or two weeks earlier by RT-PCR than the antibody detectable by serological assays (*60, 90*).

Assuming that the RT-PCR is positive before serology positivity, we divided the population of pregnant patients into five compartments: 1) RT-PCR negative and serology negative without previous exposure (X_{00}, naïve); 2) RT-PCR positive and serology negative (X_{10}, early phase infected); 3) RT-PCR positive and serology positive (X_{11}, middle-phase infected); 4) RT-PCR negative and serology positive (X_{01}, late-phase infected), and 5) both RT-PCR and serology negative with history of previous infection (Z_{00}, past infected) (Table 5-2).

We next defined four transmission quantities or parameters to link these above mentioned 5 time-based compartments: force of infection, λ_τ; average time lag between virus detectability by the RT-PCR test and antibody detectability by the serology assay, $\frac{1}{\tau}$; average time lag between antibody detectability by the serology assay and virus undetectability by the RT-PCR assay, $\frac{1}{\sigma}$; and antibody decay rate, β (Figure 5-1).

The whole length of infectious period for pregnant patients can be therefore approximated by the sum of time delay between virus detectability and antibody detectability and the average time lag between antibody detectability and virus undetectability. We developed a dynamic model to study temporal changes of both RT-PCR and serology status in pregnant

patients (Figure 5-1) with associated variables (Table 5-1) and parameters (Table 5-3). Further details about the model can be found in the Section 5.3.

Table 5-3**.** Parameter estimates (associated 90% credible intervals) among pregnant patients for each model fit.

Parameter(unit)	Definition	Model	Median	5%	95%
τ^{-1}(days)	average time lag between virus detectability and antibody detectability	1	7	4	18
		2	5	3	16
		3	5	3	10
		4	6	4	13
σ^{-1}(days)	average time lag between antibody detectability and virus undetectability	1	22	14	37
		2	18	11	32
		3	17	11	27
		4	18	12	28
β^{-1}(days)	average time lag between seroconversion and seroreversion among pregnant patients	1	152	84	336
		2	118	64	270
		3	110	65	208
		4	117	66	240
$y_{00}(-)$	proportion of patients who were giving birth and not exposed by 20 April 2020	1	0.87	0.79	0.90
		2	0.86	0.76	0.90
		3	0.86	0.74	0.89
		4	0.85	0.74	0.89
λ_τ	$\lambda_{11}(-)$	1	0.0052	0.0022	0.010
	$\lambda_{21}(-)$	2	0.0063	0.0028	0.013
	$\lambda_{22}(-)$		0.0079	0.0025	0.0182
	$\lambda_{31}(-)$	3	0.0041	0.0052	0.019
	$\lambda_{32}(-)$		0.011	0.0052	0.019
	$\lambda_{33}(-)$		0.0077	0.0030	0.019
	$\lambda_{41}(-)$	4	0.00013	0.000088	0.00072
	$\lambda_{42}(-)$		0.0095	0.0051	0.016
	$\lambda_{43}(-)$		0.0070	0.0013	0.0178
	$\lambda_{44}(-)$		0.0083	0.0033	0.019

5.4.2 Longitudinal cross-sectional RT-PCR and serology results

We modeled the exposure of 2196 pregnant patients who delivered at a New York City hospital from 20 April 2020 through 27 December 2020 based on SARS-CoV-2 testing performed on discarded samples obtained from birth admission using data from quantitative real-time polymerase chain reaction (RT-PCR) testing for SARS-CoV-2 viral infection, or serology studies assaying levels of Immunoglobulin (Ig)G and IgM as a marker of the immune response to SARS-CoV-2 infection. Of the 2196 patients that had both RT-PCR and serology results available, 2.7% were positive and 97.3% were negative for RT-PCR

testing results; and 11.2% were positive and 88.8% were negative and for serology testing results. For both tests combined, 2.2% were both positive for RT-PCR and serology, 0.5% were RT-PCR positive and serology negative, 9.0% were RT-PCR negative and serology positive, and 88.3% were both RT-PCR negative and serology negative.

5.4.3 Fitting data from pregnant patients to the dynamic model

The test results of RT-PCR and serology allow us to divide our population of pregnant patients into four data-driven categories: (a) both RT-PCR negative and serology negative; (b) RT-PCR positive and serology negative; (c) both RT-PCR positive and serology positive; and d) RT-PCR negative and serology positive. The challenge in getting from test results to dynamic model compartments is that the first compartment (X_{00}, naïve) and the last compartment (Z_{00}, past infected) in the dynamic model (Figure 5-1) both manifest as both RT-PCR and serology negative, and are thus indistinguishable. To overcome this challenge, we developed a Bayesian measurement model to fit the test result data, which connects model predictions of the five time-based modeling-compartments to the measurements of the four data-driven categories.

Different models (Model 1–4) were used to analyze different assumptions about the force infection among pregnant patients. In Model 1, we assumed the force of infection is constant over time, and then relaxed the assumptions by assuming a time-varying force of infection in Model 2–4 (for details of how these models differ, see the parameters in Table 5-3). Model fitting results showed that predictions from all four dynamic models have good agreement with measurements from the data-driven categories each calendar week (Figure 5-2).

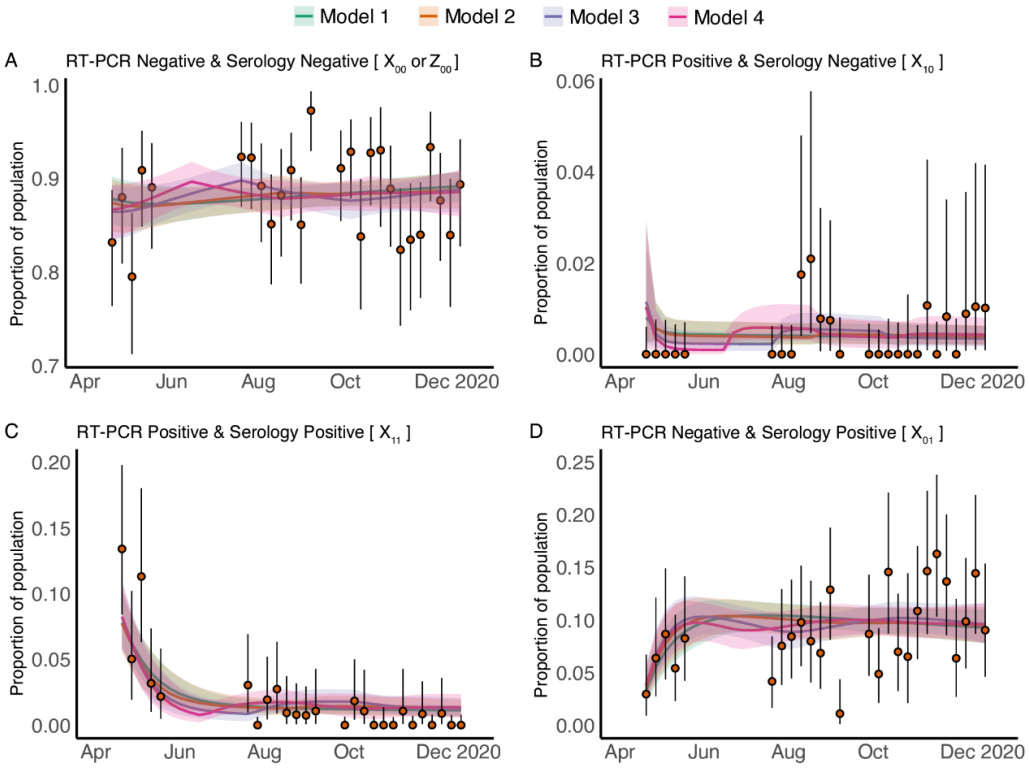

Figure 5-2**.** Time evolution measurements and fitted test-result model estimates of the SARS-CoV-2 RT-PCR and antibody status among patients who gave birth between 20 April 2020 and 21 December 2020.
Panel (A–D), respectively, shows the model fitting results for four data-driven categories: (A) both RT-PCR negative and serology negative; (B) RT-PCR positive and serology negative; (C) both RT-PCR positive and serology positive; and (D) RT-PCR negative and serology positive. In each panel, the orange solid circles and black error bars represent the measured proportion of patients who were giving birth and in one of the four RT-PCR and serology categories and their credible intervals respectively. The green, orange, purple and pink lines in each panel show the median of estimates from Model 1–4, for proportions of patients who were giving birth in each of the four categories, while the shaded areas correspond to the 90% credible intervals. The models differ in the time-dependence of the force of infection; Model 1 assumes a constant force of infection while Models 2–4 assume time-varying force of infection.

We conducted a sensitivity analysis around the choice of prior of the initial conditional of proportion of pregnant patients who were not exposed previously by 20 April 2020 (numerically equals to 1 minus the level of exposure in pregnant patients by 20 April 2020). The results showed that the median and 50% credible band of posterior estimates are very robust (Appendix Figure 20) although a heavy left tail in the 90% and 95% credible band are estimated when the priors are very weak (Appendix Figure 21), for example uniform (0,1). However, considering the transmission speed and antibody decaying rate it is

reasonable to choose a relative formative prior, such as beta (2,1) and beta (8,2) and then the posterior estimates are more concentrated around 0.85 (Appendix Figure 21).

5.4.4 Transmission parameters of COVID-19 in pregnant patients are estimated to be consistent with those estimated for general population

Data fitting allowed for the estimation of the transmission parameters. The posterior estimates of parameters for pregnant patients from the four models were summarized in Table 5-3. The model also estimated the proportion of patients who were giving birth but not exposed to SARS-CoV-2 (y_{00}) by the beginning of our study in April 2020.

We found that the estimates of the time difference between RT-PCR positivity and serology positivity, and the duration of the infectious period for pregnant patients are very robust, on average 5.5 days (95% Credible Interval, CrI (3.3, 16.7) days), and 18.8 days (95% CrI (11.3, 34.3) days), respectively. These estimates are largely comparable with those for the general population (*50, 206, 208-211*). After seroconverting, seropositivity is estimated to be maintained for 124 days on average (95% CrI: (63, 320) days) among exposed pregnant patients. This relatively rapid seroreversion is consistent with estimates from the corresponding observational study, where analysis of the relationship between the elapsed time from the date of symptom onset and the antibody levels for pregnant patients demonstrated that the IgG positivity status could last approximately 110 days on average with a lower bound of the 95% confidence interval of 82 days but with an upper bound that is uncertain and possibly very large (*196*).

5.4.5 Estimated SARS-CoV-2 exposure in pregnant patients is higher than seropositivity rates would suggest

The estimated seroprevalence (proportion of pregnant patients who are seropositive) from each of the dynamic models (Figure 5-3) match that of our data (Figure 5-2 B–D). We next

estimated the exposure to SARS-CoV-2 in the pregnant patients and found that exposure is estimated to be much higher than serology positivity (Figure 5-3). Due to the rapid decline in antibody levels after natural infection confirmed in both experimental analyses (*51, 126, 166*) and modelling analyses (*36, 108*) there is a gap between seropositivity and the cumulative level of exposure; furthermore, this gap increases with time due to increasing exposure levels over time (Figure 5-3).

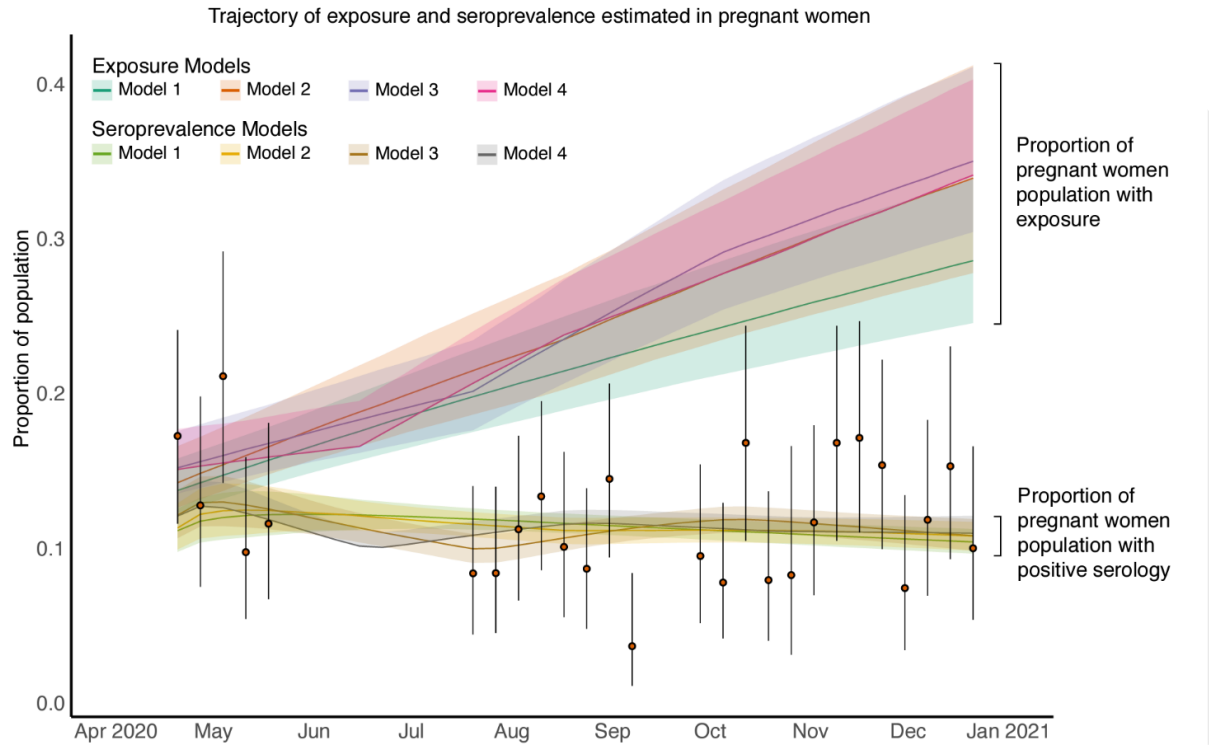

Figure 5-3**.** Time evolution of SARS-CoV-2 exposure and seroprevalence among patients who gave birth between 20 April 2020 and 21 December 2020.
The orange solid circles and black error bars represent the measured proportion of patients who were giving birth and serology positive and their credible intervals respectively. The green, orange, purple and pink lines show the median estimates of exposure for patients who were giving birth from Model 1, Model 2, Model 3 and Model 4 respectively; shaded areas correspond to 90% credible intervals. The light green, yellow, brown and grey lines show the median estimates of seroprevalence for patients who were giving birth from Model 1, Model 2, Model 3 and Model 4 respectively; shaded areas correspond to 50% credible intervals.

5.4.6 SARS-CoV-2 exposure in pregnant patients at the time of birth rose from half that of the general population to equal that of the general population by late 2020

We next compared cumulative level of exposure among pregnant patients with of the general population of New York City from the same time period. In brief, the levels of exposure in general population were estimated by applying our previously published inference methodology (*36*) to the epidemic data including mortality and seroprevalence in general population of New York City (model fitting and parameter estimation results for the general population can be found in Appendix Figure 19 and Appendix Table 10 respectively). The level of exposure in pregnant patients during April and May of 2020 is estimated to be around half of that in December 2020 in all four models (Figure 5-3 and Figure 5-4). This means that the exposure estimates of pregnant patients approaches that of the general population by November and December of 2020 (Figure 5-4).

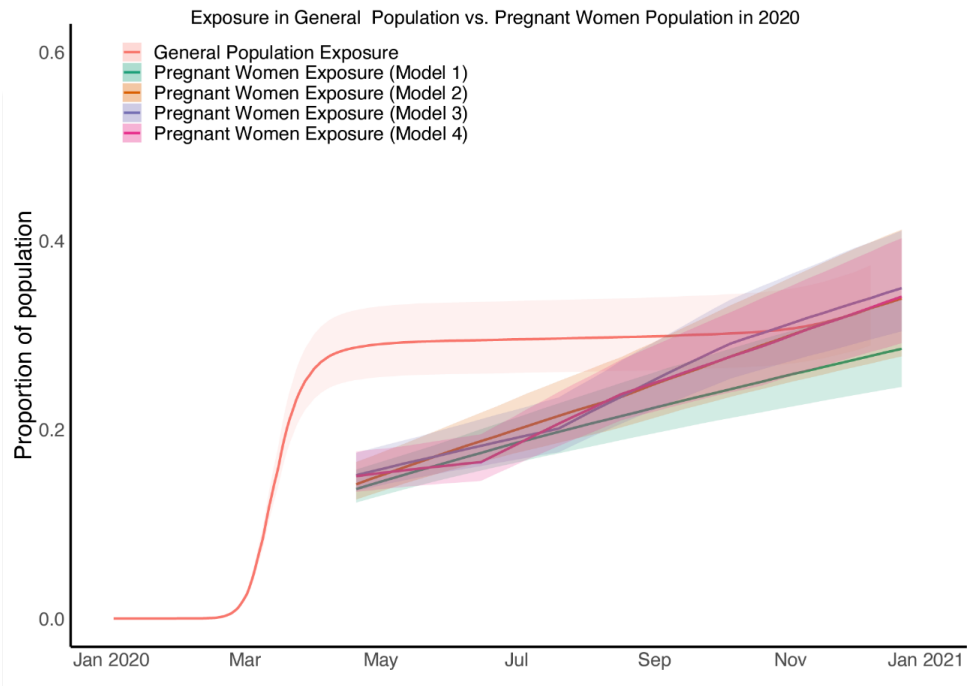

Figure 5-4**.** Comparisons of estimates of exposure in patients who were giving birth from four models and general population.
The red line shows the median estimates of exposure from general population while the shaded areas correspond to the 95% credible interval; the green, yellow, green, blue and pink line shows the median estimates of exposure from Model 1, Model 2, Model 3 and Model 4 for patients who were

giving birth, respectively, while the deep and shadow shaded areas correspond to the 50% credible intervals.

Our model was structured to recapitulate the average course of SARS-CoV-2 infection with turning RT-PCR positive occurring before becoming serology positive. However, not all disease courses follow this linear model structure. It is also possible that the state of pregnancy may alter the susceptibility to SARS-CoV-2 infection, although current evidence does not support that pregnancy increases the susceptibility of infection. In addition, the antibody decaying rate may differ during pregnancy. We should note that the thresholds of seropositive and seronegative assignment might vary between assays, and the performances of assays (including sensitivity and specificity) are different. Our study is not set up for longitudinal follow-up of our cohort, thus our data is not sufficient to evaluate the impact of pregnancy on the antibody decaying rate. While more detailed longitudinal serological data could be collected and modelled during pregnancy, incorporating antibody kinetics into transmission models may hinder the applicability of estimates resulting from different assays (*36*).

In summary, we used a novel model to evaluate SARS-CoV-2 exposure levels in different populations using seroprevalence data and RT-PCR data, comparing exposure levels in pregnant patients in New York City to the levels in the general City population. This permits us to quantify the impact of shielding measures in preventing exposure during pregnancy across the first year of the pandemic. We estimate the impact of self-protection on reducing the level of exposure among pregnant patients during early 2020 who gave birth in this New York City hospital to be approximately 50%. These results, showing time-varying differences in exposure to SARS-CoV-2 in pregnant compared to non-pregnant populations, may have led to significant reduction in maternal morbidity and mortality in the early months of the pandemic. The estimated total exposure in pregnant patients and general population of New York City are both more than double the latest serology positive measurements.

5.5 Discussion

Positive results from RT-PCR testing and serology testing can both be used to identify infected or recently infected individuals. While an infected individual turns RT-PCR positive and then RT-PCR negative within the span of days to a week, a positive serology test result can serve as a maintained marker of infection that last for months. By capturing this dynamic effect of antibody waning in our models, we found that SARS-CoV-2 exposure estimates were much higher than the seroprevalence estimates for our sample of pregnant patients and the general public in New York City. These results confirm that previous studies looking at RT-PCR positive testing rates or seroprevalence alone will substantially underestimate population-level and subgroup exposure to SARS-CoV-2.

We found that patients who gave birth between April and August of 2020 had lower levels of exposure to SARS-CoV-2 compared to the general population. In fact, in the first months of the pandemic (April and May 2020), the exposure levels of pregnant patients were half of the exposure levels of the general population in New York City, and half of the exposure levels in pregnant patients who gave birth by the end of 2020. To understand the possible variables that contribute to this lower exposure level in pregnant patients who gave birth early in 2020, we must take into account the distinctions between the experience of pregnant patients who gave birth in early 2020 vs. late 2020. Patients that gave birth before August 2020—before the level of exposure in pregnant patients became comparable to that of non-pregnant patients—were all at least in their mid to late first trimester by the time that the pandemic hit New York City. This means that most of these patients had a high probability of knowing about their pregnancy at the onset of the pandemic, and it is possible that this knowledge of pregnancy led to behavior changes that made them more cautious than the general population. In contrast, the patients giving birth towards the end of 2020 were not pregnant and/or did not know of their pregnancy before the onset of the pandemic and may

not have behaved differently than the general population; in other words, they could be considered part of general population in early 2020. During the early part of the pandemic, the population only had access to shielding measures and other non-pharmaceutical measures for prevention of disease exposures (since vaccinations only became available for the general population in early 2021). Thus, the reduction of exposure in pregnant patients by about half early in the pandemic may be attributed to effectiveness of shielding measures (Appendix Table 12). Our current data do not address whether pregnant patients (especially those that gave birth early in the pandemic) were more stringent than the general population in following recommendations for behavioral changes and other non-pharmaceutical interventions, or whether they had additional means of improving the efficacy of shielding in preventing exposure. It is less likely that biologic differences from the state of being pregnant contributed to exposure differences as the pregnant patients that gave birth later in 2020 had similar exposures to the general population.

There are some limitations of the pregnant women data. Because of lack of testing kits, some pregnant women who were giving birth from June 2020 to August 2020 were not tested by antibody tests. This might influence the calculation of weekly proportion of pregnant patients in four observed compartments (PCR negative & antibody negative; PCR positive & antibody negative; PCR positive & antibody positive; and PCR negative & antibody positive). Because of the complexity of IgG and IgM kinetics after infection, the model only regards pregnant patients who were IgG or IgM positive as serology positive. This might bias the estimation of the time lag between PCR negative & antibody negative with PCR positive & antibody negative.

Such a high-level reduction of exposure might have been associated with a reduction in infection and especially a reduction of severe COVID-19 illness and, consequently, in mortality in pregnant patients. A large-scale retrospective analysis from a database that

covers about 20% of the American population and includes 406 446 patients hospitalized for childbirth (6380 (1.6%) of whom had COVID-19) compared outcomes for pregnant patients with and without COVID-19 from April–November 2020 (*50*). It concluded that in-hospital maternal death was rare, but rates were significantly higher for patients with COVID-19 (141/100 000 patients, 95% CI 65–268) than for patients without COVID-19 (5/100 000 patients, 95% CI 3.1–7.7). The estimate of maternal death rate is consistent with the study from the UK AAP SONPM registry, where a perinatal maternal mortality rate of 167/100 000 (for patients who have COVID-19 around the time of birth) was estimated(*201, 212*). Further calculation shows that the 40% to 50% reduction on exposure to SARS-CoV-2 estimated by our study might have led to the prevention of 70 (95% CI 26–134) per 100,000 maternal deaths in New York City.

After the period included in our study, additional SARS-CoV-2 preventative measures in the form of vaccinations were introduced in 2021 although strict quarantine regulations were also lifted from the city by then. Pregnant patients were not included in studies testing the safety and efficacy of COVID-19 vaccines. Studies conducted since the start of vaccination distribution including those looking at the real-word implementation of vaccination have confirmed the safety and effectiveness of vaccines specifically for pregnant patients, their placentas, and their neonates (*51, 166, 212-214*). In fact, one study showed that vaccinated pregnant patients had almost 50:1 lower odds of severe COVID-19 infection (*214*). Our data highlights the utility of shielding measures and argues for an integrated intervention as suggested by CDC and NHS guidelines, which includes a combination of vaccination and shielding to reduce the morbidity and mortality of COVID-19 during pregnancy.

Our study has several important strengths, the two most important of which are robust data on a cohort of pregnant patients assessed over an extended period of time tested with both RT-PCR and serology throughout 2020, and the use of a novel model for reproducibly

calculating disease exposure from testing data. While the lacuna in data capture in May and June could potentially influence the performance of parameter inference, varying model assumptions on the force of infection (as detailed in the Section 5.3) found the estimated parameters and level of exposure to be robust and therefore clarified the likely minimal impact caused by missing data. While the pregnant patient population is from a single NYC institution which may not be representative of the broader population, this population allowed for uniformity in testing and the study of a large cohort of patients.

The method developed here can be used to assess whether NPIs can reduce the transmission by comparing the population exposure level before and after the implementation of NPIs in the real world. This should not replace randomized control trials (RCT) for evaluation of NPIs. However, the fact that an intervention is effective does mean it is cost effective. One can use these studies to complete the cost-effectiveness analysis for non-pharmaceutical interventions after estimating the costs of interventions. Also, the study can be extended to estimate the side effect of interventions, such as the disutility.

The evidence of shielding in pregnant women demonstrated the use of NPIs to stop/slow the spread SARS-CoV-2 in a subpopulation within a certain time period. The behaviour among general population is different from pregnant women since they have very different motivations. Also, pregnant women received different pharmaceutical interventions. Therefore, it is not propriate to generalize the results generated from pregnant women to general population. Whether shielding can stop or slow the spread of SARS-CoV-2 in the entire population is an interesting research question and worthy of future study.

Chapter 6 Discussion

Infectious disease epidemics and pandemics remain a threat to global population health. The World Health Organization declared that COVID-19 is no longer a 'global health emergency' on 4 May 2023 more than three years after originally declaring it a pandemic. Around 7 million COVID-19-related deaths have been reported to the WHO in the last three years while the true death toll is estimated to be more than three times higher (*215*). However, uncertainties around emerging variants that cause new surges in cases and deaths mean the transmission of SARS-CoV-2 does in fact remain a global health threat (*216*). Although the COVID-19 pandemic is the most widespread, a wave of other serious infectious disease outbreaks has occurred since the beginning of twenty-first century. The 2003 severe acute respiratory syndrome coronavirus outbreak (*217*), the 2009 swine flu pandemic (*218*), the 2012 Middle East respiratory syndrome coronavirus outbreak (*219*), the 2013–2016 Ebola virus disease epidemic in West Africa (*220*) and the 2015 Zika virus disease epidemic (*221*) all resulted in substantial morbidity and mortality while spreading across borders to infect people in multiple countries (*221*).

How to design and assess mitigating interventions and to minimise the impact of severe diseases during these menacing epidemics and pandemics have become important tasks for decision makers (*222*). To inform policy making, accurate estimation of population exposure by integrating epidemiological datasets collected during the outbreak while modelling its time course is crucial. Serological studies can be used to estimate levels of past exposure and thus position populations in their epidemic timeline but results from such studies need to be interpreted carefully. Several studies following individuals over time after they have had a known infection (prior vaccination) were able to determine that antibodies are only

measurable up to 6–9 months, on average. The immediate implication is that serological studies will inevitably under-estimate the number of people exposed, since some will have a lower antibody count when the study is conducted and will test negative. To circumvent biases introduced by the decay in antibody titers over time, methods for estimating population exposure should account for seroreversion, to reflect those changes in seroprevalence measures which are the net effect of increases due to recent transmission and decreases due to antibody waning.

In this thesis, I develop various mathematical models and applied Bayesian inference 1) to synthesize multiple epidemiological datasets to review the progression of exposed individuals through the various clinical and diagnostic (in both virologic and serologic) stages of infection and recovery; 2) to estimate the time course of exposure to SARS-CoV-2 in the early stage of the COVID-19 pandemic when the population consisted of naïve hosts, well before any vaccination campaign in the general population of England (Chapter 2) and New York City (Chapter 5) and in data-sparse settings (Chapter 3 and Chapter 4); 2) to assess the impact of one non-pharmaceutical intervention, namely shielding, on reducing exposure to the virus among pregnant patients (Chapter 5).

In the remainder of this discussion, I first summarise the studies presented in this thesis, before discussing important areas of ongoing and future research.

6.1 Summary of findings and implications

Levels of SARS-CoV-2 population exposure are considerably higher than suggested by seroprevalence surveys (*36*)

In Chapter 2, I present a clear and simple model to link together three key metrics for evaluating the progress of an epidemic, as applied to the context of SARS-CoV-2 in England: antibody seropositivity, infection incidence and number of deaths. I used data on these three metrics to estimate the antibody seroreversion rate and region-specific infection fatality

ratios. In doing so, the cumulative number of infections in England is estimated. I found that as a consequence of this rapid seroreversion, epidemic progression will result in an increasing gap between measured serology prevalence levels and cumulative population exposure to the virus. Ultimately, this may mean that twice as many, or more, people have been exposed to the virus relative to the number of people who are seropositive, highlighting the importance of the method in aiding the interpretation of serological survey results and their use for informing policy decisions moving forward. Estimates for the IgG (spike) seroreversion rate and infection fatality ratio (IFR) are broadly consistent with other studies, which supports the validity of these findings.

I generalised the methodology presented in Chapter 2 to account for the undocumented COVID-19 related mortality in low- and middle-income countries (LMICs) and for the sparsity of serological measurements in Chapter 4. I then applied it in the context of Afghanistan COVID-19 epidemic and found the population exposure in nine regions of Afghanistan were all higher than the seroprevalence survey suggested by July 2020.

An early pandemic diagnostic tool to reconstruct the first epidemic wave in England with minimal data (*119*)

In Chapter 3, I re-examined and evaluated the model developed in Chapter 2 while reconstructing the first COVID-19 epidemic wave in England, with a focus on how early the model could provide information about prior population exposure and how accurate the model estimate could be as more and more data became available. To approach this, I conducted a series of exercises from three perspectives: validation from the ONS Coronavirus Infection Survey, the relationship between model performance and data abundance and the time-varying case detection rate.

I found that the model I developed can reconstruct the first, unobserved, epidemic wave of COVID-19 in England from March 2020 to June 2020 as long as two or three serological

measurements are added to the model inputs, with the second wave during the winter of 2020 validated by the estimates from the ONS Coronavirus Infection Survey. Specifically, when only two serological measurements were available in each region of England, the estimates of exposure were already highly consistent with those when more serological measurements were added although the credible bands were wider. Additionally, by comparing the model-predicted exposure with the UK government official COVID-19 reported cases, I found that by the end of October 2020 the UK government's official COVID-9 online dashboard reported COVID-19 cases only accounted for less than ten percent of cumulative exposure, dramatically varying across two epidemic waves in England. The testing issue, e.g. the limited capacity of tests and symptom-based testing strategy posed a big challenge for understanding the early pandemic. Viral surveys in the general population can solve the sampling issue, but there remains the problem of not sampling early on. Serological data even from some convenient samples, e.g., blood donors, can help to pin down the progress of the pandemic when antibody decay is teased out.

Shielding among pregnant women during the beginning of COVID-19 pandemic leads to a dramatic real-world effectiveness on reducing exposure to the virus (*121*)

Pregnant patients have increased morbidity and mortality in the setting of SARS-CoV-2 infection. Before the availability of vaccinations, preventative (shielding) measures, including but not limited to wearing a mask and quarantining at home to limit contact, were recommended for pregnant patients. In Chapter 5, I assessed the impact of shielding among pregnant patients by first developing a dynamic model to link universal RT-PCR and antibody testing data from patients who gave birth from April through December 2020 from one institution in New York City and then applying Bayesian inference to estimate exposure among pregnant patients. In comparison with the estimated exposure of the general population in New York City as assessed by the method developed in Chapter 2, I found

that after considering the duration of each pregnancy pre-Covid onset and after, the impact of self-protection on reducing the level of exposure among pregnant patients during early 2020 who gave birth in this New York City hospital were approximately 50%. These results, showing time-varying differences in exposure to SARS-CoV-2 in pregnant compared to non-pregnant populations, may have led to significant reduction in maternal morbidity and mortality in the early months of the pandemic. The estimated total exposure in pregnant patients and general population of New York City are both more than double the latest serology positive measurements.

Shielding was a new intervention introduced by the UK government and also adopted by many other countries in the early day of the COVID-19 pandemic to protect population who were under high risk of severe disease after infections. However, it was also an untested public health policy based on assumptions rather than evidence of effectiveness. These estimates of shielding on reducing exposure among pregnant women presented in Chapter 5 provide important evidence and implications for future public health policy.

The relationship between exposure, serology, and immunity

It is important to note that the rate of decline in neutralizing antibodies, reflective of the effective immunity of the individual, is not the same as the rate of decline in seroprevalence. Antibodies may visibly decline in individuals yet remain above the detection threshold for antibody testing (*126*). Conversely, if the threshold antibody titer above which a person is considered immune is greater than the diagnostic test detection limit, individuals might test positive when in fact they are not effectively immune. The relationship between the presence and magnitude of antibodies (and therefore seropositive status) and protective immunity is still unclear, with antibodies that provide functional immunity only now being discovered (*130*). Furthermore, T cell-mediated immunity is detectable in seronegative individuals and

is associated with protection against disease (*61*). Therefore, the immunity profile for COVID-19 goes beyond the presence of a detectable humoral response.

I believe my methodologies to estimate total exposure levels in different countries and settings offers valuable insights and a solid evaluation metric to inform future health policies (including vaccination) that aim to disrupt transmission.

The population exposure should be interpreted in the context of the different durations of infection- and disease- blocking immunity and cross-reactive responses to other seasonal coronaviruses.

As discussed before, some studies show that the antibody level that is associated with 50% protection against new infection is estimated to be much higher than the antibody level (*43*) that is associated with 50% protection against severe infection (*90*), 28ng ml^{-1} vs 6ng ml^{-1}. This implies that a population with low seroprevalence may nonetheless be protected from severe disease and death due to extended previous exposure to SARS-CoV-2. Because of the 'cellular sensitization without seroconversion' (*64*), T cells mediated cellular immunity may play a very important role in providing protection against disease progression in an early stage of infection without seroconversion, implying that a population with low seroprevalence is still likely to be protected from cellular immunity that may be underestimated by the seroprevalence. Besides, cross-reactive responses to other seasonal coronaviruses can also contribute to a higher population immunity than the virus-specific seroprevalence level. It is important to note that sero-reversion does not prevent the establishment of herd immunity and many other factors including T cell immunity and cross protection from other human coronaviruses may play important roles in understanding population immunity. The indicators of T cells immunity are usually hard to measure compared with B cells immune responses, typically antibodies. Throughout the thesis, I did

not use any measurements directly related with T cells immunity and am not relating the serology and exposure with immunity.

6.2 Ongoing and future research

6.2.1 Using serology data to inform the assessing of the impact of non-pharmaceutical interventions (NPIs) targeted on COVID-19 on other respiratory diseases

During the COVID-19 pandemic, various nonpharmaceutical interventions (NPIs), including mask wearing and social distancing, were the major tools to reduce the transmission of SARS-CoV-2 prior to the development and deployment of vaccines (*197*). At the same time, these interventions have demonstrated a large effect on reducing the transmission of other respiratory pathogens including respiratory syncytial virus (RSV) and influenza (*197*). The US Centers for Disease Control (CDC) reported 2,857 total positive influenza specimens for the 2020/2021 season from combined clinical and public health labs when compared to 229,551 positive specimens in the 2018/2019 season (*223*). In the literature, one study (*224*) has demonstrated that the introduction of NPIs leads to a strong initial reduction in incidence on other respiratory diseases, but this effect is transient: as susceptibility increases, epidemics return while NPIs are in place although the characters of returned epidemics might vary between different basic reproduction number. However, accurate evaluations of these non-pharmaceutical interventions on other respiratory diseases are still missing. To approach this, the competition of these pathogens cannot be neglected when constructing their transmission dynamics in the population (*225*). Disentangling the transmission dynamics of multiple pathogens requires more datasets. Serological measurements can be useful since as discussed in Chapter 1, seroprevalence can best be used to track population exposure after considering antibody decay and has important implications on population immunity. I plan to develop epidemic models to couple

transmission dynamics of multiple respiratory pantheons and to disentangle the impact of NPIs on transmission based on pathogen-specific serological measurements in the population. Besides, it is also very important to note that to take the previous infection or reinfection into account, a full dynamic model with five compartments (S-E-I-R-S) can be helpful

6.2.2 Linking individual-level virologic and serologic kinetics to inform epidemic progression

I developed a compartmental model in Chapter 5 to inform the estimates of exposure by linking virology and serology datasets based on the difference of timing of virologic and serologic kinetics at the population level. In the literature, much progress in quantifying individual-level immunological and pathogen biomarkers e.g., antibody titers and Ct value after COVID-19 infections has been made. One study (*22*) has showed that individual-level viral load measurements from a single cross-sectional sample of RT-qPCR data can accurately estimate an epidemic's trajectory. I plan to revise the model in Chapter 5 to incorporate individual level virologic and serologic titers and then to couple within-host viral and antibody kinetics with population-level dynamics. Some clinical studies also showed that viral kinetics are correlated with antibody kinetics during the infections (*226*) implying that combining these two dynamics might be able to provide extra information for disease progression at the individual level and disease transmission in the population level.

6.2.3 Simulation of population assessments and economic impact of a hypothetical long-acting antibody (LAAB) on a vulnerable population

Although vaccines of COVID-19 have been shown highly safe and effective, approximately 2% of the population including immunocompromised individuals globally cannot mount an adequate immune response to COVID-19 vaccines. Others may not have been fully

vaccinated because of documented adverse reactions to the available vaccines or their components (*227*). To protect this group of vulnerable population, many efforts have been made to develop alternative therapies for prophylaxis, such as Evusheld (*228*) and AZD5156 (*229*). Considering the uncertainty of variants of concern and the timing of the availability of prophylactic therapy in the future, I aim to study a hypothetical long-acting antibody therapy. Although the exact target population of this potential therapy is still uncertain, most of these individuals have been engaging in shielding behaviour during the COVID-19 pandemic (*230*). However, it is unclear whether shielding will continue at current levels, whether or not an alternative prophylactic therapy is available. I plan to assess the potential impact of shielding and the hypothetical therapy given uncertainty of the assignment of the cost of shielding and future shielding behaviour changes.

6.3 Conclusion remarks

In this thesis, focusing on the early stages of the COVID-19 pandemic, I developed a mechanistically informed statistical model, a simple structure with few parameters, to integrate multiple epidemiological datasets and to estimate key epidemiological parameters using Bayesian inference. In doing so, I can estimate the population exposure to SARS-CoV-2. I applied these modelling frameworks in different populations and different settings. Specifically, I first demonstrated the levels of SARS-CoV-2 population exposure are considerably higher than suggested by seroprevalence surveys in the general population of England and New York City after accounting for seroreversion in Chapter 2 and Chapter 5. I derived similar results for the case of Afghanistan after accounting for the undocumented COVID-19 related mortality and sparse measurements of seroprevalence, in Chapter 4. I further described how early in the pandemic these analytic tools are able to reconstruct the first epidemic wave with minimal datasets by limiting the amount of input data and how accurate it could be by comparing with large-scale infection surveys. By comparing the

model-predicted exposure with officially reported cases, I found that by the end of October 2020 the UK government's official COVID-9 online dashboard reported COVID-19 cases only accounted for less than ten percent of cumulative exposure, dramatically varying across two epidemic waves in England. In Chapter 5, I found a dramatic real-world effectiveness of shielding on reducing exposure to SARS-CoV-2 among pregnant patients in New York City after comparing the estimates of exposure in the pregnant patients vs. the general population as assessed using the method in Chapter 2.

Emerging infectious diseases with pandemic potential in human populations will remain a significant threat going forwards. Accurately estimating population exposure has critical ramifications for preparedness plans for potential future epidemic waves. It is particularly challenging to achieve this at the beginning of a pandemic because of the tricky trade-off between sparse knowledge about pathogen and urgent demand about public health decision. The early pandemic diagnostic tools that I have described and developed in this thesis are likely to remain important for understanding epidemic dynamics at different scales and for informing public health decisions.

Appendix Figures and Tables

Appendix Table 1. The effective sample size and the Gelman-Rubin diagnostic for the eight model parameters in the default model (constant infection fatality ratio, IFR).

Parameter	n_{eff}	$\hat{R}$
β	12410	1
γ_{London}	18054	1
$\gamma_{NorthEast}$	29625	1
$\gamma_{SouthEast}$	23952	1
$\gamma_{NorthWest}$	28611	1
$\gamma_{SouthWest}$	22006	1
$\gamma_{Midlands}$	21334	1
γ_{East}	20992	1

Appendix Table 2. The effective sample size and the Gelman-Rubin diagnostic for the 15 model parameters in the time-varying IFR model.

Parameter	n_{eff}	$\hat{R}$	*Parameter*	n_{eff}	$\hat{R}$
β	35229	1	$\eta_{\mathrm{NorthWest}}$	29965	1
γ_{London}	32184	1	$\gamma_{\mathrm{SouthWest}}$	24430	1
η_{London}	26680	1	$\eta_{\mathrm{SouthWest}}$	31047	1
$\gamma_{NorthEast}$	38159	1	$\gamma_{\mathrm{Midlands}}$	31943	1
$\eta_{NorthEast}$	33166	1	η_{Midlands}	27558	1
$\gamma_{SouthEast}$	24036	1	γ_{East}	24703	1
$\eta_{SouthEast}$	24430	1	η_{East}	25506	1
$\gamma_{NorthWest}$	32887	1			

Appendix Table 3. Marginal median parameter estimates and 95% CrI for the time-varying IFR model.

Parameter	*Median (95% CrI)*
β	0.0061 (0.0054-0.0068)
γ_{London}	0.0054 (0.0048-0.0063)
η_{London}	0.30 (0.26–0.60)
$\gamma_{NorthEast}$	0.011 (0.0095–0.012)
$\eta_{NorthEast}$	0.077 (0.0029–0.33)
$\gamma_{NorthWest}$	0.0083 (0.0074–0.0098)
$\eta_{NorthWest}$	0.15 (0.0069–0.51)
$\gamma_{SouthWest}$	0.0094 (0.0086–0.011)
$\eta_{SouthWest}$	0.060 (0.0021–0.26)
$\gamma_{SouthEast}$	0.0013 (0.011-0.017)
$\eta_{SouthEast}$	0.17 (0.0070–0.53)
$\gamma_{Midlands}$	0.0088 (0.0079–0.010)
$\eta_{Midlands}$	0.14 (0.0060–0.42)
γ_{East}	0.0089 (0.0077–0.012)
η_{East}	0.18 (0.0080–0.57)

Appendix Table 4. Summary of sensitivity analyses performed for $\delta_p, \delta_\epsilon$, death inputs and β prior for both constant IFR and time varying IFR models.
Figure 2-2 and Figure 2-3 of the main text were generated using Models 2 and 7 respectively.

Model	δ_p	δ_ϵ	Prior for β	IFR	death input
1	N/A	14	Uniform	Constant	Death certificate
2	N/A	21	Uniform	Constant	Death certificate
3	N/A	28	Uniform	Constant	Death certificate
4	7	14	Uniform	Time-varying	Death certificate
5	7	21	Uniform	Time-varying	Death certificate
6	7	28	Uniform	Time-varying	Death certificate
7	14	21	Uniform	Time-varying	Death certificate
8	14	28	Uniform	Time-varying	Death certificate
9	21	28	Uniform	Time-varying	Death certificate
10	N/A	21	Uniform	Constant	28 days positive death
11	14	21	Uniform	Time-varying	28 days positive death
12	N/A	21	Weibull	Constant	Death certificate
13	14	21	Weibull	Time-varying	Death certificate

Appendix Table 5. Summary of parameter estimates for all models explored as defined in Appendix Table 4.

Parameters	***Model 1, 2, 3***	***Model 4, 5, 6***	***Model 7, 8***	***Model 9***	***Model 10***	***Model 11***	***Model 12***	***Model 13***
β	0.0057 (0.0051,0.0063)	0.0061 (0.0054 ,0.0067)	0.0061 (0.0054,0.0068)	0.0061 (0.0055,0.0069)	0.0052 (0.0046,0.0058)	0.0058 (0.0051,0.0065)	0.0057 (0.0051,0.0063)	0.0062 (0.0055,0.0068)
γ_{London}	0.0049 (0.0046,0.0053)	0.0055 (0.0048,0.0065)	0.0054 (0.0048,0.0062)	0.0053 (0.0048,0.0059)	0.0037 (0.0035,0.0040)	0.0044 (0.0037,0.0050)	0.0049 (0.0046,0.0052)	0.0054 (0.0048,0.0062)
$\gamma_{North\ West}$	0.0080 (0.0073,0.0087)	0.0084 (0.0075 ,0.010)	0.0083 (0.0074,0.0098)	0.0081 (0.0073,0.0092)	0.0063 (0.0058,0.0069)	0.0065 (0.0058,0.0075)	0.0079 (0.0073,0.0086)	0.0082 (0.0074,0.0096)
$\gamma_{North\ East}$	0.010 (0.0095,0.011)	0.011 (0.0095,0.012)	0.010 (0.0095,0.012)	0.010 (0.0094,0.011)	0.0079 (0.0073,0.0086)	0.0079 (0.0071,0.0088)	0.010 (0.0095,0.011)	0.010 (0.0094,0.012)
$\gamma_{South\ East}$	0.012 (0.011,0.013)	0.013 (0.011,0.018)	0.013 (0.011,0.017)	0.012 (0.011,0.015)	0.0082 (0.0075,0.0089)	0.0085 (0.0075,0.011)	0.012 (0.011,0.013)	0.013 (0.011,0.016)
$\gamma_{South\ West}$	0.0094 (0.0087,0.010)	0.0095 (0.0087,0.011)	0.0094 (0.0086,0.011)	0.0093 (0.0085,0.010)	0.0063 (0.0058,0.0067)	0.0062 (0.0057,0.0069)	0.0093 (0.0086,0.010)	0.0094 (0.0086,0.010)
$\gamma_{Midlands}$	0.0085 (0.0079,0.0091)	0.0088 (0.0079,0.010)	0.0088 (0.0079,0.010)	0.0087 (0.0079,0.0098)	0.0067 (0.0062,0.0072)	0.0071 (0.0063,0.0082)	0.0085 (0.0079,0.0091)	0.0087 (0.0079,0.010)
γ_{East}	0.0083 (0.0077,0.0090)	0.0092 (0.0078,0.013)	0.0089 (0.0078,0.012)	0.0086 (0.0076,0.010)	0.0069 (0.0064,0.0075)	0.0072 (0.0063,0.0090)	0.0083 (0.0076,0.0090)	0.0087 (0.0077,0.011)
η_{London}	N/A	0.28 (0.021,0.57)	0.32 (0.028,0.62)	0.38 (0.033,0.68)	N/A	0.54 (0.14,0.79)	N/A	0.33 (0.033,0.62)
$\eta_{North\ West}$	N/A	0.17 (0.0086,0.56)	0.15 (0.0059,0.49)	0.13 (0.0058,0.46)	N/A	0.14 (0.0057,0.49)	N/A	0.15 (0.0061,0.49)
$\eta_{North\ East}$	N/A	0.084 (0.0029,0.35)	0.074 (0.0031,0.31)	0.073 (0.0030,0.31)	N/A	0.076 (0.0028,0.32)	N/A	0.075 (0.0031,0.32)
$\eta_{South\ East}$	N/A	0.19 (0.0084,0.58)	0.17 (0.0069,0.53)	0.14 (0.0064,0.47)	N/A	0.15 (0.0071,0.50)	N/A	0.16 (0.0068,0.51)
$\eta_{South\ West}$	N/A	0.066 (0.0025,0.29)	0.058 (0.0020,0.25)	0.053 (0.0020,0.24)	N/A	0.058 (0.0022,0.25)	N/A	0.057 (0.0022,0.26)
$\eta_{Midlands}$	N/A	0.14 (0.0067,0.42)	0.40 (0.0064,0.13)	0.14 (0.0065,0.43)	N/A	0.23 (0.014,0.55)	N/A	0.14 (0.0070,0.43)
η_{East}	N/A	0.21 (0.0096,0.62)	0.19 (0.0085,0.57)	0.16 (0.0071,0.51)	N/A	0.16 (0.0062,0.54)	N/A	0.18 (0.0078,0.55)

Appendix Table 6. Linear regression models exploring relationships between demographic and epidemiological factors and estimated regional IFRs.
Each row refers to a unique linear regression model and indicates which covariate was used, alongside the resulting slope and intercept estimates (with accompanying 95% CIs) and p-value.

Independent Variable	Slope	Intercept	p-value
Proportion of people over 45 years of age	0.0382 [0.00292, 0.0735]	-0.00819 [-0.0239, 0.00751]	0.0388
Proportion of people over 60 years of age	0.0440 [0.000193, 0.0879]	0.001936 [0.0127, 0.00880]	0.0493
Deaths in the community relative to deaths in care homes	-0.000787 [-0.00128, -0.000290]	0.0125 [0.00987, 0.0151]	0.00962
Care home beds per 100 people over 75 years of age	0.00147 [0.000220, 0.00272]	-0.00450 [-0.0168, 0.00677]	0.0293
Diabetes prevalence	-0.000587 [-0.00574, 0.00457]	0.0128880 [-0.0236, 0.0494]	0.781
Chronic liver disease mortality (per 100,000)	8.81e-05 [-0.000650, 0.000826]	0.00764 [-0.00187, 0.0172]	0.771
Chronic obstructive pulmonary disease mortality (per 100,000)	1.28e-05 [-0.000235, 0.000261]	0.00810e-03 [-0.00461, 0.0208]	0.899

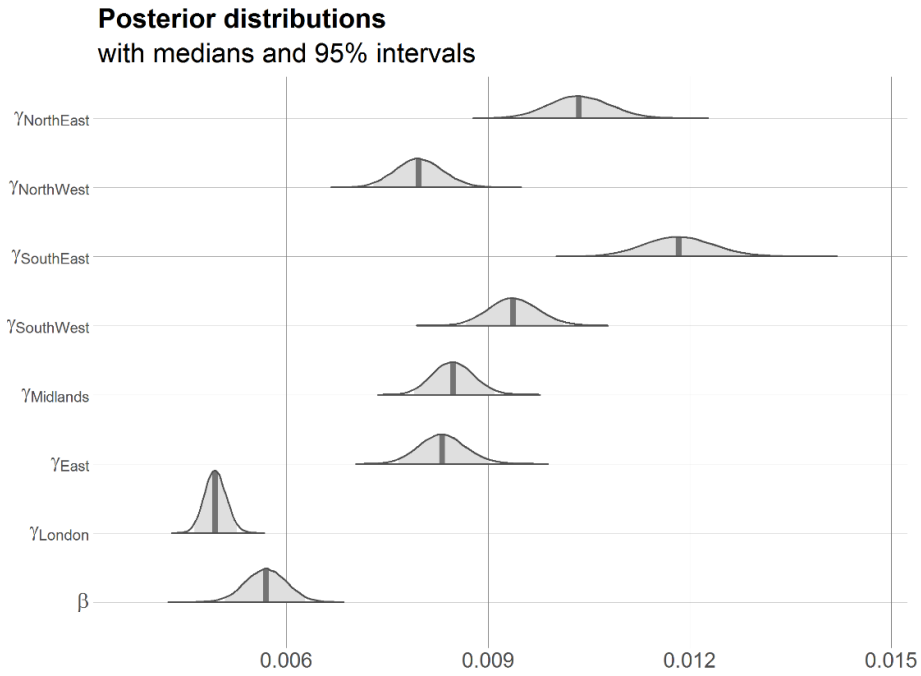

Appendix Figure 1. Marginal posterior distributions for parameters in the constant IFR model. The vertical lines show the median distributions, and the grey shaded regions show the 95% CrI.

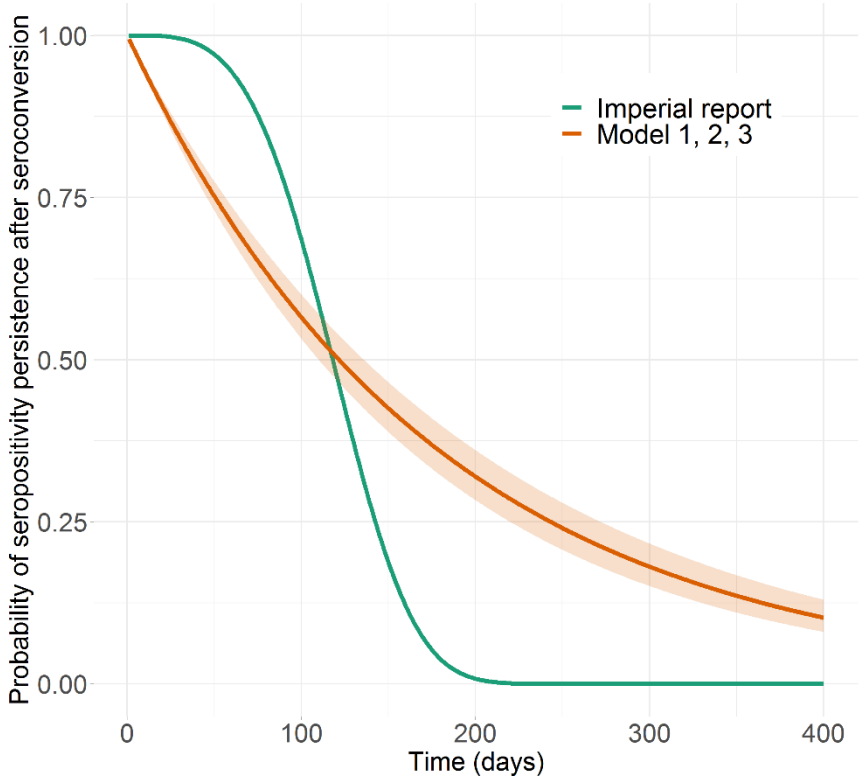

Appendix Figure 2. Probability of seropositivity persistence after seroconversion.
The green curve shows the probability curve from (*110*) and the orange curve gives the median probability curve for Models 1, 2 and 3 in our study within the corresponding 95% credible intervals defined by the shaded area. See Appendix Table 4 for details on each model's assumptions.

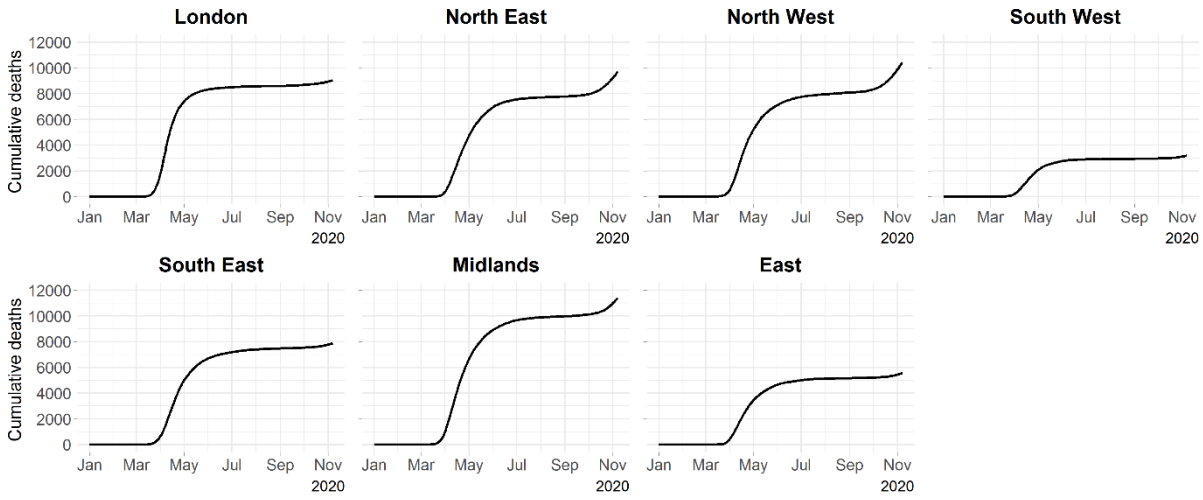

Appendix Figure 3. Cumulative deaths in the seven regions of England.

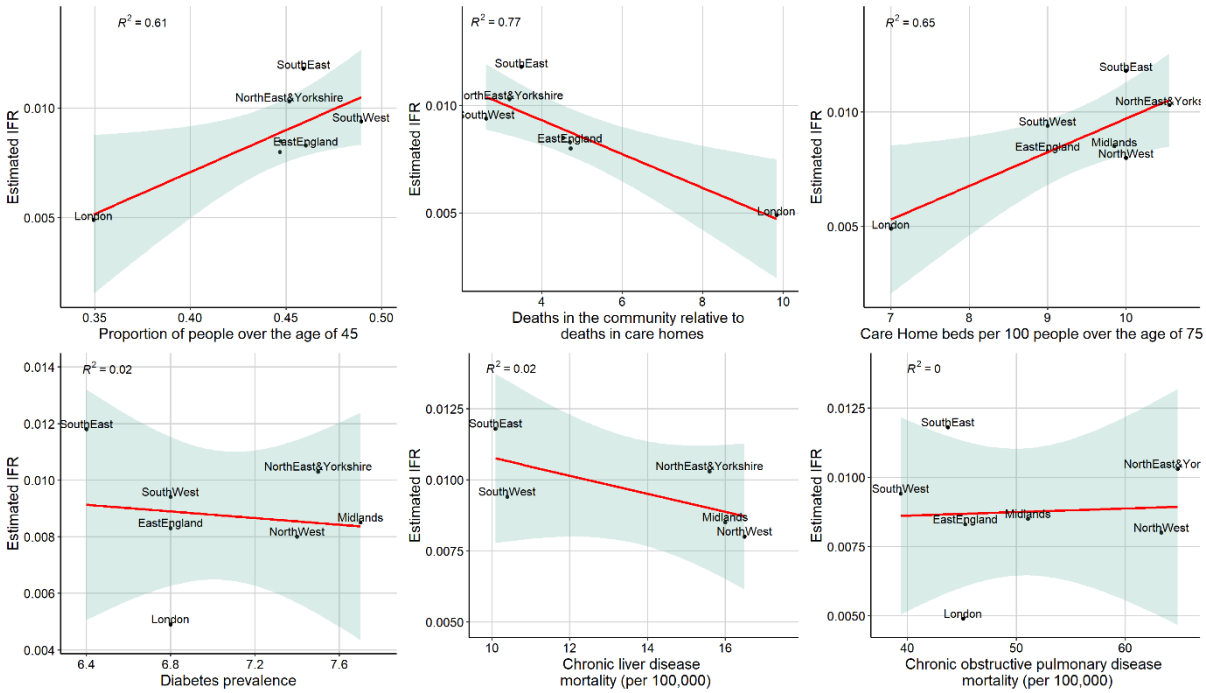

Appendix Figure 4. Relationship between demographic and epidemiological factors and estimated regional IFRs.

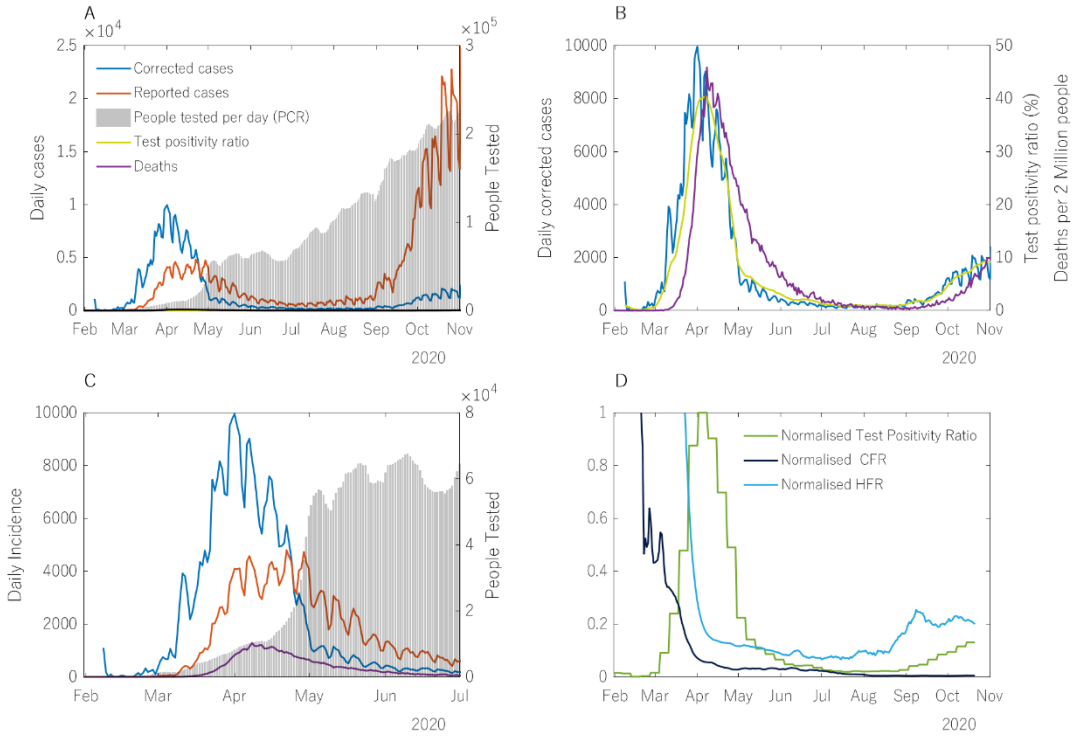

Appendix Figure 5. Relevant epidemiological metrics in England over the course of the pandemic. (A) Daily COVID-19 cases and tests in England from Feb 5th 2020 to Nov 7th, 2020, alongside the testing effort corrected case curve. Case correction was done by taking the number of daily tests done on May 1st and extrapolating the number of daily cases that would be reported if the testing effort had been constant over time, i.e., how many daily cases would be reported if 20,000 tests has been done every day. (B) Comparison of testing effort corrected case incidence (blue), test positivity ratio (yellow) and daily deaths per 2 million people (purple). (C) Daily reported incidence of cases, deaths and people tested up to July 1st, 2020. Note the different scale for mortality data used on panels (B) and (C). In panel (C) we present the absolute number of deaths reported per day as a means of comparing its scale to the reported case data. In panel (B) we modify the mortality incidence scale to more easily compared its shape over time against that of the daily corrected cases and test positivity ratio curves. (D) Normalized case fatality ratio (CFR), hospital fatality ratio (HFR) and RT-PCR test positivity ratio (yellow, blue, and green lines, respectively). We assumed fixed time lags of $\delta_p = 14$ days between RT-PCR testing and death and $\delta_h = 12$ days between RT-PCR testing and hospitalization.

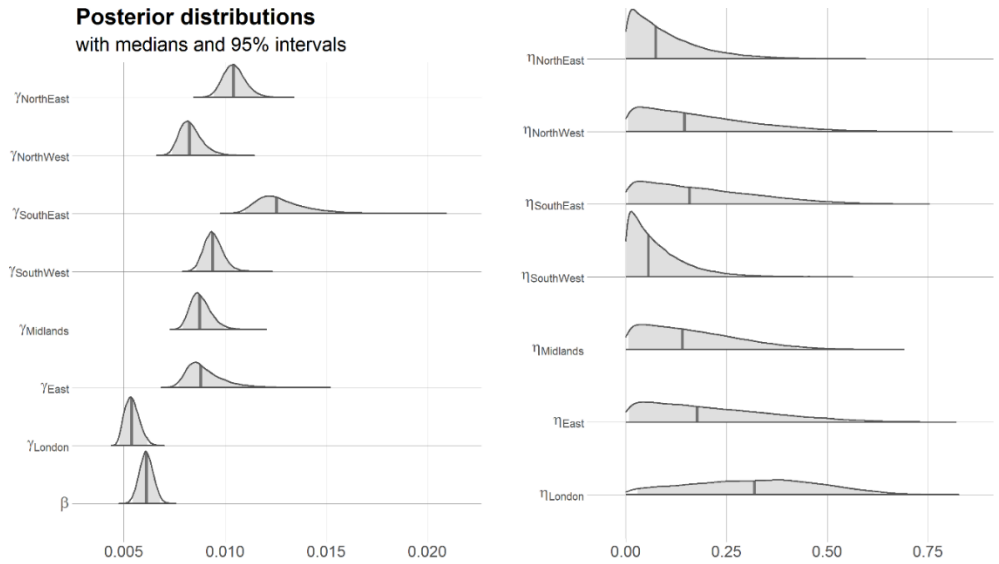

Appendix Figure 6. Marginal posterior distributions for parameters in the time-varying IFR model. The vertical lines show the median distributions, and the grey shaded regions show the 95% CrI.

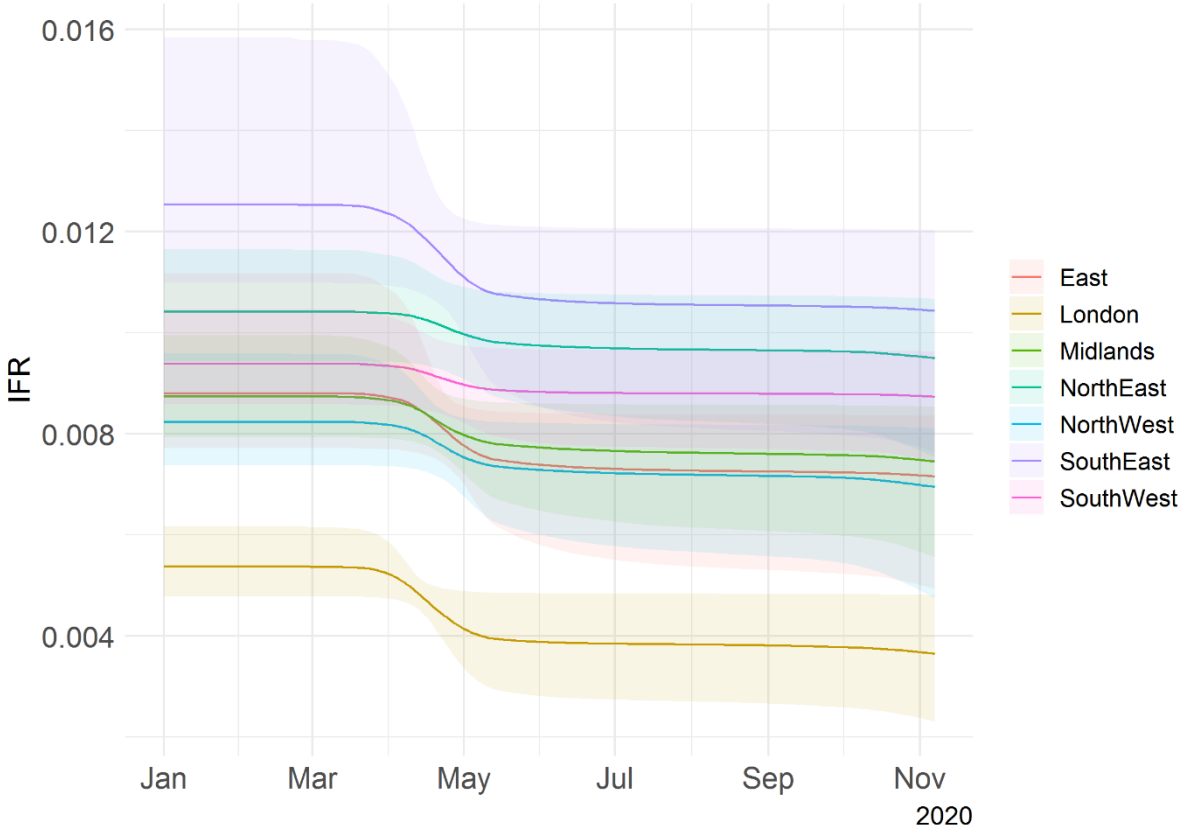

Appendix Figure 7. Posterior predictive distribution of the time-varying IFR. The solid lines show the medians and the shaded regions show the 95% CrI.

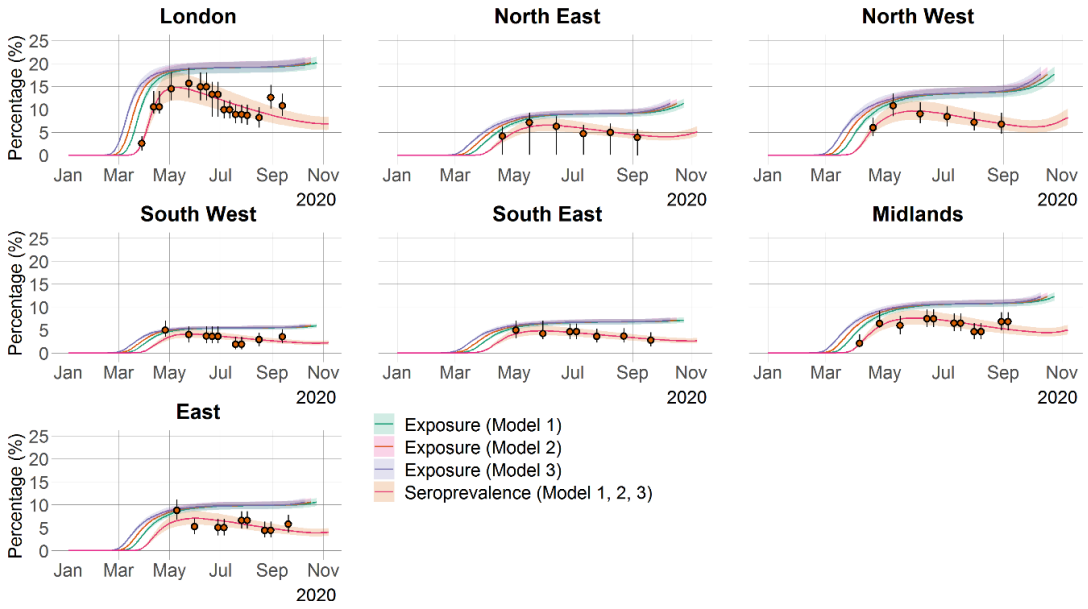

Appendix Figure 8. Comparison of the time course of the SARS-CoV-2 pandemic up to 7 November 2020 for the seven regions in England.
The figure is based on the constant IFR model, given δ_p as 2 weeks and δ_ϵ as 2, 3 and 4 weeks. The orange solid circles and black error bars in each regional panel represent the observed seroprevalence data and their credible intervals after adjusting for the sensitivity and specificity of the antibody test. The green, red and purple lines show the median constant IFR model predictions for exposure assuming δ_ϵ as 2, 3 and 4 weeks, respectively, while the shaded regions correspond to the 95% CrI. The green lines show the median constant IFR model predictions for seroprevalence while the shaded regions correspond to the 95% CrI. See Appendix Table 4 for details on each model's assumptions.

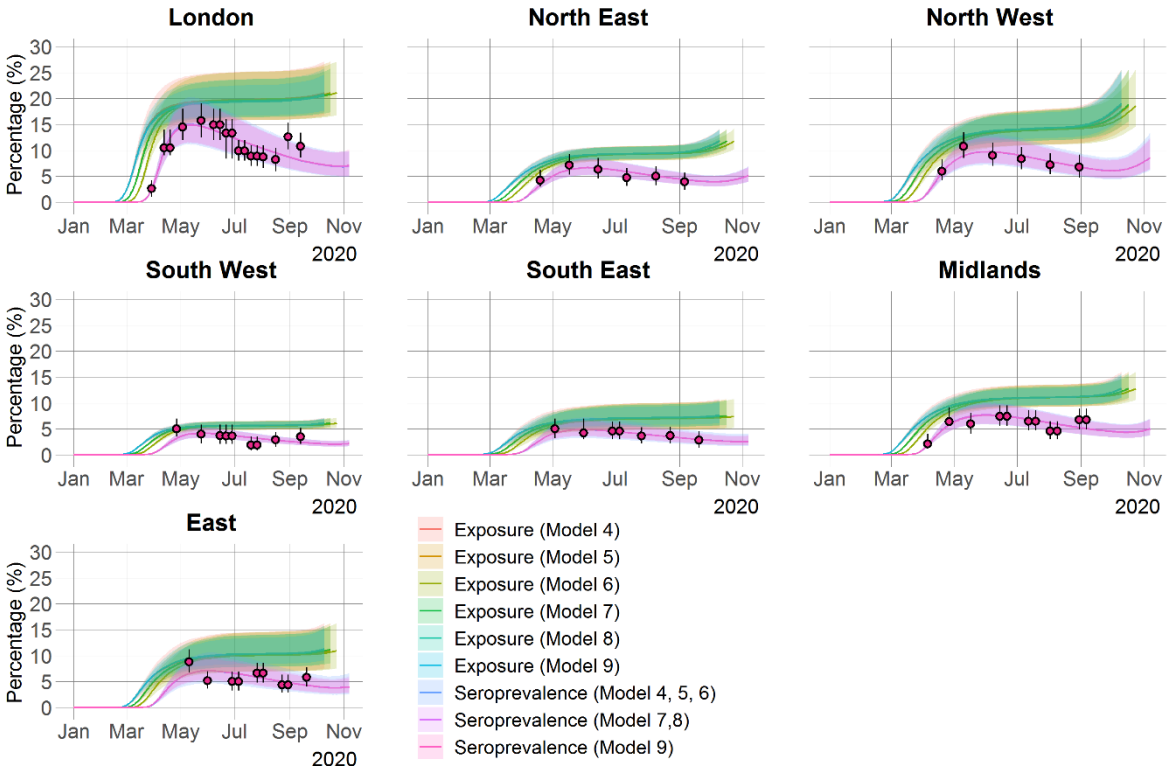

Appendix Figure 9. Comparison of time course of the SARS-CoV-2 pandemic up to 7 November 2020 for the seven regions in England for the time-varying IFR model.
The figure is generated by giving δ_p as 2 weeks and δ_ϵ as 2, 3 and 4 weeks. The orange solid circles and black error bars in each regional panel represent the observed seroprevalence data and their credible intervals after adjusting for the sensitivity and specificity of the antibody test. The lines in red, green, and blue tones show the median constant IFR model predictions for exposure assuming δ_ϵ as 2, 3 and 4 weeks, respectively, while the shaded regions correspond to their 95% CrI. The purple lines show the median constant IFR model predictions for seroprevalence while the shaded regions correspond to the 95% CrI. See Appendix Table 4 for details on each model's assumptions.

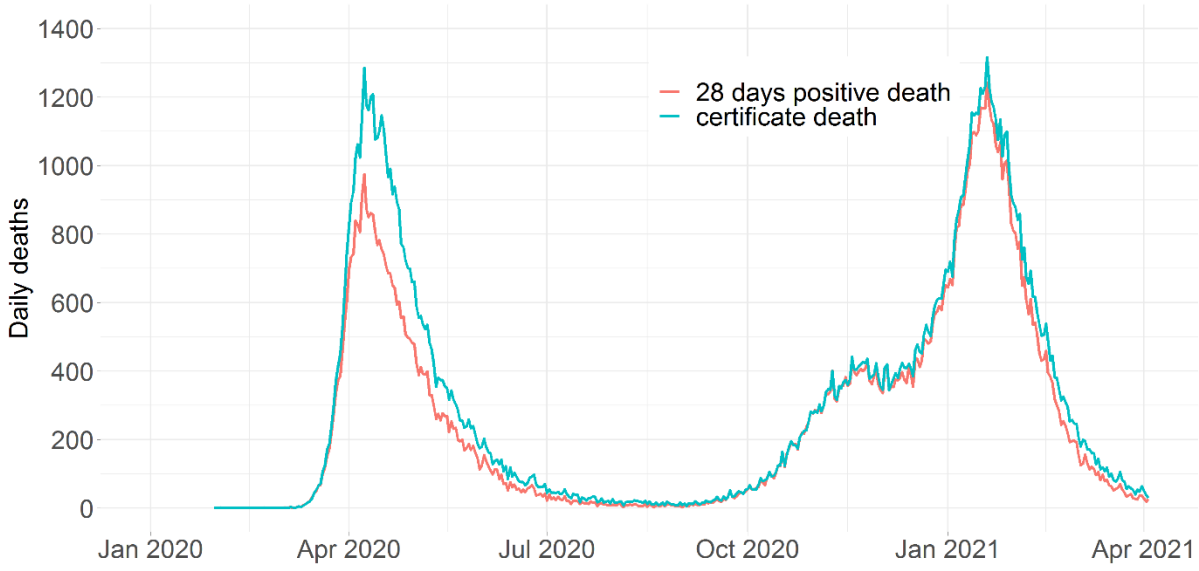

Appendix Figure 10. Daily deaths with COVID-19 on the death certificate and deaths within 28 days of positive test by date of death.

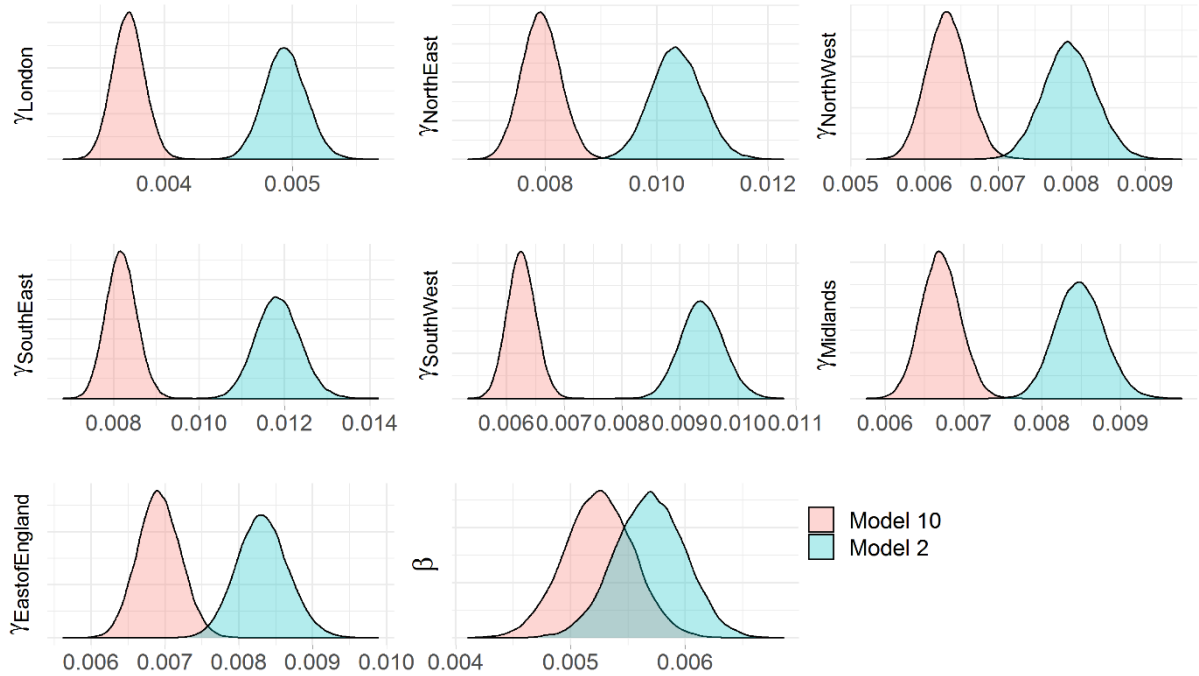

Appendix Figure 11. Comparison of marginal posterior distributions for estimated parameters in the constant IFR model.
The red regions show the posterior distributions for parameters using deaths within 28 days of positive test as model inputs while the blue regions show the posterior distributions of parameters using death certificate data as model inputs. See Appendix Table 4 for details on each model's assumptions.

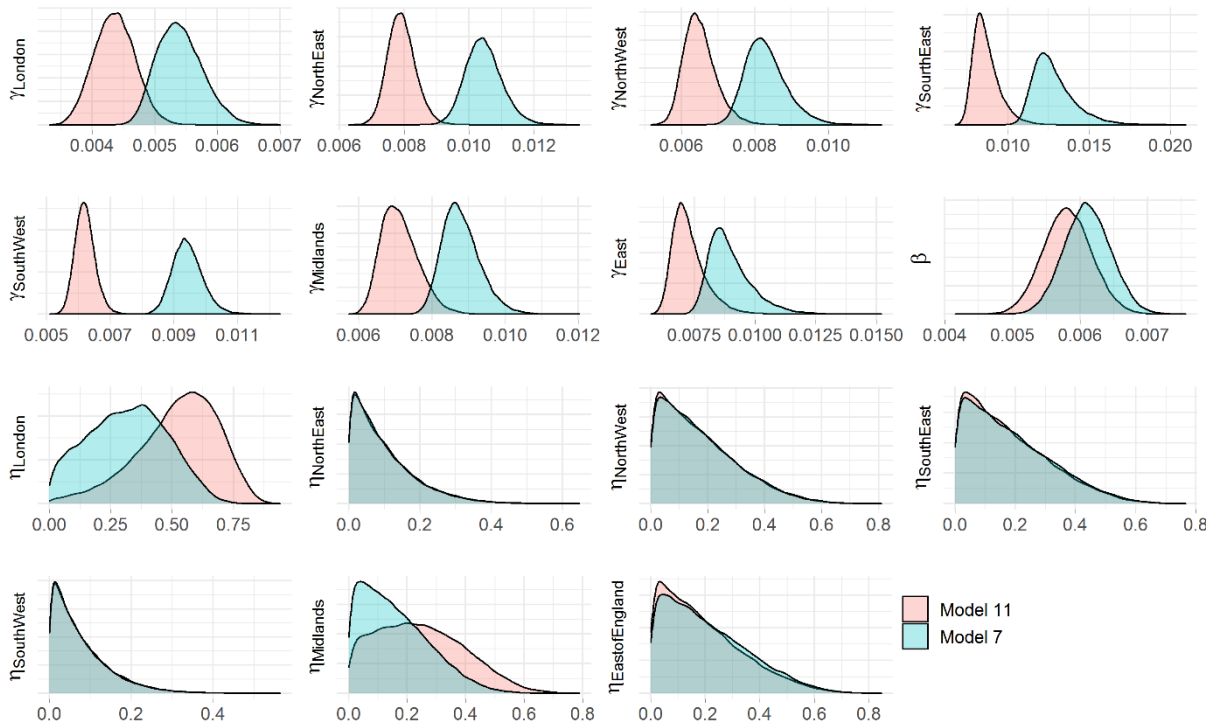

Appendix Figure 12. Comparison of marginal posterior distributions for estimated parameters in the time varying IFR model.
The red regions show the posterior distributions for parameters using deaths within 28 days of positive test as model inputs while the blue regions show the posterior distributions of parameters using death certificate data as model inputs. See Appendix Table 4 for details on each model's assumptions.

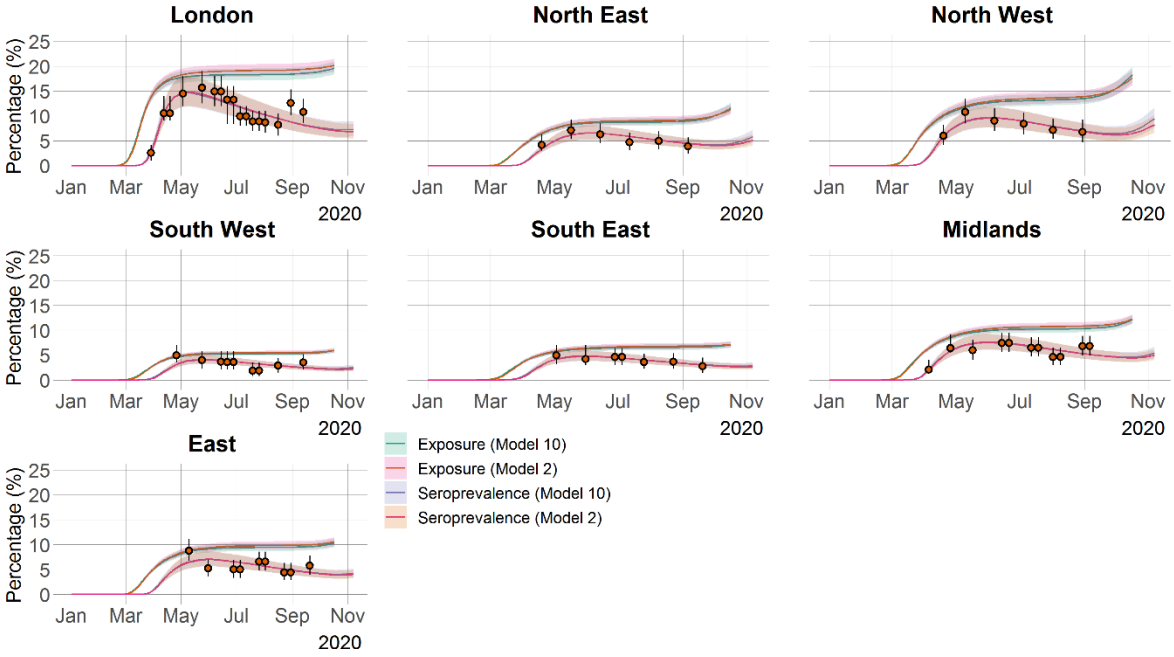

Appendix Figure 13. Comparison of the time course of the SARS-CoV-2 pandemic up to 7 November 2020 for the seven regions in England for the constant IFR model between using death within 28 days of a positive COVID-19 test and death certificate data as model inputs.
The solid orange circles and black error bars in each regional panel represent the observed seroprevalence data and their credible intervals after adjusting for the sensitivity and specificity of the antibody test. The green and pink lines show the median constant IFR model predictions for exposure using death within 28 days of a positive test and death certificate data as model inputs, respectively, while the shaded regions correspond to the 95% CrIs. The purple and orange lines show the median constant IFR model predictions for seroprevalence using death within 28 days of a positive and death certificate data as model inputs, respectively, while the shaded regions correspond to the 95% CrIs. See Appendix Table 4 for details on each model's assumptions.

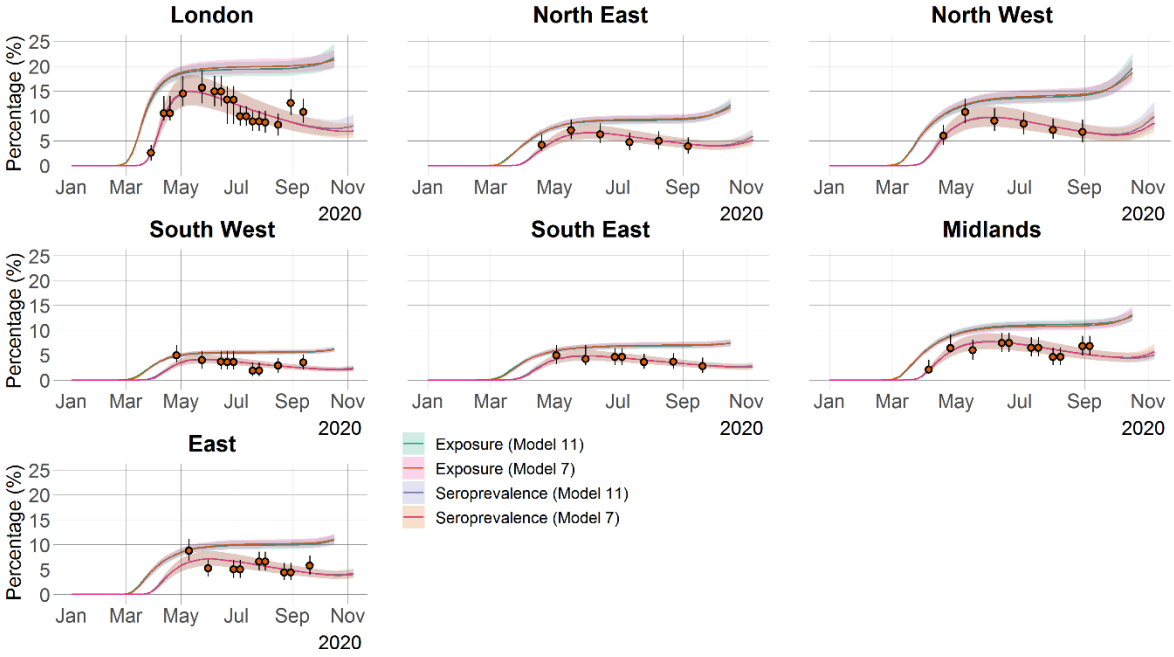

Appendix Figure 14. Comparison of the time course of the SARS-CoV-2 pandemic up to 7 November 2020 for the seven regions in England for the time-varying IFR model between using death within 28 days of a positive COVID-19 test and death certificate data as model inputs.
The solid orange circles and black error bars in each regional panel represent the observed seroprevalence data and their credible intervals after adjusting for the sensitivity and specificity of the antibody test. The green and pink lines show the median constant IFR model predictions for exposure using death within 28 days of a positive test and death certificate data as model inputs, respectively, while the shaded regions correspond to the 95% CrIs. The purple and orange lines show the median constant IFR model predictions for seroprevalence using death within 28 days of a positive and death certificate data as model inputs, respectively, while the shaded regions correspond to the 95% CrIs. See Appendix Table 4 for details on each model's assumptions.

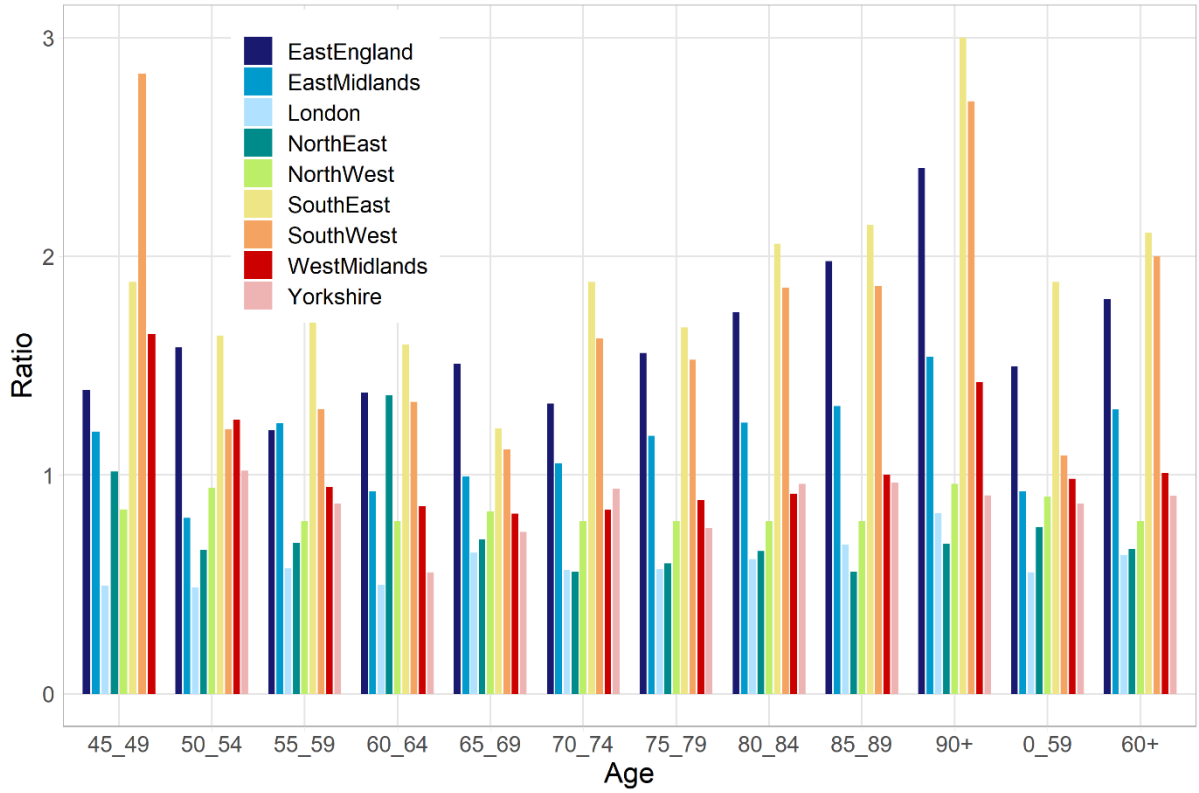

Appendix Figure 15. Ratio between relative rates of deaths of people who died within 28 days of their first positive test (per 100,000 population) in the winter wave of 2020 vs. the 2020 spring wave. A ratio greater than 1 means that the age specific rate of death was greater in the winter wave than in the preceding spring wave, and vice-versa.

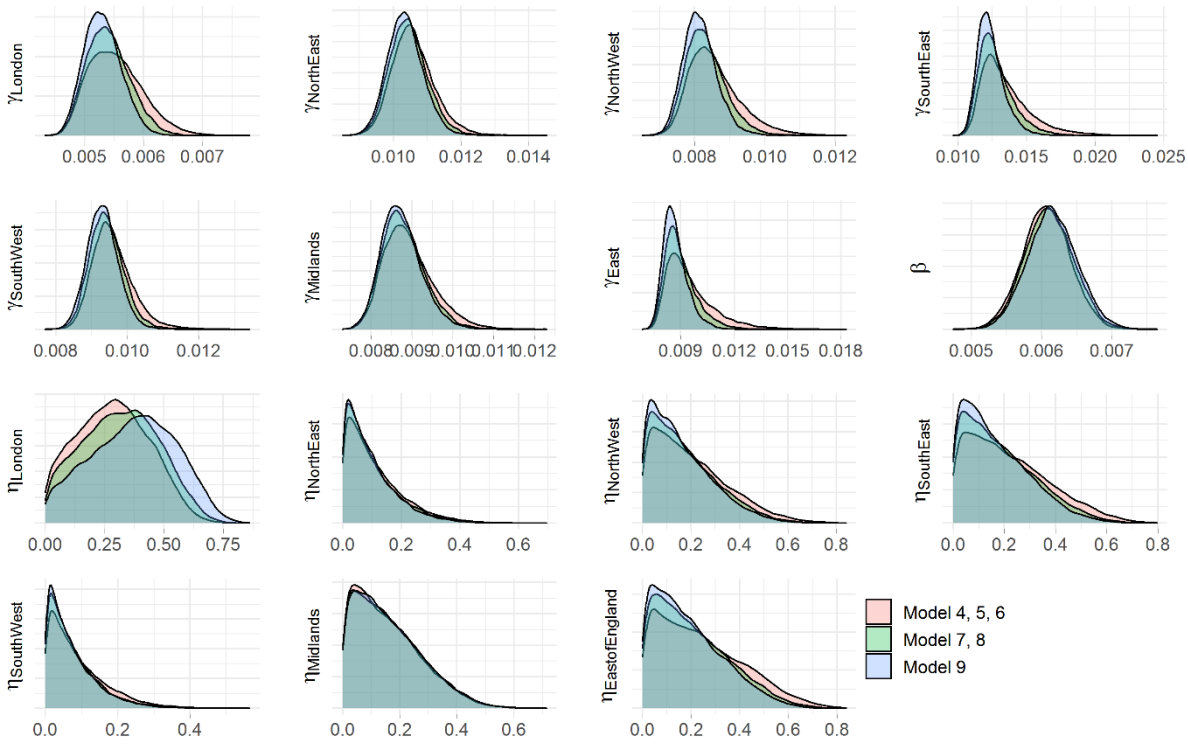

Appendix Figure 16. Comparison of parameter posterior distributions for the time-varying IFR model.
The figure uses δ_p as 7 days (Models 4, 5 and 6), 14 days (Models 7 and 8) and 21 days (Model 9). See Appendix Table 4 for details on each model's assumptions.

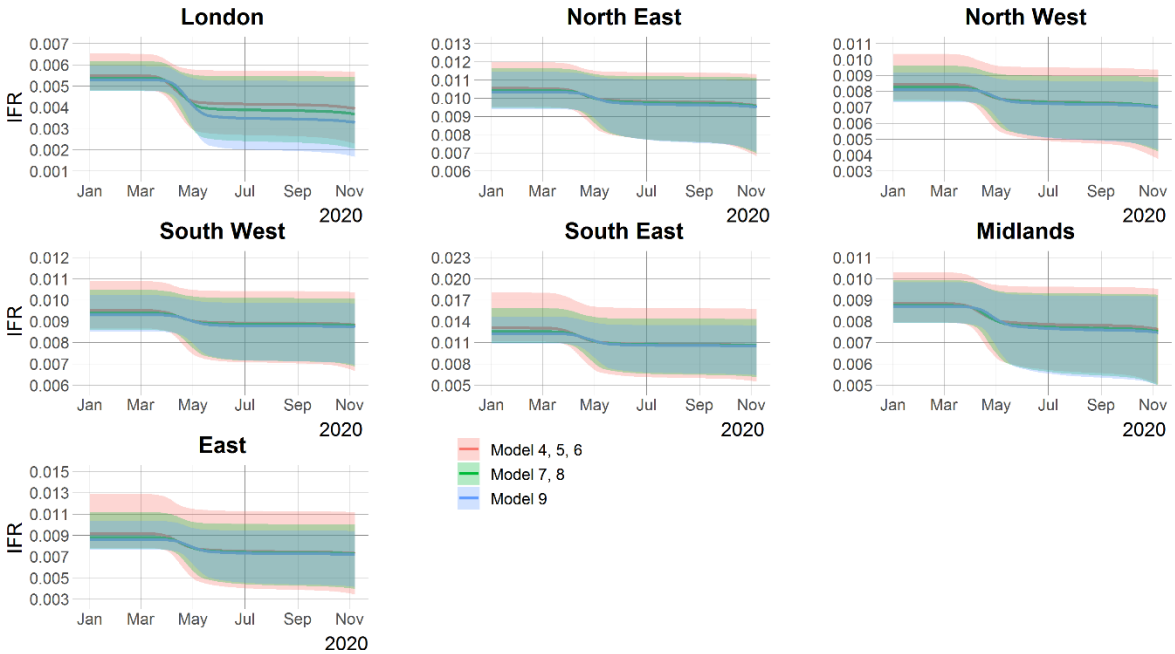

Appendix Figure 17. Comparison of IFR estimates for seven regions in England for time-varying IFR model.
The figure uses δ_p as 7 days (Models 4, 5 and 6; see Appendix Table 4 for definitions of the different Models), 14 days (Models 7 and 8) and 21 days (Model 9). See Appendix Table 4 for details on each model's assumptions.

Appendix Table 7. Sample size for the regional serology survey

Region	Sample size
Kabul	1104
Central	1056
Central highlands	902
East	1233
North	1071
South	738
North-east	1265
South-east	969
West	1176

Appendix Table 8. Characteristics of respondents

Respondents' characteristics	**Number**	**Percentage**
Total respondents	9514	100%
Sex		
Male	5128	53.9%
Female	4386	46.1%
Age		
5–17 years	4346	45.7%
18 years or more	5168	54.3%
Geographical area		
Urban	2574	27%
Rural	6940	73%
Region		
Kabul	1104	11.6%
Central	1056	11.1%
Central highlands	902	9.4%
East	1233	13.0%
North	1071	11.2%
South	738	7.8%
North-east	1265	13.3%
South-east	969	10.2%
West	1176	12.4%

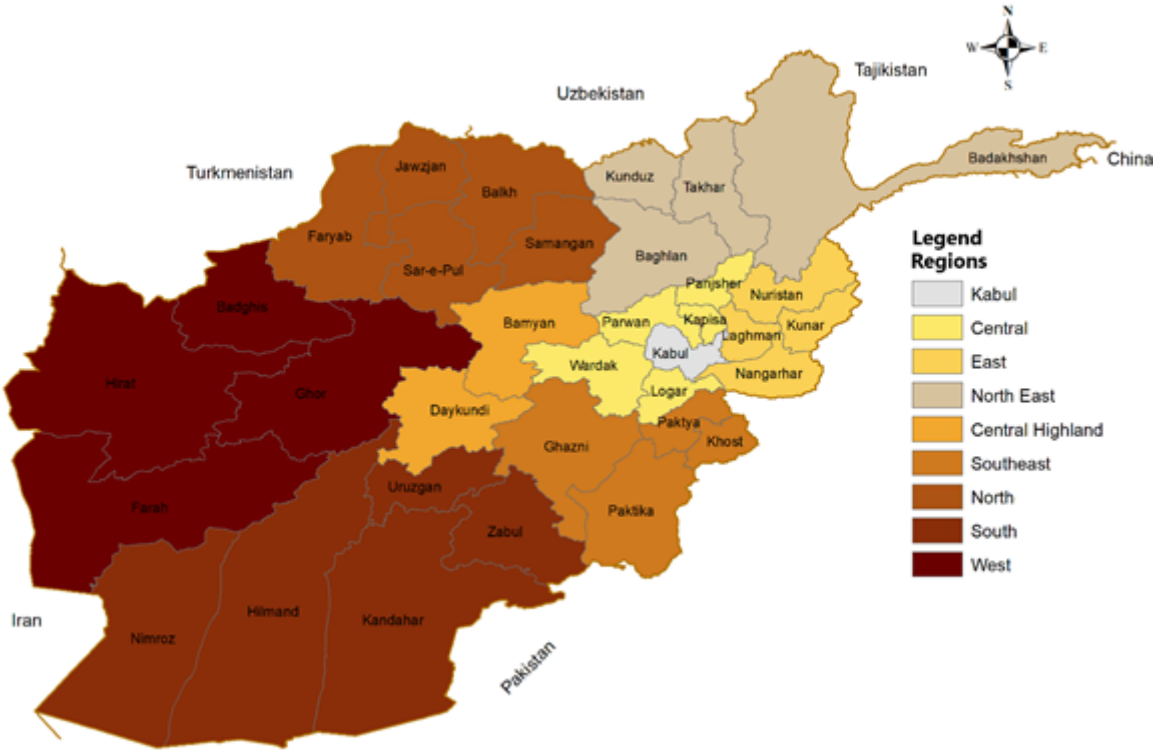

Appendix Figure 18. A map showing the nine regions in Afghanistan where the study was conducted (the eight regions of Afghanistan plus Kabul province).

Appendix Table 9. A list of parameters, definitions and priors used in the Bayesian inference in the model of pregnant patients and general population.

Parameter category	Symbol	Definition	Prior	Units	Range
Pregnant patients	λ_τ	force of infection of pregnant patients; 1 / (average time to challenge by the virus for pregnant patients)	uniform (0,1)	week^{-1}	[0,1]
	τ	1 / (average time lag between virus detection and antibody detection)	gamma (4,3)	week^{-1}	[0,5]
	σ	1 / (average time lag between middle infection and past infection)	uniform (0,1)	week^{-1}	[0,1]
	β	antibody decaying rate in pregnant patients	uniform (0,1)	na	[0,1]
	y_{00}	proportion of people who are never exposed yet by April 20th, 2020	beta (8,2)	na	[0,1]
	k_{01}	tool parameter in the initial condition reparameterization	uniform (0,1)	na	[0,1]
	k_{11}	tool parameter in the initial condition reparameterization	uniform (0,1)	na	[0,1]
	k_{10}	tool parameter in the initial condition reparameterization	uniform (0,1)	na	[0,1]
General population	α	infection fatality ratio for general population	uniform (0,1)	na	[0,1]
	ω	antibody decaying rate in general population based on ELISA test (*231*).	uniform (0,1)	na	[0,1]

Appendix Table 10. Posterior estimates of parameters in general population.

Parameter(unit)	Definition	Median	2.5%	97.5%
α (-)	Infection fatality ratio among general population	0.0077	0.0067	0.0087
ω^{-1}(days)	1/antibody decaying rate among general population	209	152	333

Appendix Table 11. The effective sample size and the Gelman-Rubin diagnostic for the four models.

Parameter	Model	n_{eff}	$\hat{R}$	Parameter	Model	n_{eff}	$\hat{R}$
τ	1	9902	1	k_{10}	1	9954	1
	2	7876	1		2	8854	1
	3	9516	1		3	11699	1
	4	8251	1		4	8544	1
σ	1	10448	1	k_{11}	1	13671	1
	2	8744	1		2	13344	1
	3	11928	1		3	13863	1
	4	8241	1		4	10818	1
β	1	9982	1	λ_{11}	1	10128	1
	2	8005	1	λ_{21}	2	9273	1
	3	9154	1	λ_{22}		8502	1
	4	7953	1	λ_{31}	3	10948	1
y_{00}	1	9330	1	λ_{32}		9698	1
	2	10350	1	λ_{33}		9549	1
	3	8152	1	λ_{41}	4	12655	1
	4	5675	1	λ_{42}		7391	1
k_{01}	1	19436	1	λ_{43}		7333	1
	2	19826	1	λ_{44}		7116	1
	3	19595	1				
	4	17016	1				

Appendix Table 12. Estimation of effectiveness of shielding from the four models.

Model	Estimation of effectiveness of shielding (95% CrI)
Model 1	53.4% (23.5%, 72.1%)
Model 2	52.0% (16.4%, 71.1%)
Model 3	48.4% (11.4%, 67.8%)
Model 4	47.3% (6.1%, 67.5%)

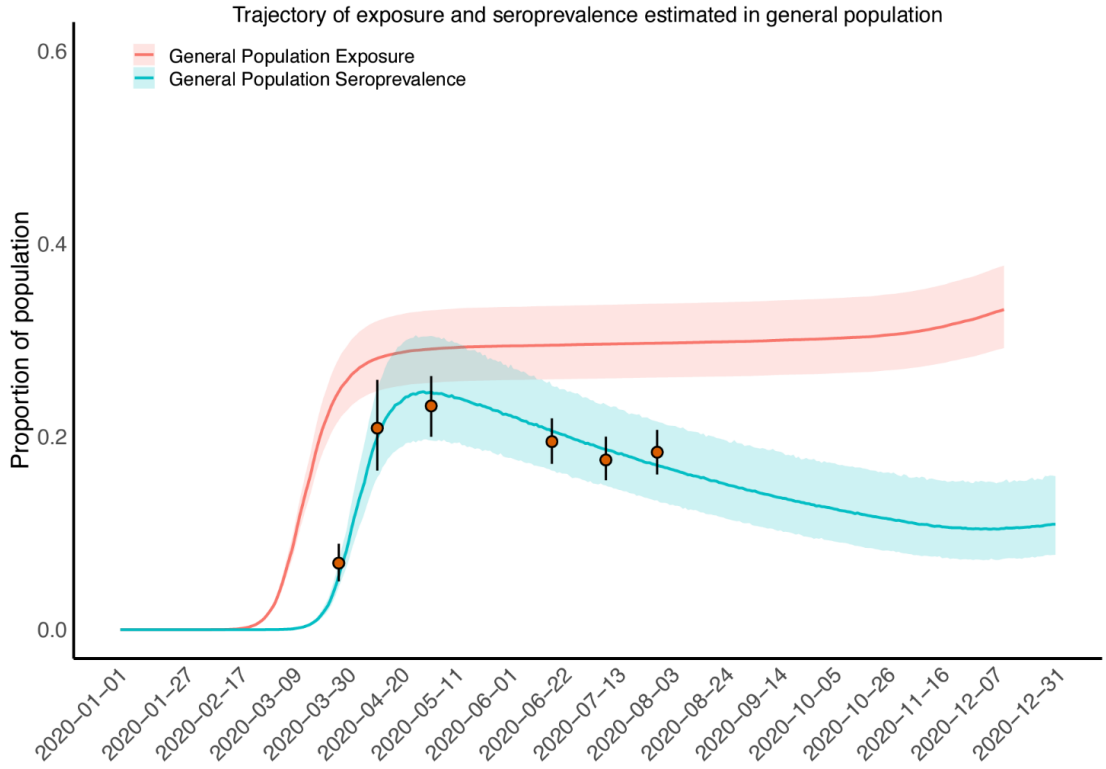

Appendix Figure 19. Time course of the SARS-CoV-2 infection among general from January 1st, 2020 to December 31st, 2020.
The orange solid circles and black error bars represent the measured seroprevalence and their credible intervals respectively. The blue and orange lines show the median of predictions of seroprevalence and exposure among general population in New York City, while the shaded areas correspond to the 95% credible intervals.

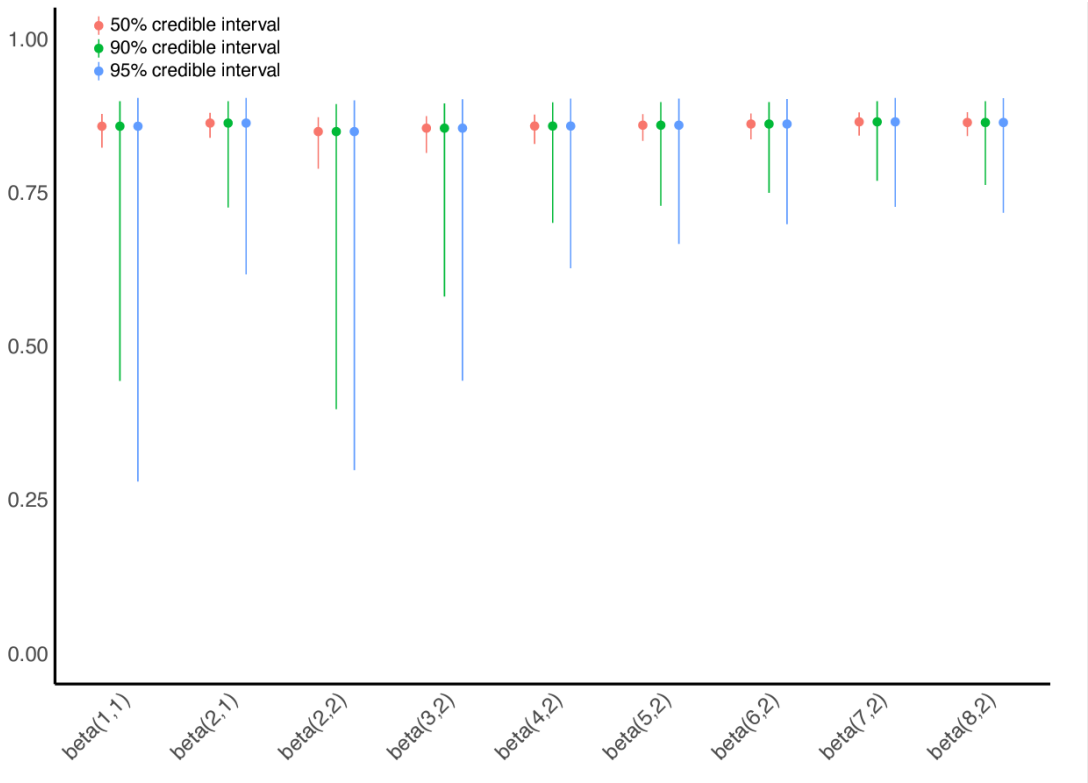

Appendix Figure 20. Comparisons of posteriors with different significant levels (50%, 90% and 95%) for the proportion of pregnant patients who were not exposed previously by 20 April 2020.

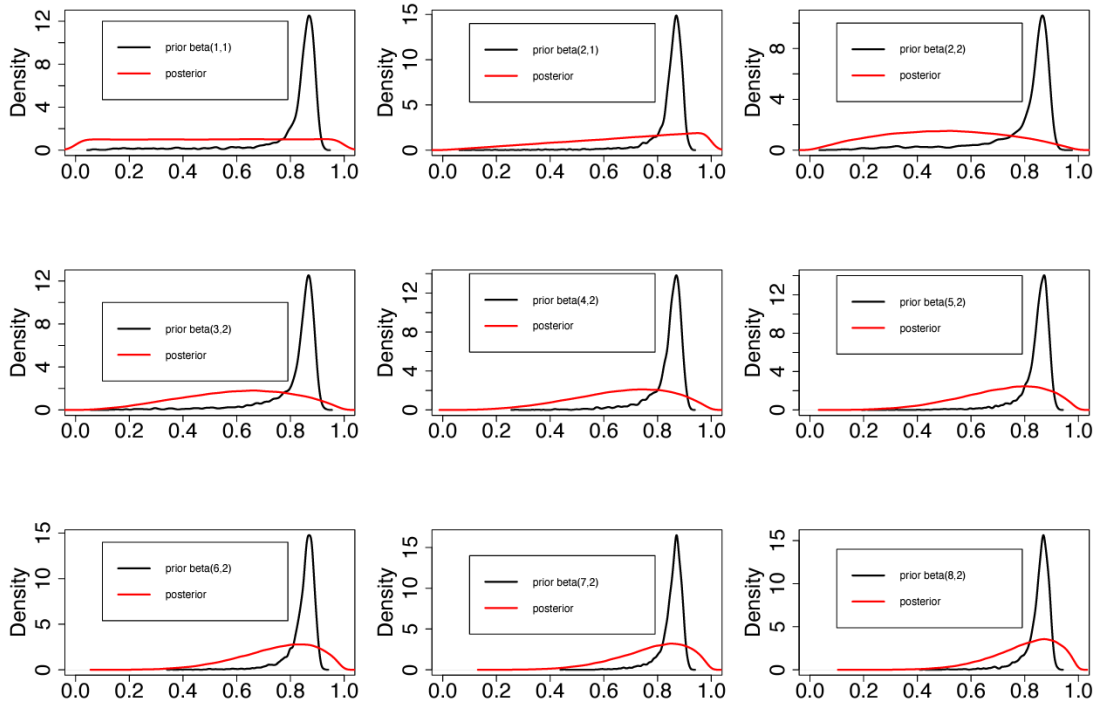

Appendix Figure 21. Comparisons of priors and posteriors for the proportion of pregnant patients who were not exposed previously by 20 April 2020.

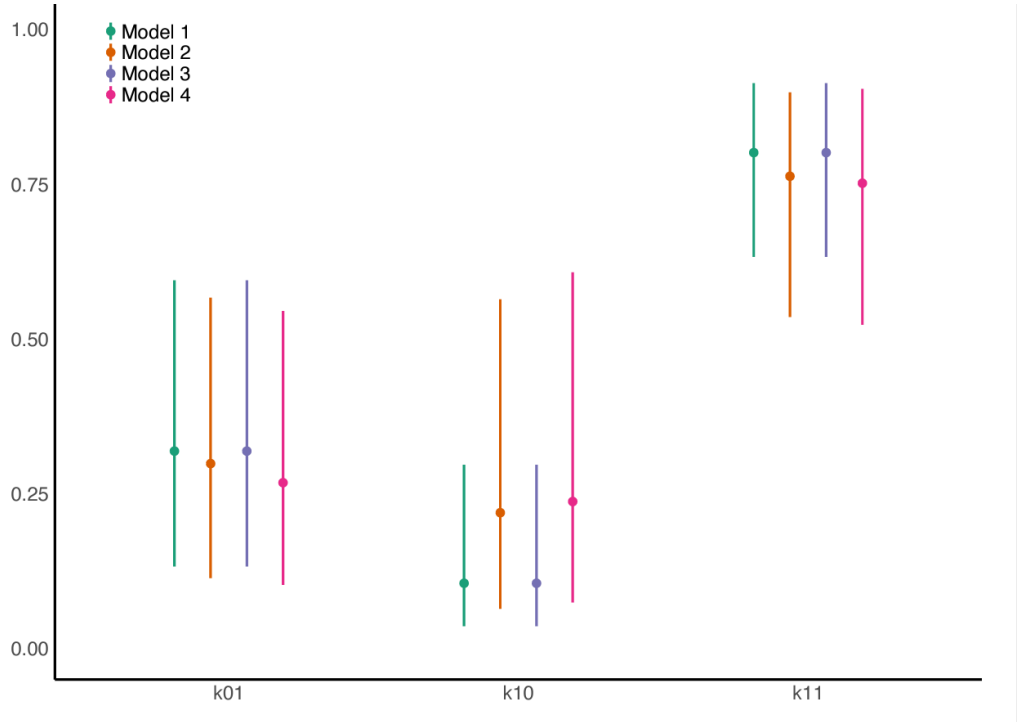

Appendix Figure 22. Comparison of estimates of 'instrumental parameters' among the four models.

Bibliography

1. D. M. Morens, G. K. Folkers, A. S. Fauci, The challenge of emerging and re-emerging infectious diseases. *Nature* 430, 242-249 (2004).
2. B. McCloskey, O. Dar, A. Zumla, D. L. Heymann, Emerging infectious diseases and pandemic potential: status quo and reducing risk of global spread. *The Lancet infectious diseases* 14, 1001-1010 (2014).
3. L. H. Taylor, S. M. Latham, M. E. Woolhouse, Risk factors for human disease emergence. *Philosophical Transactions of the Royal Society of London. Series B: Biological Sciences* 356, 983-989 (2001).
4. R. N. Thompson, E. Brooks-Pollock, Detection, forecasting and control of infectious disease epidemics: modelling outbreaks in humans, animals and plants. *Philosophical Transactions of the Royal Society B* 374, 20190038 (2019).
5. World Health Organization, WHO Health Emergency Dashboard Disclaimer, available from: https://covid19.who.int/, assessed on 1 May 2023.
6. K. M. Bubar *et al.*, Model-informed COVID-19 vaccine prioritization strategies by age and serostatus. *Science* 371, 916-921 (2021).
7. N. Banholzer *et al.*, The methodologies to assess the effectiveness of non-pharmaceutical interventions during COVID-19: a systematic review. *European Journal of Epidemiology* 37, 1003-1024 (2022).
8. Institute of Population Health, University of Liverpool for Liverpool City Region Covid-SMART Gold Command. Covid-SMART Asymptomatic Testing Pilot in Liverpool City Region: Quantitative Evaluation, available from: https://www.liverpool.ac.uk/media/livacuk/coronavirus/Liverpool_City_Region_Covid_SMART_Evaluation-Feb.pdf, assessed on 1 May 2023.
9. J. Stokes, A. J. Turner, L. Anselmi, M. Morciano, T. Hone, The relative effects of non-pharmaceutical interventions on wave one Covid-19 mortality: natural experiment in 130 countries. *BMC Public Health* 22, 1113 (2022).
10. J. M. Brauner *et al.*, Inferring the effectiveness of government interventions against COVID-19. *Science* 371, eabd9338 (2021).
11. L. Ferretti *et al.*, Quantifying SARS-CoV-2 transmission suggests epidemic control with digital contact tracing. *Science* 368, eabb6936 (2020).
12. B. C. Young *et al.*, Daily testing for contacts of individuals with SARS-CoV-2 infection and attendance and SARS-CoV-2 transmission in English secondary schools and colleges: an open-label, cluster-randomised trial. *The Lancet* 398, 1217-1229 (2021).
13. L. Geddes, Different types of immunity and why they matter to COVID-19. available from: https://www.gavi.org/vaccineswork/different-types-immunity-and-why-they-matter-covid-19#:~:text=This%20can%20happen%20through%20infection,(vaccine%2Dinduced%20immunity), assessed on 4 September 2020.
14. C. B. Jackson, M. Farzan, B. Chen, H. Choe, Mechanisms of SARS-CoV-2 entry into cells. *Nature reviews Molecular cell biology* 23, 3-20 (2022).
15. V. G. Puelles *et al.*, Multiorgan and renal tropism of SARS-CoV-2. *New England Journal of Medicine* 383, 590-592 (2020).
16. M. M. Lamers, B. L. Haagmans, SARS-CoV-2 pathogenesis. *Nature reviews microbiology* 20, 270-284 (2022).
17. O. Puhach, B. Meyer, I. Eckerle, SARS-CoV-2 viral load and shedding kinetics. *Nature Reviews Microbiology* 21, 147-161 (2023).

18. Public Health England, Understanding cycle threshold (Ct) in SARS-CoV-2 RT-PCR, available from: https://assets.publishing.service.gov.uk/government/uploads/system/uploads/attachment_data/file/926410/Understanding_Cycle_Threshold__Ct__in_SARS-CoV-2_RT-PCR_.pdf, assessed on 1 May 2022.
19. J. J. van Kampen *et al.*, Duration and key determinants of infectious virus shedding in hospitalized patients with coronavirus disease-2019 (COVID-19). *Nature communications* 12, 267 (2021).
20. S. Hakki *et al.*, Onset and window of SARS-CoV-2 infectiousness and temporal correlation with symptom onset: a prospective, longitudinal, community cohort study. *The Lancet Respiratory Medicine* 10, 1061-1073 (2022).
21. T. C. Jones *et al.*, Estimating infectiousness throughout SARS-CoV-2 infection course. *Science* 373, eabi5273 (2021).
22. J. A. Hay *et al.*, Estimating epidemiologic dynamics from cross-sectional viral load distributions. *Science* 373, eabh0635 (2021).
23. A. K. Nalla *et al.*, Comparative performance of SARS-CoV-2 detection assays using seven different primer-probe sets and one assay kit. *Journal of clinical microbiology* 58, e00557-00520 (2020).
24. S. F. Sia *et al.*, Pathogenesis and transmission of SARS-CoV-2 in golden hamsters. *Nature* 583, 834-838 (2020).
25. R. N. Binny *et al.*, Sensitivity of Reverse Transcription Polymerase Chain Reaction Tests for Severe Acute Respiratory Syndrome Coronavirus 2 Through Time. *The Journal of Infectious Diseases* 227, 9-17 (2023).
26. J. D. Challenger *et al.*, Modelling upper respiratory viral load dynamics of SARS-CoV-2. *BMC medicine* 20, 1-20 (2022).
27. S. Mallett *et al.*, At what times during infection is SARS-CoV-2 detectable and no longer detectable using RT-PCR-based tests? A systematic review of individual participant data. *BMC medicine* 18, 1-17 (2020).
28. V. T. Chu *et al.*, Comparison of home antigen testing with RT-PCR and viral culture during the course of SARS-CoV-2 infection. *JAMA Internal Medicine* 182, 701-709 (2022).
29. J. Bullard *et al.*, Predicting infectious severe acute respiratory syndrome coronavirus 2 from diagnostic samples. *Clinical infectious diseases* 71, 2663-2666 (2020).
30. M. Cevik *et al.*, SARS-CoV-2, SARS-CoV, and MERS-CoV viral load dynamics, duration of viral shedding, and infectiousness: a systematic review and meta-analysis. *The lancet microbe* 2, e13-e22 (2021).
31. L. C. Tindale *et al.*, Evidence for transmission of COVID-19 prior to symptom onset. *Elife* 9, e57149 (2020).
32. M. A. Johansson *et al.*, SARS-CoV-2 transmission from people without COVID-19 symptoms. *JAMA network open* 4, e2035057-e2035057 (2021).
33. A. Singanayagam *et al.*, Duration of infectiousness and correlation with RT-PCR cycle threshold values in cases of COVID-19, England, January to May 2020. *Eurosurveillance* 25, 2001483 (2020).
34. Q. Bi *et al.*, Epidemiology and transmission of COVID-19 in 391 cases and 1286 of their close contacts in Shenzhen, China: a retrospective cohort study. *The Lancet infectious diseases* 20, 911-919 (2020).
35. R. Verity *et al.*, Estimates of the severity of coronavirus disease 2019: a model-based analysis. *The Lancet infectious diseases* 20, 669-677 (2020).

36. S. Chen, J. A. Flegg, L. J. White, R. Aguas, Levels of SARS-CoV-2 population exposure are considerably higher than suggested by seroprevalence surveys. *PLOS Computational Biology* 17, e1009436 (2021).
37. D. R. Burton, Antibodies, viruses and vaccines. *Nature Reviews Immunology* 2, 706-713 (2002).
38. K. Wang *et al.*, Longitudinal dynamics of the neutralizing antibody response to severe acute respiratory syndrome coronavirus 2 (SARS-CoV-2) infection. *Clinical Infectious Diseases* 73, e531-e539 (2021).
39. L. Grzelak *et al.*, A comparison of four serological assays for detecting anti–SARS-CoV-2 antibodies in human serum samples from different populations. *Science translational medicine* 12, eabc3103 (2020).
40. Technology Networks Diagnostics, COVID-19 Antibody Testing: S vs. N Protein, available from: https://www.technologynetworks.com/diagnostics/blog/covid-19-antibody-testing-s-vs-n-protein-340327, assessed on 1 May 2023.
41. L. Mazzini *et al.*, Comparative analyses of SARS-CoV-2 binding (IgG, IgM, IgA) and neutralizing antibodies from human serum samples. *Journal of Immunological Methods* 489, 112937 (2021).
42. UK Health Security Agency, Antibody testing for SARS-CoV-2 Extended information for medical professionals and researchers on using and interpreting SARS-CoV-2 antibody tests, available from: https://assets.publishing.service.gov.uk/government/uploads/system/uploads/attachment_data/file/1066325/Extended-guidance-antibody-testing.pdf, assessed on 1 May 2023.
43. D. S. Khoury *et al.*, Neutralizing antibody levels are highly predictive of immune protection from symptomatic SARS-CoV-2 infection. *Nature medicine* 27, 1205-1211 (2021).
44. C. Lucas *et al.*, Delayed production of neutralizing antibodies correlates with fatal COVID-19. *Nature medicine* 27, 1178-1186 (2021).
45. S. A. Ejazi, S. Ghosh, N. Ali, Antibody detection assays for COVID-19 diagnosis: an early overview. *Immunology and cell biology* 99, 21-33 (2021).
46. M. Stone *et al.*, Evaluation of commercially available high-throughput SARS-CoV-2 serologic assays for serosurveillance and related applications. *Emerging infectious diseases* 28, 672 (2022).
47. C. H. Chau, J. D. Strope, W. D. Figg, COVID-19 clinical diagnostics and testing technology. *Pharmacotherapy: The Journal of Human Pharmacology and Drug Therapy* 40, 857-868 (2020).
48. M. Yüce, E. Filiztekin, K. G. Özkaya, COVID-19 diagnosis—A review of current methods. *Biosensors and Bioelectronics* 172, 112752 (2021).
49. R. T. Suhandynata *et al.*, Longitudinal monitoring of SARS-CoV-2 IgM and IgG seropositivity to detect COVID-19. *The journal of applied laboratory medicine* 5, 908-920 (2020).
50. K. K.-W. To *et al.*, Temporal profiles of viral load in posterior oropharyngeal saliva samples and serum antibody responses during infection by SARS-CoV-2: an observational cohort study. *The Lancet infectious diseases* 20, 565-574 (2020).
51. Q.-X. Long *et al.*, Antibody responses to SARS-CoV-2 in patients with COVID-19. *Nature medicine* 26, 845-848 (2020).
52. L. R. Petersen *et al.*, Lack of antibodies to severe acute respiratory syndrome coronavirus 2 (SARS-CoV-2) in a large cohort of previously infected persons. *Clinical Infectious Diseases* 73, e3066-e3073 (2021).

53. J. Van Elslande *et al.*, Longitudinal follow-up of IgG anti-nucleocapsid antibodies in SARS-CoV-2 infected patients up to eight months after infection. *Journal of Clinical Virology* 136, 104765 (2021).
54. K. Oved *et al.*, Multi-center nationwide comparison of seven serology assays reveals a SARS-CoV-2 non-responding seronegative subpopulation. *EClinicalMedicine* 29, 100651 (2020).
55. S. F. Lumley *et al.*, The duration, dynamics, and determinants of severe acute respiratory syndrome coronavirus 2 (SARS-CoV-2) antibody responses in individual healthcare workers. *Clinical Infectious Diseases* 73, e699-e709 (2021).
56. F. Anna *et al.*, High seroprevalence but short-lived immune response to SARS-CoV-2 infection in Paris. *European journal of immunology* 51, 180-190 (2021).
57. L. Piccoli *et al.*, Mapping neutralizing and immunodominant sites on the SARS-CoV-2 spike receptor-binding domain by structure-guided high-resolution serology. *Cell* 183, 1024-1042. e1021 (2020).
58. J. Van Elslande, L. Gruwier, L. Godderis, P. Vermeersch, Estimated half-life of SARS-CoV-2 anti-spike antibodies more than double the half-life of anti-nucleocapsid antibodies in healthcare workers. *Clinical Infectious Diseases* 73, 2366-2368 (2021).
59. N. Owusu-Boaitey, T. W. Russell, G. Meyerowitz-Katz, A. T. Levin, D. Herrera-Esposito, Dynamics of SARS-CoV-2 seroassay sensitivity: a systematic review and modeling study. *medRxiv*, 2022.2009.2008.22279731 (2023).
60. N. Sethuraman, S. S. Jeremiah, A. Ryo, Interpreting diagnostic tests for SARS-CoV-2. *Jama* 323, 2249-2251 (2020).
61. T. Sekine *et al.*, Robust T cell immunity in convalescent individuals with asymptomatic or mild COVID-19. *Cell* 183, 158-168. e114 (2020).
62. A. Nelde *et al.*, SARS-CoV-2-derived peptides define heterologous and COVID-19-induced T cell recognition. *Nature immunology* 22, 74-85 (2021).
63. R. da Silva Antunes *et al.*, Differential T-cell reactivity to endemic coronaviruses and SARS-CoV-2 in community and health care workers. *The Journal of infectious diseases* 224, 70-80 (2021).
64. F. Gallais *et al.*, Intrafamilial exposure to SARS-CoV-2 associated with cellular immune response without seroconversion, France. *Emerging infectious diseases* 27, 113 (2021).
65. J. A. Juno *et al.*, Humoral and circulating follicular helper T cell responses in recovered patients with COVID-19. *Nature medicine* 26, 1428-1434 (2020).
66. S. Boppana *et al.*, SARS-CoV-2-specific circulating T follicular helper cells correlate with neutralizing antibodies and increase during early convalescence. *PLoS pathogens* 17, e1009761 (2021).
67. E. Stephenson *et al.*, Single-cell multi-omics analysis of the immune response in COVID-19. *Nature medicine* 27, 904-916 (2021).
68. A. K. Wheatley *et al.*, Evolution of immune responses to SARS-CoV-2 in mild-moderate COVID-19. *Nature communications* 12, 1162 (2021).
69. J. Zuo *et al.*, Robust SARS-CoV-2-specific T cell immunity is maintained at 6 months following primary infection. *Nature immunology* 22, 620-626 (2021).
70. J. H. Jung *et al.*, SARS-CoV-2-specific T cell memory is sustained in COVID-19 convalescent patients for 10 months with successful development of stem cell-like memory T cells. *Nature communications* 12, 4043 (2021).
71. T. Bilich *et al.*, T cell and antibody kinetics delineate SARS-CoV-2 peptides mediating long-term immune responses in COVID-19 convalescent individuals. *Science translational medicine* 13, eabf7517 (2021).

72. K. W. Cohen *et al.*, Longitudinal analysis shows durable and broad immune memory after SARS-CoV-2 infection with persisting antibody responses and memory B and T cells. *Cell Reports Medicine* 2, (2021).
73. P. A. Szabo *et al.*, Longitudinal profiling of respiratory and systemic immune responses reveals myeloid cell-driven lung inflammation in severe COVID-19. *Immunity* 54, 797-814. e796 (2021).
74. J. Grau-Expósito *et al.*, Peripheral and lung resident memory T cell responses against SARS-CoV-2. *Nature communications* 12, 3010 (2021).
75. K. W. Ng *et al.*, Preexisting and de novo humoral immunity to SARS-CoV-2 in humans. *Science* 370, 1339-1343 (2020).
76. M. Sagar *et al.*, Recent endemic coronavirus infection is associated with less-severe COVID-19. *The Journal of clinical investigation* 131, (2021).
77. A. Sette, S. Crotty, Pre-existing immunity to SARS-CoV-2: the knowns and unknowns. *Nature Reviews Immunology* 20, 457-458 (2020).
78. P. Moss, The T cell immune response against SARS-CoV-2. *Nature immunology* 23, 186-193 (2022).
79. R. Kundu *et al.*, Cross-reactive memory T cells associate with protection against SARS-CoV-2 infection in COVID-19 contacts. *Nature communications* 13, 80 (2022).
80. E. Head, T cells from common colds cross-protect against infection with SARS-CoV-2, available from: https://www.imperial.ac.uk/news/233018/cells-from-common-colds-cross-protect-against/, assessed on 10 September 2023.
81. M. Lipsitch, Y. H. Grad, A. Sette, S. Crotty, Cross-reactive memory T cells and herd immunity to SARS-CoV-2. *Nature Reviews Immunology* 20, 709-713 (2020).
82. H. Salje *et al.*, Estimating the burden of SARS-CoV-2 in France. *Science* 369, 208-211 (2020).
83. S. Flaxman *et al.*, Estimating the effects of non-pharmaceutical interventions on COVID-19 in Europe. *Nature* 584, 257-261 (2020).
84. S. F. Lumley *et al.*, Antibody status and incidence of SARS-CoV-2 infection in health care workers. *New England Journal of Medicine* 384, 533-540 (2021).
85. R. A. Harvey *et al.*, Association of SARS-CoV-2 seropositive antibody test with risk of future infection. *JAMA internal medicine* 181, 672-679 (2021).
86. A. G. Letizia *et al.*, SARS-CoV-2 seropositivity and subsequent infection risk in healthy young adults: a prospective cohort study. *The Lancet Respiratory Medicine* 9, 712-720 (2021).
87. V. J. Hall *et al.*, SARS-CoV-2 infection rates of antibody-positive compared with antibody-negative health-care workers in England: a large, multicentre, prospective cohort study (SIREN). *The Lancet* 397, 1459-1469 (2021).
88. D. Michlmayr *et al.*, Observed protection against SARS-CoV-2 reinfection following a primary infection: A Danish cohort study among unvaccinated using two years of nationwide PCR-test data. *The Lancet Regional Health-Europe* 20, 100452 (2022).
89. L. J. Abu-Raddad *et al.*, SARS-CoV-2 antibody-positivity protects against reinfection for at least seven months with 95% efficacy. *EClinicalMedicine* 35, 100861 (2021).
90. J. Wei *et al.*, Anti-spike antibody response to natural SARS-CoV-2 infection in the general population. *Nature Communications* 12, 6250 (2021).
91. D. Menges *et al.*, Heterogenous humoral and cellular immune responses with distinct trajectories post-SARS-CoV-2 infection in a population-based cohort. *Nature Communications* 13, 4855 (2022).

92. W. O. Kermack, A. G. McKendrick, A contribution to the mathematical theory of epidemics. *Proceedings of the royal society of london. Series A, Containing papers of a mathematical and physical character* 115, 700-721 (1927).
93. R. Aguas *et al.*, Modelling the COVID-19 pandemic in context: an international participatory approach. *BMJ global health* 5, e003126 (2020).
94. M. Fyles *et al.*, Using a household-structured branching process to analyse contact tracing in the SARS-CoV-2 pandemic. *Philosophical Transactions of the Royal Society B* 376, 20200267 (2021).
95. L. Danon, L. Lacasa, E. Brooks-Pollock, Household bubbles and COVID-19 transmission: insights from percolation theory. *Philosophical Transactions of the Royal Society B* 376, 20200284 (2021).
96. C. E. Overton *et al.*, EpiBeds: Data informed modelling of the COVID-19 hospital burden in England. *PLoS Computational Biology* 18, e1010406 (2022).
97. T. Crellen *et al.*, Dynamics of SARS-CoV-2 with waning immunity in the UK population. *Philosophical transactions of the royal society b* 376, 20200274 (2021).
98. P. Birrell, J. Blake, E. Van Leeuwen, N. Gent, D. De Angelis, Real-time nowcasting and forecasting of COVID-19 dynamics in England: the first wave. *Philosophical Transactions of the Royal Society B* 376, 20200279 (2021).
99. E. S. Knock *et al.*, Key epidemiological drivers and impact of interventions in the 2020 SARS-CoV-2 epidemic in England. *Science Translational Medicine* 13, eabg4262 (2021).
100. S. Pei, T. K. Yamana, S. Kandula, M. Galanti, J. Shaman, Burden and characteristics of COVID-19 in the United States during 2020. *Nature* 598, 338-341 (2021).
101. N. Hoertel *et al.*, A stochastic agent-based model of the SARS-CoV-2 epidemic in France. *Nature medicine* 26, 1417-1421 (2020).
102. S. Venkatramanan *et al.*, Using data-driven agent-based models for forecasting emerging infectious diseases. *Epidemics* 22, 43-49 (2018).
103. R. Hinch *et al.*, OpenABM-Covid19—An agent-based model for non-pharmaceutical interventions against COVID-19 including contact tracing. *PLoS computational biology* 17, e1009146 (2021).
104. C. C. Kerr *et al.*, Covasim: an agent-based model of COVID-19 dynamics and interventions. *PLOS Computational Biology* 17, e1009149 (2021).
105. A. C. Miller *et al.*, Statistical deconvolution for inference of infection time series. *Epidemiology (Cambridge, Mass.)* 33, 470 (2022).
106. Office for National Statistics, Coronavirus (COVID-19) Infection Survey, UK Statistical bulletins, available from: https://www.ons.gov.uk/peoplepopulationandcommunity/healthandsocialcare/conditionsanddiseases/bulletins/coronaviruscovid19infectionsurveypilot/previousReleases, assessed on 1 May 2023. (2023).
107. E. Colman, G. A. Puspitarani, J. Enright, R. R. Kao, Ascertainment rate of SARS-CoV-2 infections from healthcare and community testing in the UK. *Journal of Theoretical Biology* 558, 111333 (2023).
108. K. Shioda *et al.*, Estimating the cumulative incidence of SARS-CoV-2 infection and the infection fatality ratio in light of waning antibodies. *Epidemiology (Cambridge, Mass.)* 32, 518 (2021).
109. S. J. Phipps, R. Q. Grafton, T. Kompas, Robust estimates of the true (population) infection rate for COVID-19: a backcasting approach. *Royal Society Open Science* 7, 200909 (2020).

110. N. F. Brazeau *et al.*, Estimating the COVID-19 infection fatality ratio accounting for seroreversion using statistical modelling. *Communications medicine* 2, 54 (2022).
111. P. S. Sullivan *et al.*, Severe acute respiratory syndrome coronavirus 2 cumulative incidence, United States, August 2020–December 2020. *Clinical Infectious Diseases* 74, 1141-1150 (2022).
112. K. Lamba *et al.*, SARS-CoV-2 cumulative incidence and period seroprevalence: results from a statewide population-based serosurvey in California. *Open Forum Infectious Diseases* 8, ofab379 (2021).
113. A. T. Chamberlain *et al.*, Cumulative incidence of SARS-CoV-2 infections among adults in Georgia, United States, August to December 2020. *The Journal of Infectious Diseases* 225, 396-403 (2022).
114. A. Gelman *et al.*, *Bayesian data analysis*. (CRC press, 2013).
115. W. R. Gilks, S. Richardson, D. Spiegelhalter, *Markov chain Monte Carlo in practice*. (CRC press, 1995).
116. M. D. Hoffman, A. Gelman, The No-U-Turn sampler: adaptively setting path lengths in Hamiltonian Monte Carlo. *J. Mach. Learn. Res.* 15, 1593-1623 (2014).
117. Stan Development Team, RStan: the R interface to Stan, available from: https://cran.r-project.org/web/packages/rstan/vignettes/rstan.html, assessed on 1 May 2023.
118. Stan development team, Convergence and efficiency diagnostics for Markov Chains, available from: https://mc-stan.org/rstan/reference/Rhat.html, assessed on 1 May 2023.
119. S. Chen, J. A. Flegg, K. A. Lythgoe, L. J. White, Reconstructing the first COVID-19 pandemic wave with minimal data in the UK. *medRxiv*, 2023.2003. 2017.23287140 (2023).
120. S. A. Saeedzai *et al.*, COVID-19 morbidity in Afghanistan: a nationwide, population-based seroepidemiological study. *BMJ open* 12, e060739 (2022).
121. S. Chen *et al.*, Estimating the effectiveness of shielding during pregnancy against SARS-CoV-2 in New York City during the first year of the COVID-19 pandemic. *Viruses* 14, 2408 (2022).
122. M. Nicole *et al.*, The socio-economic implications of the coronavirus and covid-19 pandemic: A review. *International journal of surgery* 78, 185-193 (2020).
123. A. Mahdi *et al.*, OxCOVID19 Database, a multimodal data repository for better understanding the global impact of COVID-19. *Scientific Reports* 11, 9237 (2021).
124. C. J. E. Metcalf, C. Viboud, D. J. Spiro, B. T. Grenfell, Using serology with models to clarify the trajectory of the SARS-CoV-2 emerging outbreak. *Trends in Immunology* 41, 849-851 (2020).
125. J. Watson, A. Richter, J. Deeks, Testing for SARS-CoV-2 antibodies. *bmj* 370, (2020).
126. J. Seow *et al.*, Longitudinal observation and decline of neutralizing antibody responses in the three months following SARS-CoV-2 infection in humans. *Nature microbiology* 5, 1598-1607 (2020).
127. A. Grifoni *et al.*, Targets of T cell responses to SARS-CoV-2 coronavirus in humans with COVID-19 disease and unexposed individuals. *Cell* 181, 1489-1501. e1415 (2020).
128. R. K. Arora *et al.*, SeroTracker: a global SARS-CoV-2 seroprevalence dashboard. *The Lancet Infectious Diseases* 21, e75-e76 (2021).

129. H. Ward *et al.*, Antibody prevalence for SARS-CoV-2 in England following first peak of the pandemic: REACT2 study in 100,000 adults. *Nature communications* 12, 905 (2020).
130. T. J. Ripperger *et al.*, Orthogonal SARS-CoV-2 serological assays enable surveillance of low-prevalence communities and reveal durable humoral immunity. *Immunity* 53, 925-933. e924 (2020).
131. A. S. Iyer *et al.*, Persistence and decay of human antibody responses to the receptor binding domain of SARS-CoV-2 spike protein in COVID-19 patients. *Science immunology* 5, eabe0367 (2020).
132. H. Ward *et al.*, Declining prevalence of antibody positivity to SARS-CoV-2: a community study of 365,000 adults. *MedRxiv*, 2020.2010. 2026.20219725 (2020).
133. Public Health England, National flu and COVID-19 surveillance reports, available from: https://www.gov.uk/government/statistics/national-flu-and-covid-19-surveillance-reports, assessed on 1 May 2023.
134. J. Zhao *et al.*, Antibody responses to SARS-CoV-2 in patients with novel coronavirus disease 2019. *Clinical infectious diseases* 71, 2027-2034 (2020).
135. H. Ward *et al.*, Antibody prevalence for SARS-CoV-2 in England following first peak of the pandemic: REACT2 study in 100,000 adults. (2020).
136. T. Nicol *et al.*, Assessment of SARS-CoV-2 serological tests for the diagnosis of COVID-19 through the evaluation of three immunoassays: Two automated immunoassays (Euroimmun and Abbott) and one rapid lateral flow immunoassay (NG Biotech). *Journal of Clinical Virology* 129, 104511 (2020).
137. Public Health England, Evaluation of the Euroimmun Anti-SARS-CoV-2 ELISA (IgG) serology assay for the detection of anti-SARS-CoV-2 antibodies, available from: https://assets.publishing.service.gov.uk/government/uploads/system/uploads/attachment_data/file/893433/Evaluation_of_Euroimmun_SARS_CoV_2_ELISA_IgG__1_.pdf, assessed on 1 May 2023.
138. F. Muecksch *et al.*, Longitudinal serological analysis and neutralizing antibody levels in coronavirus disease 2019 convalescent patients. *The Journal of infectious diseases* 223, 389-398 (2021).
139. R. J. Harris *et al.*, Serological surveillance of SARS-CoV-2: Six-month trends and antibody response in a cohort of public health workers. *Journal of Infection* 82, 162-169 (2021).
140. G. Meyerowitz-Katz, L. Merone, A systematic review and meta-analysis of published research data on COVID-19 infection fatality rates. *International Journal of Infectious Diseases* 101, 138-148 (2020).
141. S. Stringhini *et al.*, Seroprevalence of anti-SARS-CoV-2 IgG antibodies in Geneva, Switzerland (SEROCoV-POP): a population-based study. *The Lancet* 396, 313-319 (2020).
142. N. Brazeau *et al.*, COVID-19 Infection Fatality Ratio: Estimates from Seroprevalence.(Imperial College London 2020) DOI: https://doi.org/10.25561/83545.
143. C. Manisty *et al.*, Time series analysis and mechanistic modelling of heterogeneity and sero-reversion in antibody responses to mild SARS-CoV-2 infection. *EBioMedicine* 65, 103259 (2021).
144. UK Health Security Agency, GOV.UK Coronavirus (COVID-19) dashboard in the UK, available from: https://coronavirus.data.gov.uk/, assessed on 1 May 2023.
145. Office for National Statistics, Population age structure by single year of age and sex for local authorities, counties, regions and England as a whole, mid-2018 to

mid-2043. 2021, available from: https://www.ons.gov.uk/peoplepopulationandcommunity/populationandmigration/populationestimates/articles/ukpopulationpyramidinteractive/2020-01-08. assessed on 1 May 2023.
146. Public Health England, Public health profiles, available from: https://fingertips.phe.org.uk/search/care%20home#page/10/gid/1/pat/15/par/E92000001/ati/6/are/E12000004/iid/93500/age/1/sex/4/cid/4/tbm/1/page-options/car-do-0. assessed on 1 May 2023.
147. K. Mohd Hanafiah, J. Groeger, A. D. Flaxman, S. T. Wiersma, Global epidemiology of hepatitis C virus infection: new estimates of age-specific antibody to HCV seroprevalence. *Hepatology* 57, 1333-1342 (2013).
148. Public Health England, COVID-19: review of disparities in risks and outcomes. 2020, available from: https://www.gov.uk/government/publications/covid-19-review-of-disparities-in-risks-and-outcomes, assessed on 1 May 2023.
149. W. N. Chia *et al.*, Dynamics of SARS-CoV-2 neutralising antibody responses and duration of immunity: a longitudinal study. *The Lancet Microbe* 2, e240-e249 (2021).
150. G. den Hartog *et al.*, Persistence of antibodies to severe acute respiratory syndrome coronavirus 2 in relation to symptoms in a nationwide prospective study. *Clinical Infectious Diseases* 73, 2155-2162 (2021).
151. E. Duysburgh *et al.*, Persistence of IgG response to SARS-CoV-2. *The Lancet Infectious Diseases* 21, 163-164 (2021).
152. The Centre for Evidence-Based Medicine, Estimating the infection fatality ratio in England. 2020, available from: https://www.cebm.net/covid-19/estimating-the-infection-fatality-ratio-in-england/, assessed on 28 June 2021.
153. O. Dyer, Covid-19: Study claims real global deaths are twice official figures. *BMJ: British Medical Journal (Online)* 373, (2021).
154. L. F. Buss *et al.*, Three-quarters attack rate of SARS-CoV-2 in the Brazilian Amazon during a largely unmitigated epidemic. *Science* 371, 288-292 (2021).
155. P. C. Hallal *et al.*, SARS-CoV-2 antibody prevalence in Brazil: results from two successive nationwide serological household surveys. *The Lancet Global Health* 8, e1390-e1398 (2020).
156. J. Lourenco *et al.*, Fundamental principles of epidemic spread highlight the immediate need for large-scale serological surveys to assess the stage of the SARS-CoV-2 epidemic. *MedRxiv*, 2020.2003. 2024.20042291 (2020).
157. U. Akkucuk, *Managing inflation and supply chain disruptions in the global economy*. (IGI Global, 2022).
158. J. M. Aburto *et al.*, Quantifying impacts of the COVID-19 pandemic through life-expectancy losses: a population-level study of 29 countries. *International journal of epidemiology* 51, 63-74 (2022).
159. C. J. E. Metcalf, D. H. Morris, S. W. Park, Mathematical models to guide pandemic response. *Science* 369, 368-369 (2020).
160. C. Pagel, C. A. Yates, Role of mathematical modelling in future pandemic response policy. *bmj* 378, (2022).
161. T. J. Bollyky *et al.*, Pandemic preparedness and COVID-19: an exploratory analysis of infection and fatality rates, and contextual factors associated with preparedness in 177 countries, from Jan 1, 2020, to Sept 30, 2021. *The Lancet* 399, 1489-1512 (2022).

162. B. Kennedy *et al.*, App-based COVID-19 syndromic surveillance and prediction of hospital admissions in COVID Symptom Study Sweden. *Nature Communications* 13, 2110 (2022).
163. M. R. Desjardins, Syndromic surveillance of COVID-19 using crowdsourced data. *The Lancet Regional Health–Western Pacific* 4, (2020).
164. K. B. Pouwels *et al.*, Community prevalence of SARS-CoV-2 in England from April to November, 2020: results from the ONS Coronavirus Infection Survey. *The Lancet Public Health* 6, e30-e38 (2021).
165. H. Clapham *et al.*, Seroepidemiologic study designs for determining SARS-COV-2 transmission and immunity. *Emerging Infectious Diseases* 26, 1978 (2020).
166. F. J. Ibarrondo *et al.*, Rapid decay of anti–SARS-CoV-2 antibodies in persons with mild Covid-19. *New England Journal of Medicine* 383, 1085-1087 (2020).
167. B. Böger *et al.*, Systematic review with meta-analysis of the accuracy of diagnostic tests for COVID-19. *American journal of infection control* 49, 21-29 (2021).
168. Office for National Statistics, Coronavirus (COVID-19) Infection Survey technical article: Cumulative incidence of the number of people who have tested positive for COVID-19, UK: 22 April 2022, available from: https://www.ons.gov.uk/peoplepopulationandcommunity/healthandsocialcare/conditionsanddiseases/articles/coronaviruscovid19infectionsurveytechnicalarticlecumulativeincidenceofthenumberofpeoplewhohavetestedpositiveforcovid19uk/22april2022, assessed on 1 May 2023.
169. T. W. Russell *et al.*, Reconstructing the early global dynamics of under-ascertained COVID-19 cases and infections. *BMC medicine* 18, 332 (2020).
170. J. Shah *et al.*, COVID-19: the current situation in Afghanistan. *The Lancet Global Health* 8, e771-e772 (2020).
171. Ministry of Public Health, Measures taken by the Ministry of Public Health for preventing and controlling the spread of the coronavirus in Afghanistan, available from: https://moph.gov.af/. accessed on 4 June 2020.
172. World Health Organization, Afghanistan Brief: COVID-19, No 52, available from https://www.humanitarianresponse.info/sites/www.humanitarianresponse.info/files/documents/files/daily_brief_covid-19_11_june_2020.pdf, assessed on 1 May 2023.
173. Our World in Data: Afghanistan: Coronavirus Pandemic Country Profile, available from: https://ourworldindata.org/coronavirus/country/afghanistan, assessed on 1 May 2023.
174. World Health Organization, The true death toll of COVID-19: estimating global excess mortality, available from: https://www.who.int/data/stories/the-true-death-toll-of-covid-19-estimating-global-excess-mortality, assessed on 1 May 2023.
175. M. Y. Essar *et al.*, COVID-19 and multiple crises in Afghanistan: an urgent battle. *Conflict and Health* 15, 1-3 (2021).
176. N. Ortega *et al.*, Seven-month kinetics of SARS-CoV-2 antibodies and role of pre-existing antibodies to human coronaviruses. *Nature communications* 12, 4740 (2021).
177. World Health Organization, Population-based age-stratified seroepidemiological investigation protocol for COVID-19 virus infection, 17 March 2020. available from: https://apps.who.int/iris/handle/10665/331656. License: CC BY-NC-SA 3.0 IGO, assessed on 1 May 2023.
178. Healgen Scientific, LCC, Rapid COVID-19 Antigen Test, available from: https://www.healgen.com/if-respiratory-covid-19-antigen, assessed on 1 May 2023.
179. S. Burgess, M. J. Ponsford, D. Gill, Are we underestimating seroprevalence of SARS-CoV-2? *BMJ* 370, (2020).

180. Healgen Scientific LLC. COVID-19 IgG/IgM Rapid Test Cassette (Whole Blood/Serum/Plasma) Instruction for Use 2020, Available from: https://www.fda.gov/media/138438/download., (2020).
181. National Statistics and Information Authority (NSIA), NSIA estimates general population at 33.6 million, available from: https://www.ariananews.af/nsia-estimates-general-population-at-33-6-million/, assessed on 1 May 2023.
182. S. L. Wu *et al.*, Substantial underestimation of SARS-CoV-2 infection in the United States. *Nature communications* 11, 4507 (2020).
183. The COVID-19 International Modelling Consortium, available from: https://como.bmj.com/.
184. R. M. Anderson, R. M. May, Vaccination and herd immunity to infectious diseases. *Nature* 318, 323-329 (1985).
185. H. E. Randolph, L. B. Barreiro, Herd immunity: understanding COVID-19. *Immunity* 52, 737-741 (2020).
186. K. O. Kwok, F. Lai, W. I. Wei, S. Y. S. Wong, J. W. Tang, Herd immunity–estimating the level required to halt the COVID-19 epidemics in affected countries. *Journal of Infection* 80, e32-e33 (2020).
187. M. G. M. Gomes *et al.*, Individual variation in susceptibility or exposure to SARS-CoV-2 lowers the herd immunity threshold. *Journal of theoretical biology* 540, 111063 (2022).
188. D. M. Altmann, D. C. Douek, R. J. Boyton, What policy makers need to know about COVID-19 protective immunity. *The Lancet* 395, 1527-1529 (2020).
189. Maryland: Johns Hopkins Bloomberg school of public health, What is herd immunity and how can we achieve it with COVID-19? available from: https://www.jhsph.edu/covid-19/articles/achieving-herd-immunity-with-covid19.html2021, assessed on 1 May 2023.
190. D. Pople *et al.*, Burden of SARS-CoV-2 infection in healthcare workers during second wave in England and impact of vaccines: prospective multicentre cohort study (SIREN) and mathematical model. *bmj* 378, (2022).
191. J. J. Lau *et al.*, Real-world COVID-19 vaccine effectiveness against the Omicron BA. 2 variant in a SARS-CoV-2 infection-naive population. *Nature Medicine*, 1-1 (2023).
192. K. B. Pouwels *et al.*, Effect of Delta variant on viral burden and vaccine effectiveness against new SARS-CoV-2 infections in the UK. *Nature medicine* 27, 2127-2135 (2021).
193. T. Britton, F. Ball, P. Trapman, A mathematical model reveals the influence of population heterogeneity on herd immunity to SARS-CoV-2. *science* 369, 846-849 (2020).
194. A. Fontanet, S. Cauchemez, COVID-19 herd immunity: where are we? *Nature Reviews Immunology* 20, 583-584 (2020).
195. M. Prabhu *et al.*, Pregnancy and postpartum outcomes in a universally tested population for SARS-CoV-2 in New York City: a prospective cohort study. *BJOG: An International Journal of Obstetrics & Gynaecology* 127, 1548-1556 (2020).
196. J. M. Kubiak *et al.*, Severe acute respiratory syndrome coronavirus 2 serology levels in pregnant women and their neonates. *American journal of obstetrics and gynecology* 225, 73. e71-73. e77 (2021).
197. R. E. Baker *et al.*, The impact of COVID-19 nonpharmaceutical interventions on the future dynamics of endemic infections. *Proceedings of the National Academy of Sciences* 117, 30547-30553 (2020).

198. S. Singh, M. Shaikh, K. Hauck, M. Miraldo, Impacts of introducing and lifting nonpharmaceutical interventions on COVID-19 daily growth rate and compliance in the United States. *Proceedings of the National Academy of Sciences* 118, e2021359118 (2021).
199. Centers for Disease Control and Prevention, COVID-19 in Pregnant and Recently Pregnant People Guideline; US Department of Health and Human Services, CDC: Atlanta, GA, USA, 2022, available online: https://www.cdc.gov/coronavirus/2019-ncov/need-extra-precautions/pregnant-people.html#:~:text=of%20Severe%20Illness-,If%20you%20are%20pregnant%20or%20were%20recently%20pregnant%2C%20you%20are,one%20that%20causes%20COVID%2D19 , accessed on 20 April 2021.
200. National Health Service, Pregnancy and coronavirus (COVID-19), available online: https://www.nhs.uk/conditions/coronavirus-covid-19/people-at-higher-risk/pregnancy-and-coronavirus/ , accessed on 27 September 2022.
201. E. I. Ortiz, E. Herrera, A. De La Torre, Coronavirus (COVID 19) infection in pregnancy. *Colombia médica* 51, (2020).
202. J. Qiao, What are the risks of COVID-19 infection in pregnant women? *The lancet* 395, 760-762 (2020).
203. Centers for Disease Control and Prevention, COVID Data Tracker; US Department of Health and Human Services, CDC: Atlanta, GA, USA, 2022, available online: https://covid.cdc.gov/covid-data-tracker, accessed on 20 April 2021.
204. N. Vousden *et al.*, Severity of maternal infection and perinatal outcomes during periods in which Wildtype, Alpha and Delta SARS-CoV-2 variants were dominant: Data from the UK Obstetric Surveillance System national cohort. *BMJ Medicine* 1, (2022).
205. F. P. Havers *et al.*, Seroprevalence of antibodies to SARS-CoV-2 in 10 sites in the United States, March 23-May 12, 2020. *JAMA internal medicine* 180, 1576-1586 (2020).
206. W. Wang *et al.*, Detection of SARS-CoV-2 in different types of clinical specimens. *Jama* 323, 1843-1844 (2020).
207. K. Li *et al.*, Dynamic changes in anti-SARS-CoV-2 antibodies during SARS-CoV-2 infection and recovery from COVID-19. *Nature communications* 11, 6044 (2020).
208. S. Zheng *et al.*, Viral load dynamics and disease severity in patients infected with SARS-CoV-2 in Zhejiang province, China, January-March 2020: retrospective cohort study. *bmj* 369, (2020).
209. R. Wölfel *et al.*, Virological assessment of hospitalized patients with COVID-2019. *Nature* 581, 465-469 (2020).
210. L. Guo *et al.*, Profiling early humoral response to diagnose novel coronavirus disease (COVID-19). *Clinical infectious diseases* 71, 778-785 (2020).
211. F. Xiang *et al.*, Antibody detection and dynamic characteristics in patients with coronavirus disease 2019. *Clinical Infectious Diseases* 71, 1930-1934 (2020).
212. E. Mullins *et al.*, Pregnancy and neonatal outcomes of COVID-19: coreporting of common outcomes from PAN-COVID and AAP-SONPM registries. *Ultrasound in Obstetrics & Gynecology* 57, 573-581 (2021).
213. K. S. Jering *et al.*, Clinical characteristics and outcomes of hospitalized women giving birth with and without COVID-19. *JAMA internal medicine* 181, 714-717 (2021).

214. M. C. Smithgall *et al.*, Placental pathology in women vaccinated and unvaccinated against SARS-CoV-2. *American Journal of Obstetrics and Gynecology*, (2022).
215. World Health Organization, Statement on the fifteenth meeting of the IHR (2005) Emergency Committee on the COVID-19 pandemic, available from: https://www.who.int/news/item/05-05-2023-statement-on-the-fifteenth-meeting-of-the-international-health-regulations-(2005)-emergency-committee-regarding-the-coronavirus-disease-(covid-19)-pandemic, assessed on 5 May 2023.
216. J. Wise, Covid-19: WHO declares end of global health emergency. *BMJ*, (2023).
217. J. D. Cherry, P. Krogstad, SARS: the first pandemic of the 21st century. *Pediatric research* 56, 1-5 (2004).
218. S. Al Hajjar, K. McIntosh, The first influenza pandemic of the 21st century. *Annals of Saudi medicine* 30, 1-10 (2010).
219. S. Al Hajjar, Z. A. Memish, K. Mcintosh, Middle East respiratory syndrome coronavirus (MERS-CoV): a perpetual challenge. *Annals of Saudi medicine* 33, 427-436 (2013).
220. R. T. Kamorudeen, K. A. Adedokun, A. O. Olarinmoye, Ebola outbreak in West Africa, 2014–2016: Epidemic timeline, differential diagnoses, determining factors, and lessons for future response. *Journal of infection and public health* 13, 956-962 (2020).
221. R. E. Baker *et al.*, Infectious disease in an era of global change. *Nature Reviews Microbiology* 20, 193-205 (2022).
222. A. Handel, I. M. Longini Jr, R. Antia, What is the best control strategy for multiple infectious disease outbreaks? *Proceedings of the Royal Society B: Biological Sciences* 274, 833-837 (2007).
223. Centers for Diseases Control and Prevention, Weekly U.S. Influenza Surveillance Report (FluView), available from: https://www.cdc.gov/flu/weekly/index.htm, assessed on 9 June 2023.
224. R. E. Baker *et al.*, Long-term benefits of nonpharmaceutical interventions for endemic infections are shaped by respiratory pathogen dynamics. *Proceedings of the National Academy of Sciences* 119, e2208895119 (2022).
225. J. Cohen, Will viral interference hold off the tripledemic? available from: https://www.science.org/doi/epdf/10.1126/science.adf8989, assessed on 1 May 2023. 378, 815.
226. M. Masiá *et al.*, SARS-CoV-2 seroconversion and viral clearance in patients hospitalized with COVID-19: viral load predicts antibody response. *Open forum infectious diseases* 8, ofab005 (2021).
227. National Institutes of Health, COVID-19 Treatment Guidelines, The COVID-19 Treatment Guidelines Panel's Statement on Tixagevimab Plus Cilgavimab (Evusheld) as Pre-Exposure Prophylaxis of COVID-19, available from: https://files.covid19treatmentguidelines.nih.gov/guidelines/archive/statement-on-evusheld-01-10-2023.pdf, assessed on 5 May 2023.
228. M. J. Levin *et al.*, Intramuscular AZD7442 (tixagevimab–cilgavimab) for prevention of COVID-19. *New England Journal of Medicine* 386, 2188-2200 (2022).
229. AstraZeneca's global website, First participant dosed in SUPERNOVA Phase I/III trial evaluating AZD5156, a next-generation long-acting antibody combination, for prevention of COVID-19, available from: https://www.astrazeneca-us.com/media/statements/2022/first-participant-dosed-in-supernova-phase-I-III-trial-evaluating-azd5156-a-next-generation-long-acting-antibody-combination-for-prevention-of-covid-19.html, assessed on 5 May 2023.

230. Office for National Statistics, Coronavirus and clinically extremely vulnerable (CEV) people in England: 4 April to 23 April 2022, available from: https://www.ons.gov.uk/peoplepopulationandcommunity/healthandsocialcare/conditionsanddiseases/bulletins/coronavirusandclinicallyextremelyvulnerablepeopleinengland/4aprilto23april2022, assess on 10 May 2023.
231. M. Prabhu *et al.*, Antibody response to coronavirus disease 2019 (COVID-19) messenger RNA vaccination in pregnant women and transplacental passage into cord blood. *Obstetrics and Gynecology* 138, 278 (2021).